



HAL
open science

Catalytic reactivity at high coverage : a theoretical approach

Sarah Gautier

► **To cite this version:**

Sarah Gautier. Catalytic reactivity at high coverage : a theoretical approach. Theoretical and/or physical chemistry. Ecole normale supérieure de lyon - ENS LYON, 2015. English. NNT : 2015ENSL1015 . tel-01407346

HAL Id: tel-01407346

<https://theses.hal.science/tel-01407346>

Submitted on 2 Dec 2016

HAL is a multi-disciplinary open access archive for the deposit and dissemination of scientific research documents, whether they are published or not. The documents may come from teaching and research institutions in France or abroad, or from public or private research centers.

L'archive ouverte pluridisciplinaire **HAL**, est destinée au dépôt et à la diffusion de documents scientifiques de niveau recherche, publiés ou non, émanant des établissements d'enseignement et de recherche français ou étrangers, des laboratoires publics ou privés.

THÈSE

en vue de l'obtention du grade de

Docteur de l'Université de Lyon, délivré par l'École Normale Supérieure de Lyon

DISCIPLINE : CHIMIE

LABORATOIRE DE CHIMIE

ÉCOLE DOCTORALE DE CHIMIE (CHIMIE, PROCÉDÉS, ENVIRONNEMENT)

présentée et soutenue publiquement le 28 septembre 2015

par Madame **Sarah GAUTIER**

**Réactivité catalytique à haut recouvrement :
une approche théorique**

Directeur de thèse : M. Philippe SAUTET

Après l'avis de :

M. Guy MARIN

M. Jean-François PAUL

Devant le jury composé de :

Mme Céline CHIZALLET	IFPEN	Examinatrice
M. Guy MARIN	Université de Gand	Rapporteur
Mme Carine MICHEL	ENS de Lyon	Examinatrice
M. Jean-François PAUL	Université Lille 1	Rapporteur
M. Laurent PICCOLO	IRCELYON	Examineur
M. Philippe SAUTET	ENS de Lyon	Directeur

Remerciements

Je souhaite remercier toutes les personnes qui m'ont grandement aidée tout au long de ce travail.

- Mes collègues de bureau Yuemei et Torsten, puis Romain et Enza, qui partageront toujours avec générosité leurs connaissances et leur sagesse. Leur bienveillance m'a permis de m'intégrer plus facilement dans un environnement nouveau, et d'achever sereinement ce travail de longue haleine.
- Ronan Madec et Romain Goffe, amis de toujours, m'ont initiée à l'art subtil de la programmation ce qui m'a permis de gagner un temps considérable et de me concentrer sur la chimie de mon travail.
- Ludovic Briquet, mon compagnon de cordée lors de l'ascension du Butadiène, et Tanguy Le Bahers, ami précieux et collègue brillant, m'ont apporté leur soutien en partageant leur connaissance et en me montrant la voie de la persévérance.
- Je remercie aussi les chercheurs, ingénieurs, techniciens et notre cher administrateur, pour leur ouverture d'esprit et leur accueil au sein du laboratoire.
- C'est grâce à mes collègues enseignants, et en particulier à Bastien Mettra, que j'ai pu assumer sans trop de difficulté mon service d'activité complémentaire d'enseignement, notamment les travaux pratiques de chimie organique de troisième année !

- Filippo Ronzani, mon compagnon de vie lui même chimiste, m'a soutenue tout au long de ces trois années, et n'a pas pour autant renoncé à rester à mes côtés.
- Merci aussi à Tahar Boulmezaoud et Michel Rérat, deux enseignants qui m'ont marquée par leur investissement personnel et m'ont donné le goût des sciences.
- Paul Fleurat-Lessard, toujours patient, m'a motivée et aiguillée quand je doutais ou me heurtais à des difficultés d'ordre technique et organisationnel. De plus, nos discussions scientifiques ont fortement contribué au bon développement de ce travail.
- Carine Michel m'a consacré beaucoup de son temps, m'a initiée avec patience au calcul périodique, et m'a conseillée avec efficacité sur des points essentiels à des moments critiques.
- Enfin, mon directeur de thèse, Philippe Sautet, a bien voulu croire en moi et m'a embauchée malgré mon parcours atypique. Bien qu'extrêmement demandé, il a su trouver le temps et la disponibilité d'esprit pour des interventions décisives quant à l'avancement de notre travail, constamment irrigué par son intérêt passionné pour la chimie.

Sarah

Contents

1	Introduction	9
2	Methodology	13
2.1	Schrödinger equation	13
2.2	Density Functional Theory	15
2.3	The Kohn-Sham method	17
2.4	The PBE and optPBE functionals	19
2.5	Periodic systems	21
2.6	Supercell	22
2.7	Thermodynamic model	24
3	Molecular adsorption at Pt(111). How accurate are DFT functionals ?	29
3.1	Introduction	30
3.2	Computational details	34
3.3	Results and discussion	35
3.4	Conclusion	51
4	Hydrogen adsorption and coverage dependency on Pt(111) and Sn/Pt-Pt(111)	55
4.1	Introduction	56
4.2	Computational details	57
4.3	Pt(111): results and discussion	61

4.4	Sn/Pt-Pt(111): results and discussion	69
4.5	Conclusion	76
5	Butadiene and Hydrogen co-adsorption and coverage dependency on Pt(111)	79
5.1	Introduction	79
5.2	Computational details	80
5.3	Before co-adsorption, butadiene adsorption on Pt(111)	80
5.4	Screening of the co-adsorption of butadiene with one hydrogen	81
5.5	How chemisorbed butadiene modifies the coverage of hydrogen	87
5.6	Competitive chemisorption of butadiene and hydrogen	93
5.7	What about butadiene physisorption ?	96
5.8	Conclusion	100
6	Butadiene and Hydrogen co-adsorption and coverage dependency on Sn/Pt-Pt(111)	105
6.1	Introduction	106
6.2	Before co-adsorption, butadiene adsorption on Sn/Pt-Pt(111)	106
6.3	Screening of the co-adsorption of butadiene with one hydrogen	108
6.4	How chemisorbed butadiene modifies the coverage of hydrogen	109
6.5	Competitive chemisorption of butadiene and hydrogen	116
6.6	What about butadiene physisorption ?	116
6.7	Conclusion	120
7	Butadiene hydrogenation as a function of the coverage on Pt(111) and Sn/Pt-Pt(111)	125
7.1	Introduction	126
7.2	Pt(111)	128
7.3	Sn/Pt-Pt(111)	150

8 Conclusion	165
Appendices	171
A Hydrogen adsorption sites on a (2×2) cell of Pt(111)	173
B Screening of hydrogen adsorption sites on a (3×3) cell of Pt(111)	181
C Molecular adsorption at Pt(111). How accurate are DFT functionals ?	187
Bibliography	203

Chapter 1

Introduction

Reaction mechanisms in heterogeneous catalysis are the subject of a particular attention since many years. Researches in that field of chemistry are numerous and their applications are of paramount importance. Selective hydrogenation of fat acids for the food industry and hydrogenation of polyunsaturated hydrocarbons for the petroleum industry¹⁻⁴ are two examples of these applications. These reactions are catalysed by metallic particles or bimetallic alloys, and happen under pressure of hydrogen. Since chemists are able to model surfaces, simulations of the surface state remain minimalist. Indeed the complexity of such systems combined to computing time limits is a real challenge for the theoretician community. The usual way to treat surface reaction in ab initio studies is to consider only one molecule of each reactant adsorbed on the surface, this for each step of the reaction, and conclude on the most favourable pathway. In other words, reactivity studies are usually modelled in conditions corresponding to ultra-high vacuum (UHV) even though some reactions are demanding "normal" conditions (room temperature and pressure). This kind of simplified approach brings insights on the reaction mechanisms especially by proposing a description of the transition states, but the question remains: do we describe the co-adsorption of the reactant accurately enough to be able to conclude on the mechanism ? Thanks to technical and computational

recent developments, surface chemists have tried to bridge the gap between their simple surface model and real catalytic conditions⁵. In particular, the pressure issue is a real challenge as it implies a high coverage on the surface and thus the exploration of several conditions. Our aim is to develop an approach to treat such surface systems as accurately as possible by taking into account the partial pressure of the species and the temperature. Thus, we organized a thermodynamic model based on the principles of Boltzmann's statistic physics in order to know what is the coverage of the surface species when the reaction occurs.

We applied this methodology to the study of the selective hydrogenation of butadiene in 1-butene on Pt(111) and Sn/Pt-Pt(111). We used the VASP program (Vienna Ab-initio Simulation Package)^{6,7} which allows the simulation of solids and surfaces within the Density Functional Theory (DFT) framework. The choice of the surface catalyst was dictated by the experimental community which uses platinum most often because of its high activity, or tin-platinum alloys that are less active but more selective for partial hydrogenation of polyolefins.^{8,9} DFT studies of butadiene hydrogenation on Pt(111) and Sn/Pt-Pt(111) were already carried out^{4,10} without taking into account the operating conditions for this reaction which are $T = 300\text{-}400\text{ K}$ and $P_{H_2} = 1\text{-}10\text{ bar}$. Thus, a low coverage of hydrogen is considered which leads to a conclusion supporting the Langmuir-Hinshelwood mechanism. At such conditions and when the thermodynamic equilibrium is reached, we expect the hydrogen coverage to be high and thus a potential modification of the reaction mechanism. On top of that, we wonder if the description of the relative stability of hydrogen and butadiene brought by GGA functionals is accurate enough. Indeed, butadiene is a larger molecule than hydrogen and may involve dispersion interactions with the surface when adsorbing. As the relative stability of the reactants on the surface may have strong consequences on the reaction mechanism, we investigated methods that propose the treatment of van der Waals (vdW) interactions. A benchmark of recently developed functionals, also called vdW functionals, was carried

out on a group of molecules to which butadiene and butene belongs to. The study of hydrogen adsorption alone on Pt(111) and Sn/Pt-Pt(111) in a first place, and the investigation of hydrogen and butadiene co-adsorption on both surface catalyst in a second part, are presented to stress the importance of the thermodynamic study of the surface species. The final aim of this work is to understand the kinetics of butadiene hydrogenation and how realistic hydrogen coverage might affect the mechanisms. For this, a study of the reaction pathways at different coverages is proposed in the last part. A comparison between Pt(111) and Sn/Pt-Pt(111) is developed along this document in order to understand and analyse the different observations made on both catalysts and the better selectivity of the alloy.

Chapter 2

Methodology

Contents

2.1 Schrödinger equation	13
2.2 Density Functional Theory	15
2.3 The Kohn-Sham method	17
2.4 The PBE and optPBE functionals	19
2.5 Periodic systems	21
2.6 Supercell	22
2.7 Thermodynamic model	24

2.1 Schrödinger equation

The aim of this work is to study the adsorption of molecules on a metallic surface. As the surface is a periodic system, it has to be studied with a periodic approach. For this, we used *ab initio* methods which try to solve the non relativist time-independent Schrödinger equation. This allows to describe at the quantum level the electronic structure of atoms and molecules.

$$H\Psi = E\Psi \quad (2.1)$$

In this equation, the operator H is the Hamiltonian of the system, E is one eigenvalue of H (the energy of the system) and Ψ is the associated eigenvector, which corresponds to the multi electronic wave function of the system. In the case of polyatomic molecules, the Hamiltonian becomes (in atomic units):

$$H = T_N + T_e + V_{NN} + V_{NE} + V_{ee} \quad (2.2)$$

$$\begin{aligned} H = & -\frac{1}{2} \sum_A^{nuclei} \frac{\nabla_A^2}{M_A} - \frac{1}{2} \sum_i^{electrons} \nabla_i^2 + \sum_A^{nuclei} \sum_{B>A}^{nuclei} \frac{Z_A Z_B}{R_{AB}} \\ & - \sum_A^{nuclei} \sum_i^{electrons} \frac{Z_A}{R_{iA}} + \sum_i^{electrons} \sum_{j>i}^{electrons} \frac{1}{r_{ij}} \end{aligned} \quad (2.3)$$

In this equation, the first term corresponds to the kinetic energy of the nuclei, the second to the kinetic energy of the electrons, the third to the Coulomb repulsion of the nuclei, the fourth to the Coulomb attraction of the electrons and the nuclei and the last one to the Coulomb repulsion of the electrons. ∇_A^2 is the Laplace operator, M_A is the mass of the nucleus A , Z_A and Z_B are the atomic numbers of the nuclei A and B , R_{AB} , R_{iA} and r_{ij} are the distances between two nuclei A and B , the electron i and the nucleus A , and two electrons i and j .

In order to simplify this equation, a first approximation called Born-Oppenheimer approximation is usually done. As the nuclei mass is much larger than the electrons mass, one can consider that the electronic cloud adapts instantaneously to the movement of the nuclei. In other words, the electrons see only the potential generated by the immobile nuclei. This allows to uncouple the movement of the electrons and that of the nuclei. The Hamiltonian becomes the sum of a nuclear Hamiltonian, H_{nucl} , and an electronic Hamiltonian, H_{el} (equation 2.4). If we fix the position of the nuclei, it is possible

to write a Schrödinger equation who depends only on the electrons positions (the nuclei positions being only parameters in this new equation). Within this approximation, the total wave function of the system is the product of an electronic wave function, Ψ_{el} , and a nuclear wave function, Ψ_{nucl} .

$$H = H_{el} + H_{nucl} \quad (2.4)$$

$$H_{el}\Psi_{el}^{R_A}(r_i) = E_{el}^{R_A}\Psi_{el}^{R_A}(r_i) \quad (2.5)$$

$$H_{el} = -\frac{1}{2} \sum_i^{electrons} \nabla_i^2 - \sum_A^{nuclei} \sum_i^{electrons} \frac{Z_A}{R_{iA}} + \sum_i^{electrons} \sum_{j>i}^{electrons} \frac{1}{r_{ij}} \quad (2.6)$$

The total energy of the system is :

$$E_{tot} = E_{el}^{R_A} + \sum_A^{nuclei} \sum_{B>A}^{nuclei} \frac{Z_A Z_B}{R_{AB}} \quad (2.7)$$

The Born-Oppenheimer approximation will be adopted from this point forward. The Hamiltonian of the system will be the electronic Hamiltonian and the wave function of the system will be the multi electronic wave-function, Ψ_{el} .

Many methods were developed to solve the electronic Schrödinger equation by means of different types of approximations. They can be sorted in two categories : the methods based on the Hartree-Fock theory and the methods based on the Density Functional Theory (DFT). The latter were used for the studies presented in this document.

2.2 Density Functional Theory

The DFT is a quantum method that allow to study the electronic structure of systems. It differs from the methods called "post-Hartree-Fock" because of the use of the electronic

density of the system instead of its multi electronic wave function. The initial principle of DFT comes historically from the Thomas-Fermi model elaborated in 1927. According to that model, the kinetic energy of a non-interacting electrons gas depends only on the electronic density of that cloud. It was then completed by Dirac, who added an exchange energy also depending only on the electronic density of the system. Instead of working with a wave function, Ψ , depending on the $3N$ cartesian coordinates of the N electrons of a system, one could use the electronic density, $\rho(\vec{r})$, who only depends on 3 coordinates. The electronic density and the wave function are related by the following formula :

$$\rho(\vec{r}) = \int_{\vec{r}_2} \dots \int_{\vec{r}_N} \Psi(\vec{r}_1, \vec{r}_2 \dots \vec{r}_N) \Psi^*(\vec{r}_1, \vec{r}_2 \dots \vec{r}_N) d\vec{r}_2 \dots d\vec{r}_N \quad (2.8)$$

However, the idea of using the electronic density as founding principle of quantum calculations will be formulated in 1964 by Hohenberg and Kohn in the form of two theorems.

1) Existence theorem

According to this theorem, any observable of a system in its fundamental state, and in particular its energy, is a functional of the electronic density. A functional is an application which associates a number to a function (i.e. a functional is a function of function). Thus, the electronic energy of a chemical system can be written as :

$$E[\rho(\vec{r})] = T_e[\rho(\vec{r})] + V_{ee}[\rho(\vec{r})] + V_{Ne}[\rho(\vec{r})] \quad (2.9)$$

where each one of the terms has the same signification than in equation 2.3. The potential generated by the nuclei can be considered as a particular case of external potential, v_{ext} , felt by the electrons. It is possible to generalize the equation 2.9 in the form of equation 2.10.

$$E[\rho(\vec{r})] = F_{HK}[\rho(\vec{r})] + \int v_{ext}(\vec{r})\rho(\vec{r})d\vec{r} \quad (2.10)$$

The F_{HK} function groups the kinetic energy of the electrons and their interactions. This last functional is called universal functional as it does not depend on the external potential and therefore on the studied system.

2) Variational principle

This second theorem applies the variational principle of quantum mechanics to the particular case of DFT. Thus, the energy of a system calculated with an approximate electronic density will always be superior to the exact energy obtained with the exact density.

$$F_{HK}[\rho(\vec{r})] + \int v_{ext}(\vec{r})\rho(\vec{r})d\vec{r} = E[\rho(\vec{r})] \geq E_{exact}[\rho_{exact}(\vec{r})] \quad (2.11)$$

The variational principle allows to select the electronic density the closest to the real one within a set of test densities. This selected density minimises the total energy.

These two theorems show that only the electronic density of a system defines both the Hamiltonian and the resulting observable value. However, they do not help to determine the electronic density as the interelectronic interaction term, V_{ee} , is still present in the equation. This prevents to determine the exact analytical form of the universal functional.

2.3 The Kohn-Sham method

Kohn and Sham proposed an exact method in 1965 to determine the electronic density of the fundamental state of a system as well as its energy.¹¹ Their method (the Kohn-Sham

method) is based on the following assessment: the kinetic energy of a non-interacting electrons gas, T_s , has a known analytical expression. This expression, given in equation 2.12, requires the introduction of the monoelectronic molecular orbitals ψ_i .

$$T_s = -\frac{1}{2} \sum_i^{electrons} \langle \psi_i | \nabla_i^2 | \psi_i \rangle \quad (2.12)$$

The molecular orbitals are used to form the multi electronic wave function of the system also called Slater determinant. This determinant is a mathematical way to approach the multi electronic wave function of a system as it respects the antisymmetry principle of the wave function for the fermions. This is required by the non discernability of the particules in quantum mechanics.

$$\Psi_{Slater}(\vec{r}_1, \vec{r}_2 \dots \vec{r}_N) = \frac{1}{\sqrt{N!}} \begin{vmatrix} \psi_1(\vec{r}_1) & \dots & \psi_N(\vec{r}_1) \\ \vdots & \ddots & \vdots \\ \psi_1(\vec{r}_N) & \dots & \psi_N(\vec{r}_N) \end{vmatrix} \quad (2.13)$$

The introduction of orbitals and the use of the free electron gas kinetic energy leads to a system of N coupled monoelectronic equations of which the solutions allow to calculate the wave function and, consequently, the electronic density (equations 2.14 to 2.16). To sum up, this method allows to calculate the electronic structure of a non interacting electron gas submitted to an effectif potential, v_{eff} , which has the same electronic density than the real system.

$$H_{KS}\psi_i = \varepsilon_i\psi_i \quad (2.14)$$

$$H_{KS} = -\frac{1}{2}\nabla^2 + \int \frac{\rho(\vec{r}')\rho(\vec{r})}{|\vec{r}-\vec{r}'|} d\vec{r}' + v_{ext}(\vec{r}) + v_{xc}[\rho(\vec{r})] = -\frac{1}{2}\nabla^2 + v_{eff}[\rho(\vec{r})] \quad (2.15)$$

$$v_{xc}[\rho(\vec{r})] = \frac{\delta E_{xc}}{\delta \rho} \quad (2.16)$$

The first term of the Hamiltonian correspond to the kinetic energy, the second represents the classical part of the Coulomb interaction between electrons, the third one is the external potential (i.e. the interaction with the nuclei) and the last one, v_{xc} , represents the exchange-correlation potential and E_{xc} is the exchange-correlation energy. The latter is expressed as follows :

$$E_{xc} = (T_{real} - T_s) + (V_{ee} - \int \frac{\rho(\vec{r})\rho(\vec{r}')}{|\vec{r} - \vec{r}'|} d\vec{r}') \quad (2.17)$$

This relation allows to correct the replacement of the real kinetic energy with the kinetic energy of a non interacting electrons system and allows to take into account the non classical interaction between the electrons (term in parenthesis).

By replacing the electronic density of a real system by that of a non interacting electrons system, Kohn and Sham instaurated a method to calculate the energy of a system in its fundamental state. This method is in theory exact if the exchange correlation potential is known. Unfortunately, this is not the case. Thus, it is required to develop approximate exchange-correlation functionals.

2.4 The PBE and optPBE functionals

As seen before, the whole method developp by Kohn and Sham to use DFT in practice is based on the exchange-correlation functional. Many functionals were developped both on pure theoretical considerations and on empirical considerations. Indeed, one can adjust the functional parameters to a set of experimental data. It is important to note that, today, there is no such a thing as one perfect functional that would be able to describe correctly any type of physical-chemical properties (structures, excitation energies, energy barriers...) for each of all kinds of systems (molecules, surface, solide...).

In this work we used two different kind of functional. The first is the PBE functional

which was developed by Perdew, Burke and Ernzerhof in 1996.¹² It belongs to the Generalized Gradient Approximation (GGA) family and does not contain any empirical parameter. The second functional, optPBE, is a non local functional also called van der Waals functional (vdw-DF) that allow to take into account the dispersion forces of a system. It is a quite recent functional developed by J. Klimeš et al. in 2010.¹³ The energy of a system calculated with optPBE can be expressed as the sum of three terms :

$$E_{XC}^{optPBE} = E_X^{GGA} + E_C^{LDA} + E_C^{nl} \quad (2.18)$$

The first term is a GGA exchange component optimized from the initial PBE exchange energy. The second term is the LDA correlation component which is the same than the PBE correlation term. The last term is the non local part of the correlation which contains the dispersion energy. The latter is defined as follows :

$$E_C^{nl} = \int \int d\vec{r}_1 d\vec{r}_2 n(\vec{r}_1) \varphi(\vec{r}_1, \vec{r}_2) n(\vec{r}_2) \quad (2.19)$$

with $n(\vec{r}_1)$ and $n(\vec{r}_2)$ the local electronic densities and $\varphi(\vec{r}_1, \vec{r}_2)$ the non local electronic density.

Those two functionals were chosen because of two different reasons :

- The GGA level of theory is a good compromise to describe a heterogeneous system such as an organic molecule adsorbed on a metallic surface
- PBE does not describe the dispersion forces that may exist between a hydrocarbon and a metallic surface while optPBE does

The comparison of the traditional method (using PBE) and this other approach (using vdW functionals) is treated in Chapter 3.

2.5 Periodic systems

When passing from a molecular system to an extensive system, the number of atoms composing it increases considerably. This modifies its electronic structure. Indeed, we will not speak anymore about molecular orbitals, localised in energy, but about energy bands spreading on a whole range of energy. From a methodologic point of view, those systems can have a periodicity in their structure i.e. the global structure is the repetition in space of an elementary structure called elementary lattice. Crystalline systems for example, are part of this kind of architecture. In these conditions, the system can be studied in quantum mechanics thanks to a Hamiltonian having the same periodicity than the system itself. One must also impose some periodic conditions at the limits of the elementary lattice called Periodic Boundary Conditions (PBC) of Born-Von Karman. Bloch demonstrated, in these conditions, that the mono electronic wave functions must be written as follows :

$$\Psi_{\vec{k}}(\vec{r}) = u(\vec{r})e^{i\vec{k}\cdot\vec{r}} \quad (2.20)$$

$$u(\vec{r} + \vec{T}) = u(\vec{r}) \quad (2.21)$$

where \vec{k} is a vector of the reciprocal space and \vec{T} a vector of the direct space. The \vec{k} vectors can be any possible value of the Brillouin zone (which is the elementary lattice of the reciprocal space). In the periodic calculation codes, the basic functions which form the crystalline orbitals (twin of the molecular orbitals) are Bloch functions. Within the Kohn-Sham method applied to periodic systems, one should solve $N_{\vec{k}}$ times the set of mono-electronic equations (with $N_{\vec{k}}$ the number of \vec{k} vectors). This is impossible if $N_{\vec{k}}$ is infinite. In practice, the calculated properties of a system, such as the total energy, converge with the number of $N_{\vec{k}}$ used. It is enough to determine the finite number of those vectors, with a convergence criterion, to consider that those properties meet the

convergence. From now on, we will talk about k-points to name the \vec{k} vectors.

Several models were developed to study the surfaces of materials. Among them, one of the most utilized is the so called "slab model". It consists in cutting a surface in the bulk of the solid, following the Miller index (hkl). The surface is defined by the Miller index and has a finite thickness which is given in number of layers of atoms. The periodicity is kept in the three directions of space (3D-periodic). Following the direction perpendicular to the surface, the lattice parameter is chosen large enough to avoid interactions between the slabs (see Figure 2.1). The influence of the thickness of the slab on the different electronic parameter was studied for each system. The convergence criteria were chosen to meet the best compromise between the accuracy of the results and the calculation time spent to obtain those results.

As a consequence, the number of layers of the slab chosen for each system will be specified in the different studies presented in this work.

2.6 Supercell

The surface elementary lattice, also called elementary cell, is usually too small to realise the adsorption of molecules. That is why we work with supercells. A supercell is the multiplication of the elementary cell in both direction of the periodicity of the surface. The size of the supercell is chosen so that the interactions between adsorbates from one cell to another are negligible. The concept of supercell is represented in Figure 4.3 of Chapter 4. As the dimensions of the supercell depend on the adsorbate, they will be specified in the computational details of each study.

The number of k-points necessary to realise the meshing of the first Brillouin zone depends on the size of the supercell. Indeed, the volume of the first Brillouin zone is inversely proportional to that of the supercell. Thus, the larger the supercell, the smaller the first Brillouin zone and the smaller the number of k-points needed to obtain

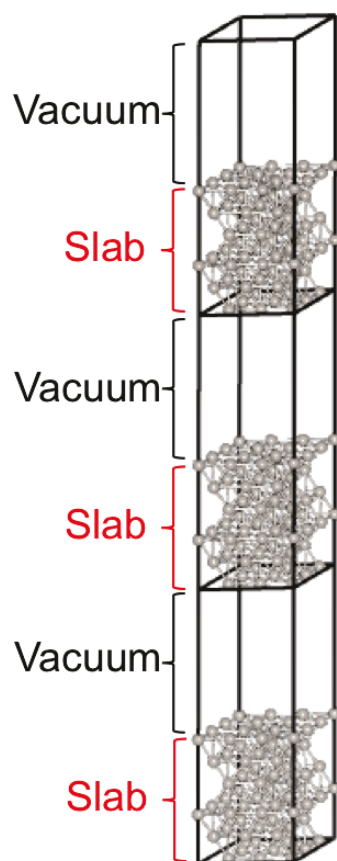


Figure 2.1: Example of a six layer slab, repeated three times in the z direction of the space, illustrating the vacuum imposed between the slab

the desired k-points density. A k-points convergence study was systemically realised for each supercell in order to determine the optimal number of k-points to use for the calculations.

2.7 Thermodynamic model

The adsorption energy, E_{ads} , of a system is calculated at 0 K as follows:

$$E_{ads}^{Tot} = E_{Tot} - E_{slab} - \sum_{i=1}^x n_i E_i(g) \quad (2.22)$$

with E_{Tot} being the energy of the entire system, E_{slab} the energy of the slab alone, n_i the number of molecule i adsorbed, x the number of different molecules and $E_i(g)$ the energy of the molecule in the gas phase; a negative value indicates an exothermic adsorption process.

The differential adsorption energy, E_{ads}^{diff} , is calculated to analyse the stability of a system. It will be used in the study of the co-adsorption of molecules, to understand the effect of adding one more molecule on a pre-covered surface. It is defined as follows when considering one type of molecule:

$$E_{ads}^{diff} = E_{ads}^{Tot}(n_i, n_j + 1) - E_{ads}^{Tot}(n_i, n_j) \quad (2.23)$$

A positive value indicates that the global system is destabilized by adding one molecule of type j.

The coverage of a system is defined as:

$$\theta_i = \frac{n_i}{n_{At,surf}} \quad (2.24)$$

with $n_{At,surf}$ the number of atom belonging to the surface. These atoms can be of different nature depending on the catalyst. The coverage is given in monolayer (ML)

with 1 ML corresponding to a surface completely covered, thus, with as many molecule adsorbed as atom of the surface.

Butadiene hydrogenation reactions are run under a pressure of hydrogen of about 5 bar with temperature ranging from 300 to 400 K. The adsorption free energies were calculated by using default statistical thermodynamics. When considering strongly adsorbed systems, we didn't take into consideration any rotational and translational contribution of the entropy. Moreover, at low coverage, the amount of molecule being small on the surface, we didn't include the vibrational entropy. At high coverage, and for strongly adsorbed molecules, we took into account the vibrational entropy. For weakly adsorbed systems, we added a contribution of a 2D translational entropy in order to allow the molecules to diffuse on the surface. The gas phase of the system was treated within the ideal gas approximation.

The adsorption free energy is defined as follows:

$$G_{ads}^{Tot}(T, P) = G_{Tot} - G_{slab} - \sum_{i=1}^x n_i G_i(g) \quad (2.25)$$

If we work in the approximation assuming that the entropic contribution of the adsorbed phases is negligible, we can write :

$$G_{ads}^{Tot}(T, P) = E_{Tot} - E_{slab} - \sum_{i=1}^x n_i G_i(g) \quad (2.26)$$

We now need to define $G_i(g)$. The free energy is calculated as follows :

$$G = H - TS = U + PV - TS = PV + F \quad (2.27)$$

With F the free energy of the system, expressed as follows :

$$F = -k_B T \ln[Z] \quad (2.28)$$

with Z the total partition function.

$$Z = Z_{conf} \times Z_{nucl} \times Z_{elec} \times Z_{trans} \times Z_{rot} \times Z_{vib} \quad (2.29)$$

with nucl for nuclear partition function, conf for configurational, elec for electronic, trans for translational, rot for rotational and vib for vibrational partition function.

As we don't consider nuclear contribution, it comes :

$$Z = Z_{conf} \times Z_{elec} \times Z_{trans} \times Z_{rot} \times Z_{vib} \quad (2.30)$$

Because of the paradoxe, we have :

$Z = \frac{z^n}{n!}$ with z the partition function of each molecule, n the number of molecules.

$$\text{So } G = PV - k_B T \ln[Z_{conf} \times Z_{elec}] - k_B T \ln \left[\frac{(z_{trans} \times z_{rot} \times z_{vib})^n}{n!} \right]$$

The Stirling formula gives : $\ln(n!) = n \ln(n) - n$

$$G = PV - k_B T \ln[Z_{conf} \times Z_{elec}] - k_B T (n \ln[z_{trans} \times z_{rot} \times z_{vib}] - (n \ln(n) - n))$$

$$G = -k_B T \ln[Z_{conf} \times Z_{elec}] - nk_B T \ln \left[\frac{z_{trans} \times z_{rot} \times z_{vib}}{n} \right]$$

$$G = F_{conf} + F_{elec} - nk_B T \ln \left[\frac{z_{trans} \times z_{rot} \times z_{vib}}{n} \right]$$

The translational partition function is :

$$z_{trans, M_i}(T, P) = \left(\frac{2\pi m_{M_i} k_B T}{h^2} \right)^{3/2} V \quad (2.31)$$

if we note $z_{trans}^*(T) = \left(\frac{2\pi mk_B T}{h^2}\right)^{3/2}$ then

$$G = F_{conf} + F_{elec} - nk_B T \ln \left[\frac{V \times z_{trans}^* \times z_{rot} \times z_{vib}}{n} \right]$$

as $n = \frac{PV}{k_B T}$, it comes :

$$G = F_{conf} + F_{elec} - nk_B T \ln \left[\frac{V \times z_{trans}^* \times z_{rot} \times z_{vib}}{\frac{PV}{k_B T}} \right]$$

$$G = F_{conf} + F_{elec} - nk_B T \ln \left[\frac{k_B T}{P} \times z_{trans}^* \times z_{rot} \times z_{vib} \right]$$

$$G = F_{conf} + F_{elec} - nk_B T \ln [z_{trans}^* \times z_{rot} \times z_{vib}] + nk_B T \ln \left[\frac{P}{k_B T} \right]$$

For a molecule in the gas phase, the contribution of the configurational free energy F_{conf} can be neglected as it is very small. Moreover, the following approximation was adopted :

$$F_{elec}^i = n_i E_{elec}^i \quad (2.32)$$

considering that the electronic entropy was negligible. Therefore, the adsorption free energy of a given molecule in the gas phase comes as :

$$G_i(g) = n_i E_i(g) - k_B T \ln [(z_{trans}^{*,i} \times z_{rot}^i \times z_{vib}^i)^{n_i}] + n_i k_B T \ln \left[\frac{P^i}{k_B T} \right] \quad (2.33)$$

After the first approximation assuming that the vibrational contribution of the entropy is negligible, we obtain:

$$G_i(g) = n_i E_i(g) - k_B T \ln [(z_{trans}^{*,i} \times z_{rot}^i)^{n_i}] + n_i k_B T \ln \left[\frac{P^i}{k_B T} \right] \quad (2.34)$$

Finally, the adsorption free energy for a given system with i different molecules adsorbed on the surface becomes :

$$G_{ads}^{Tot}(T, P) = E_{Tot} - E_{slab} - \sum_{i=1}^x n_i E_i(g) + k_B T \sum_{i=1}^x \ln[(z_{trans}^{*,i} \times z_{rot}^i)^{n_i}] - k_B T \sum_{i=1}^x n_i \ln \left[\frac{P^i}{k_B T} \right] \quad (2.35)$$

$$G_{ads}^{Tot}(T, P) = E_{ads}^{Tot} + k_B T \sum_{i=1}^x \ln[(z_{trans}^{*,i} \times z_{rot}^i)^{n_i}] - k_B T \sum_{i=1}^x n_i \ln \left[\frac{P^i}{k_B T} \right] \quad (2.36)$$

with the rotational partition functions:

$$z_{rot}(T) = \frac{1}{\sigma_r} \left(\frac{T}{\theta_r} \right) = \frac{1}{\sigma_r} \left(\frac{8\pi^2 I k_B T}{h^2} \right) \quad (2.37)$$

for a linear molecule, and

$$z_{rot}(T) = \frac{\pi^{1/2}}{\sigma_r} \left(\frac{T}{\theta_r^a \theta_r^b \theta_r^c} \right) = \frac{\pi^{1/2}}{\sigma_r} \left(\frac{8\pi^2 k_B T}{h^2} \right)^{\frac{3}{2}} I_a I_b I_c \quad (2.38)$$

for a non linear molecule.

Chapter 3

Molecular adsorption at Pt(111). How accurate are DFT functionals ?

Contents

3.1 Introduction	30
3.2 Computational details	34
3.3 Results and discussion	35
3.3.1 Structures	35
3.3.2 Binding mode and electronic structure	39
3.3.3 Experimental adsorption energies	40
3.3.4 Adsorption energies - General performance	41
3.3.5 Adsorption energies – Performance for each family	43
3.4 Conclusion	51

3.1 Introduction

Chemisorption of a molecule on a surface is a key elementary step in many processes such as catalysis, electrochemistry, surface treatment, tribology and friction.¹⁴ Our knowledge of bond energies of adsorbates is still scarce and obtaining accurate data is central to our understanding of surface chemistry and of its implications in the just mentioned processes.^{15,16} During chemisorption, bonds are formed between the molecule and the surface atoms, and bonds within the molecule and within the surface are rearranged.¹⁷ These new bonds are not different in nature from the ones already present in the molecule or in the surface, but their description with quantum chemical methods can be difficult especially in the case of transition metal surfaces.^{18,19} Indeed this requires a method that can describe adequately, at the same time, the localized bonding within molecule, the extended electronic structure of the transition metal, and the interactions at the interface. Such systems are nowadays mainly described using Density Functional Theory (DFT), more precisely with one of the approximations for the exchange-correlation functional of DFT. The hierarchy of available functionals is usually classified using the Jacob's ladder introduced by Perdew.²⁰ The first rung of the ladder consists of the Local Density approximation (LDA), while the second (resp. third) rung introduces semi-local dependence on the density (GGA) (resp. kinetic energy density, meta-GGA). Rung 4 and 5 respectively introduce an explicit dependence on occupied orbitals (e.g. hybrid functionals) and virtual orbitals (e.g. RPA). LDA yields severe over-binding in molecules and solids and is now rarely used in chemistry.²¹ The GGA level brings considerable improvement and is still a very popular method for the description of extended metallic solids and their surfaces. In molecular chemistry however, organic molecules or transition metal complexes, these GGA methods tend to underestimate the electronic

gap of molecules, and a popular and accurate approach is to use hybrid functionals, such as the vastly used B3LYP²², where GGA exchange is mixed with Hartree-Fock exchange. However these hybrid functionals are not well adapted for transition metal solids, yielding a severe underestimation of their atomization energy and an overestimation of their d-band width.^{23,24} Hence the choice of a functional for our molecule-metal surface problem appears as a real headache. On top of that, none of these GGA or hybrid functionals describe correctly the van der Waals (vdW) dispersion forces that could play a significant role in the molecular adsorption energy. Such vdW interactions can be described by an ad-hoc addition of a force field, by using double hybrid functionals that incorporate a fraction of second order perturbation correlation energy an explicitly correlated energy term, by accessing the fifth rung of Jacob's ladder with the calculations of correlation energy using unoccupied KS orbitals (e.g. RPA method) or by calling for explicitly non-local descriptions of the correlation functional, such in the vdW-DF method.²⁵ The vdW-DF approaches however do not describe well transition metal bulk structure in their original implementations, and the choice of the optimal exchange functional accompanying the vdW-DF correlation is still a matter of debate. Hence the users of DFT methods are faced with many different approximations, with various advantages and limitations, and it is not clear which one is adequate for describing the interaction between a molecule and a metal surface. In this paper, we aim at determining the most adequate and applicable DFT method for studying gas phase adsorption processes at metallic surfaces. To assess the accuracy of DFT functionals, we gather a set of highly accurate experimental data and carefully compare the experimental adsorption energies with the theoretical ones. The quantification of the chemisorption energy of molecules at surfaces is also an acute experimental problem. The development of single crystal adsorption calorimetry (SCAC) has allowed a strong advance in the field by the determination of accurate data at well-defined surfaces, although nowadays less than a handful of such apparatus exist worldwide.²⁶⁻²⁹ An important point is that the adsorption en-

ergy of a molecule strongly depends on the presence of co-adsorbed species, the usual behavior being a decrease of the chemisorption energy upon increased molecule coverage, so that the evaluation of both the energy and the coverage is of key importance. Recent tools allow the detailed measurement of the adsorption energy as a function of coverage with an accuracy of 6 %.²⁶ The adsorption energy as a function of coverage has therefore been accurately measured for a series of unsaturated molecules. We have gathered a set of ten molecular chemisorption processes on a Pt(111) surface, for which accurate SCAC data is available. This set includes hydrogen, carbon monoxide, saturated hydrocarbons (methane, ethane), and unsaturated molecules of various size and number of π electrons with ethylene, cyclohexene, benzene and naphthalene. While methane and ethane are just weakly physisorbed due to dispersion forces, most of these molecules chemisorb intact on the Pt(111) surface at low temperature, hence forming molecule-surface chemical bonds, except H_2 which is dissociated in H atoms. Ethylene reacts at room temperature to form an ethylidyne species CCH_3 and hydrogen,^{26,30,31} while cyclohexene is either chemisorbed intact or dehydrogenated into $c-C_6H_9$ and hydrogen.³² This benchmark-set is described in more details in Appendix C. Besides this set, we have also added unsaturated molecules of importance in catalysis, such as butene or butadiene. Although SCAC data are not available for these molecules, the comparison of ethylene with butadiene and butene allows us to understand the influence on the chemisorption energy of conjugation length and of alkyl substituents, respectively.

The comparison between these micro-calorimetry data with published calculation using the GGA approximation shows contrasting results. The calculated and measured adsorption energy for cyclohexene seem to match within 8 %, while for benzene and naphthalene, the measured energy exceeds the computed one by 60 % (in absolute value).¹⁶ This situation is not satisfactory, and although the contribution of missing van der Waals interactions was pointed out as a possible origin of the discrepancy, our understanding of the situation is far from complete. Hence, in this paper, we compare

results using the largely employed PBE GGA functional¹² with a set a vdW functionals. Two of them (optPBE-vdW, optB86b-vdW)¹³ use the vdW-DF non-local correlation functional (vdW-DF)³³ with different exchange functionals, while the third one (BEEF-vdW)³⁴ is based on the second version on this non-local correlation functional (vdW-DF2)³⁵. The original vdW-DF and vdW-DF2 functionals had been considered at first as well, but they were discarded due to their poor description of the lattice parameter of Pt metal. The optB88-vdW¹³ functional was also tested but its poor numerical stability to describe surfaces limited its usefulness and we did not pursue these tests further. In addition to these non-local correlation functionals, we also considered the PBE-dDsC functional^{36,37} which represents here the family of a posteriori corrections where a vdW term is added on top of a GGA functional, PBE in this case. In PBE-dDsC, van der Waals interactions are calculated from an atom pair wise dispersion correction, damped in the short-range where the parent density functional provides a reasonable description. The atom pair specific parameters (dispersion coefficients and short range damping strength) are determined from the electron density. This dispersion correction has not, so far, been tested for molecular adsorption on metal surfaces.

These five exchange-correlation functionals (PBE, optPBE-vdW, optB86b-vdW, BEEF-vdW and PBE-dDsC) were considered on the complete selected set of adsorbates. In the specific case on benzene, and in order to broaden the discussion, the optB88-vdW non-local functional was also added, together with two well tested representatives of the a posteriori dispersion correction: Grimme's PBE-D3³⁸ (with zero or BJ damping³⁹) and Tkatchenko and Scheffler's PBE-TS⁴⁰ (standard or with self-consistent screening, SCS⁴¹).

After the computational details we will present the geometries adopted by the various systems and discuss the influence of the functional on the electronic structure in these systems, before rationalizing trends in adsorption energies and analyzing the performance of the various approximations for the adsorption energies with respect to ex-

perimental data.

3.2 Computational details

The calculations were performed within the density functional theory (DFT) framework using the Vienna Ab Initio Simulation Package (VASP) which achieves periodic calculations based on a plane-wave basis set. The projector augmented wave (PAW) method is used to describe the electron-ion interaction, with an automatic optimization of the real-space projection operators. The Pt atom was described with 10 electrons in the valence. The basis set cutoff was set to 400 eV. The precision setting of VASP is set to "normal" and the wave function convergence threshold was set to 10^{-6} eV. The atom pair wise dispersion correction dDsC was implemented in VASP 5.3.5, as an extension of the vdW-TS implementation by Tomas Bucko.⁴² The results were validated against previous implementations for molecules. For atoms separated by more than a unit cell, we took their overlap, which determines a part of the short range damping, to be zero. The implemented gradients are purely "classical", i.e., they neglect derivatives due to changes in the electron distribution, as is customary in such approaches and has been validated recently for dDsC.⁴³

The Pt(111) surfaces were modeled by a two-dimensional slab in a three dimensional periodic cell generated by introducing a vacuum spacing in the direction perpendicular to the surface (12 Å). The coverage (θ) given in monolayers (ML) is defined by the ratio of the number of molecules adsorbed on the surface and the number of Pt atom from the surface. The geometry of all molecules except naphthalene were optimized on Pt(111) using a (3×3) super-cell, hence giving a coverage of 1/9 ML. Naphthalene was chemisorbed on a (4×4) super-cell i.e. with a coverage of 1/16 ML. The slab was six layer thick. A $7 \times 7 \times 1$ Monkhorst-Pack grid was used to sample the Brillouin-zone together with a second-order Methfessel-Paxton smearing of 0.2 eV. The geometric

optimizations were carried out allowing the entire molecules and the uppermost two layers of the metallic surface to relax with a force criterion of 0.01 eV/Å; the other layers were kept fixed in the bulk geometry. For the PBE-dDsC functional, while the geometry optimization was converged to the same accuracy as for the other functionals (0.01 eV/Å), a value of 0.02 eV/Å would be more realistic considering the approximate nature of the gradients and the accuracy of the numerical integration, defined by the FFT grid. For each system the convergence of the adsorption energy with respect to the thickness of the slab and the Monkhorst-Pack grid was tested to determine the most accurate and computationally efficient set up, with respect to the convergence criteria on the adsorption energy fixed at 0.01 eV (see Supporting Informations).

The Pt-Pt distance was optimized from Pt bulk calculation for each functional and was used for the frozen part of the slab. The Pt-Pt distance is 2.814 Å in the case of PBE, 2.806 Å for PBE-dDsC, 2.821 Å for optPBE-vdW, 2.793 Å for optB86b-vdW and 2.829 Å for BEEF-vdW.

The adsorption energy (E_{ads}) corresponds to the difference between the energy of the molecule adsorbed on the slab of Pt ($E_{mol+slab}$) and the sum of the free slab (E_{slab}) and the gas phase molecule (E_{mol}) energies:

$$E_{ads} = -(E_{mol+slab} - E_{slab} - E_{mol}) \quad (3.1)$$

3.3 Results and discussion

3.3.1 Structures

As just underlined, the five selected exchange correlation functionals give a similar value for the bulk atomic distance of Pt, with an overestimation with respect to experimental value of 2.77 Å ranging from 0.8 % (optB86b-vdW) to 2 % (BEEF-vdW). The Pt cohesive energy varies more. PBE underestimates it by 0.32 eV (−60 %) and PBE-

dDsC gives a small additional vdW contribution and hence a smaller underestimation (by 0.25 eV, -4%). The three non-local vdW functionals give, in contrast, a slight overestimation by the same amount (ca -0.35 eV, $+6\%$).

Each molecule can be adsorbed with several potential modes on Pt(111). For cyclohexene, butadiene and benzene, we checked in detail that the most stable adsorption mode remained unchanged for the five functionals considered (see Appendix C). For the other adsorbates we hence used the adsorption mode determined with PBE in the literature. The only exception is CO, which is considered in the experimental top site (and not in the optimal PBE fcc site) to better compare with recent studies that constrain the molecule on this top site.

The different structures for the associatively or dissociatively chemisorbed molecules are presented in Figure 3.3.1, while characteristic atomic distances and coordinates are given in the Appendix C. The main result of these geometry optimizations is that the vdW functionals tested give very similar geometries compared to PBE, with almost unmodified bond distances for chemisorption, while physisorbed systems (methane and ethane) show differences up to 0.4 \AA for optB86b-vdW (see Appendix C).

The most stable adsorption configuration of mono-olefins (ethylene, butene and cyclohexene) is known to be $\text{di}\sigma$, from experimental and computational studies with GGA functionals (Figure 3.3.1-a, c and d).^{44,45,2} Atomic coordinates are only slightly modified when changing the functional. For example with ethylene the Pt-C bond distance only varies by $+0.017/-0.003 \text{ \AA}$ compared to the PBE values and the C-C bond distance by $\pm 0.002 \text{ \AA}$ (see Appendix C). As already indicated, ethene does not stay intact upon adsorption on Pt(111) and is transformed at room temperature to ethylidyne CCH_3 , bound vertically at a fcc hollow site and H a neighboring site (corresponding to the preferential site given by the functional). Thus, the first species seen by SCAC at room temperature is not $\text{di}\sigma$ ethylene but the co-adsorption between ethylidyne and hydrogen which is shown in Figure 3.3.1-b. With butene (Figure 3.3.1-c) and cyclohexene (Figure 3.3.1-

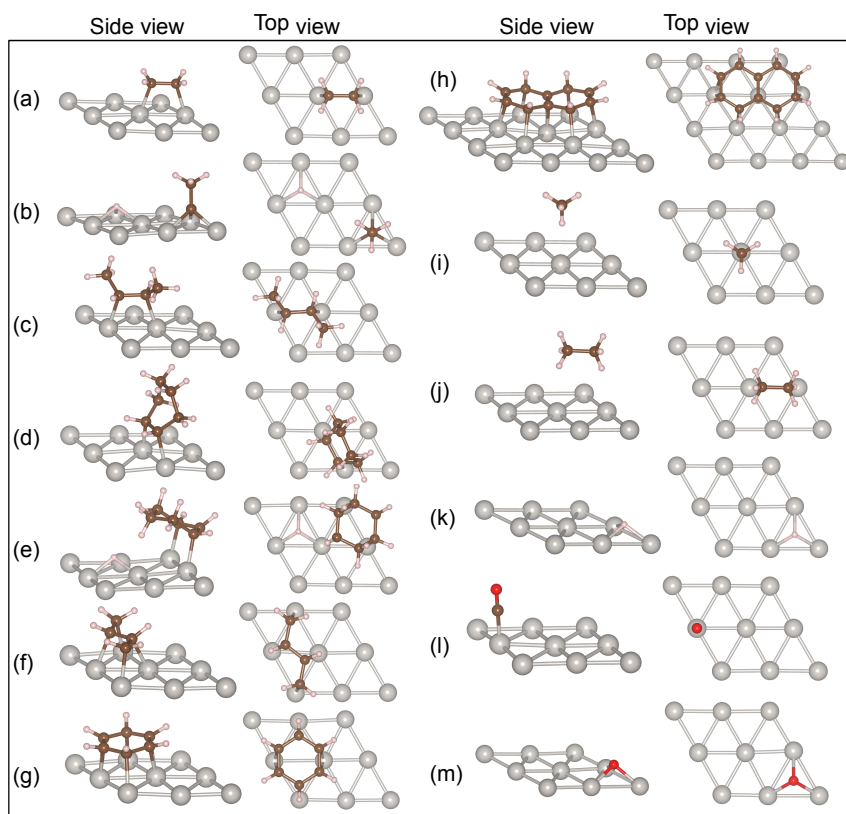


Figure 3.1: Side view and top view of the adsorption geometry on Pt(111) for a: ethylene C_2H_4 , b: ethynylidyne CCH_3 and one H, c: butene C_4H_8 , d: cyclohexene C_6H_{10} , e: C_6H_9 and one H, f: butadiene C_4H_6 , g: benzene C_6H_6 , h: naphthalene $C_{10}H_8$, i: methane CH_4 , j: ethane C_2H_6 , k: H atom, in fcc position, l: CO, m: O atom

d), an intact $d\sigma$ molecular chemisorption is found at low temperature.^{39,46} Cyclohexene shows four $d\sigma$ geometries, depending on the configuration of the cycle and its position with respect to the surface. Energy differences between these configurations are small (total range is 0.05-0.13 eV depending on the functional) and the most stable one is the “boat up” configuration, even if the chair cis configuration is very close with PBE and iso-energetic for BEEF-vdW (see Appendix C). At 281 K cyclohexene dehydrogenates and forms 2-cyclohexenyl (noted c-C₆H₉) and co-adsorbed H (Figure 3.3.1-e).³² Polyunsaturated hydrocarbons in our set start with butadiene. This molecule is found in the tetra σ conformation for all functionals (Figure 3.3.1-f) in agreement with experiments at room temperature and previous calculations.^{10,47-50} Benzene is the prototype aromatic molecule and its adsorption on Pt(111) was vastly studied experimentally as well as theoretically. With all selected functionals, the most stable geometry on Pt(111) is the bridge-30° site (Figure 3.3.1-g) in agreement with all previously published calculations.^{1,2,51-55} The second most stable form (hcp-0°) is significantly less stable whatever the functional (by at least 0.3 eV). The chemisorption structure of benzene on Pt(111) was studied by diffuse LEED.⁵⁶ Among the structures explored by LEED, bridge-0° (rotated by 30° versus Figure 3.3.1-g)) (resp. bridge-30°) gave a R-factor of 0.05 (resp 0.08). These values of R factor are both very small and indicate a good match.¹

The adsorption mode of naphthalene was shown by GGA calculations to be the double

¹The authors argued that the accuracy in the R-factor was good enough to conclude that bridge-0° is the optimum structure and that bridge-30° can be discarded. All published DFT calculations (whatever the functional) indicate that the bridge-0° structure is 0.6-0.7 eV less stable than the bri-30° one. Such a difference is markedly beyond the error bar. In addition the bond distances obtained by LEED and DFT agree well for the bridge-30° minimum (exp: Pt-C= 2.18 ± 0.02 Å, C-C= 1.39 ± 0.1 Å; DFT: Pt-C= 2.18, C-C= 1.44-1.48 Å), while those of the bridge-0° minimum do not agree especially Pt-C and C-C₂ (exp: Pt-C= 2.02 ± 0.02 Å, C-C₁ = 1.45 ± 0.1 Å; DFT: Pt-C= 2.15 Å, C-C₁ = 1.46 Å, C-C₂ = 1.40 Å). All this tends to the conclusion that the LEED assignment was incorrect, and the bri-30° is in fact the true structure.

bridge-30°, geometry which was selected here (Figure 3.3.1-h).⁵⁷ Methane and ethane were also considered, mainly for discussion purpose. Methane was placed on the top site and ethane on a pseudo di-top (or bridge) site. We found the staggered adsorption mode to be the most stable for ethane, compared to the eclipsed modes. Finally, H, CO and O were considered as references, and in relation with other published benchmarks on small adsorbates. O and H are at the fcc hollow site, although with optPBE-vdW and BEF-vdW the on top H geometry for H can be marginally more stable than the fcc site (by 0.04 and 0.03 eV respectively, see Appendix C).

3.3.2 Binding mode and electronic structure

In this section, we analyse the Kohn-Sham orbitals in order to determine if the covalent part of the bond is affected by the choice of the functional. The first point that we have underlined already is that the geometry of the adsorbates are markedly distorted compared to their gas phase structure, with the CH bond bent away from the surface. The resulting mixing of σ and π molecular orbitals provides orbitals that have a good energy match and a strong overlap with the Pt surface. These molecular deformations are very similar for the five selected functionals, already an indication that the covalent orbital mixing is of similar nature and magnitude. In order to confirm this, we plot in Figure 3.2 the density of states projected on the pz orbitals of carbon for ethylene and benzene adsorbed on the Pt(111) surface. In each plot two functionals are considered: PBE and optPBE-vdW.

The molecular orbitals of the deformed ethylene and benzene strongly mix with the d band of Pt, resulting in a continuous density of state, even if only the pz component on the carbon is considered here in the projection. The main and clear result is that the projected DOS are nearly identical for the two considered functionals, so that the covalent part of the surface-molecule bond is identical, in agreement with the quasi-identical geometries. Hence, although this might seem surprising at first sight, the difference in

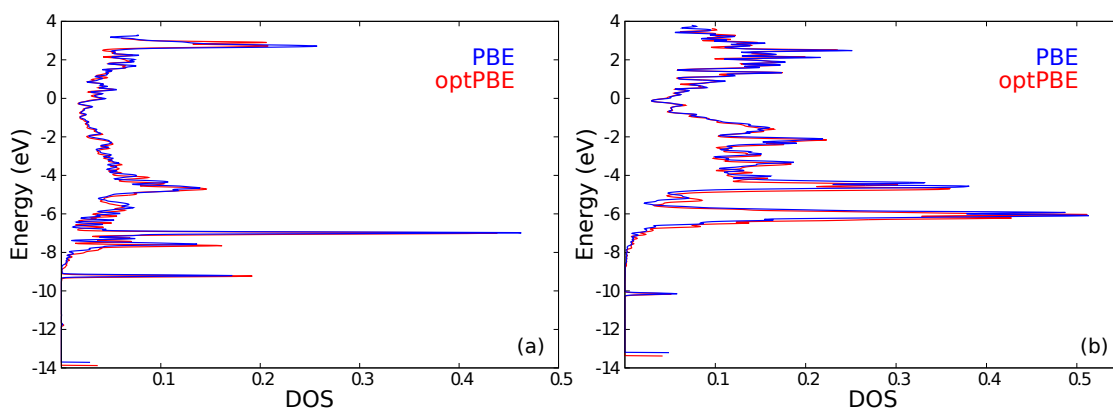


Figure 3.2: Density of state projected on the carbon p_z orbitals for: a) ethylene, b) benzene, adsorbed on Pt(111). The z direction is perpendicular to the surface. In each case the result for the PBE functional (resp. optPBE-vdW) is shown in red (resp blue)

the two functionals, semi-local PBE and non-local optPBE-vdW is solely focused on the dispersion energy term. This justifies the analogy between optPBE-vdW and PBE-dDsC results for interpretative purposes (vide infra). Indeed, in the case of PBE-dDsC, for a given geometry, the electronic density is strictly that of PBE.

3.3.3 Experimental adsorption energies

The estimation of the experimental adsorption energy value to be compared with our calculations deserves some comments, since the differential heat of adsorption might strongly depend on the coverage. In most cases, the evolution of the differential heat of adsorption has been given as a quadratic function of the coverage. This function was integrated from 0 to $1/9$ ML to obtain the integral heat of adsorption. This integrated heat of adsorption is the energy difference between the bare surface and that covered with $1/9$ ML of adsorbates, which corresponds to the calculated data. Note that here $1/9$ ML is defined by one molecule (or atom for H and O) for nine surface Pt atoms. In the case of ethylidene, H, CO and O, where no coverage dependent fit is given the

integral was performed graphically. A word of caution must be given for ethylidyne, O and CO where published calorimetric data are incorrect, due to a wrong value used for the reflectivity of Pt(111). Accordingly, all values have been scaled by 0.7059.⁵⁸ This experimental set is gathered in Table C.1 in Appendix C.

One should underline here that although the coverage has been carefully matched between experiment and theory, the specific molecular arrangement on the Pt(111) surface might differ in some cases. At the low coverage considered here, these different configurations should not affect strongly the chemisorption energy.

3.3.4 Adsorption energies - General performance

The chemisorption energies for the selected molecules and exchange correlation functionals are summarized in Figure 3.3. The microcalorimetry data is also indicated when available. In order to compare with the experimental value, we use the convention where positive energy corresponds to a stabilizing adsorption. In the case of the BEEF-vdW functional, the statistical error bar is also indicated. The difference between the calculated and the experimental value when available is reported in Figure 3.3-b and the general performance of each functional in predicting the experimental adsorption energy is quantified by the Mean Absolute Deviation (MAD), the Mean Absolute Percentage Deviation (MAPD) and the maximal deviation (MAX) in Table 3.1. PBE is a widely used exchange correlation function but nevertheless, calculated adsorption energies range between 8 % and 141 % of the experimental data. Vdw-bonded systems (methane, ethane) are strongly under-bound (8-10 % of the experimental adsorption energy). For unsaturated hydrocarbons, the situation is contrasted. When laterally π -bonded, their PBE adsorption energy represents between 50 and 70 % of the experimental adsorption energy. In contrast σ -bonded molecules like CO or ethylidyne are markedly over-bound (by ca 30 %). Note that the simple case of H (referenced to $\frac{1}{2}$ H₂ in gas phase) gives an over-binding of 41 % (although this is only by 0.15 eV in absolute value). On the

complete set, the MAPD for PBE is 45 %, and a remarkably high maximum error of 1.28 eV is obtained for naphthalene.

Let us now see how the vdW functionals modify the picture. Clearly, chemisorption energies strongly differ between the various functionals, up to 2 eV for the larger naphthalene molecule, and already 0.7 eV for ethylene, which represent a very large fraction of the adsorption energy. As expected, the results with the GGA PBE strongly differ from that of vdW functionals. However, the three vdW-functionals also provide very different results. These large variations show that the choice of the exchange part of the functional is crucial in the case of those molecules. This is a concern for the accuracy of DFT calculations since each functional has been fitted, so that more similar values could have been expected. A rigorous comparison with experiment is clearly needed. If we now consider the average deviation from the experiments on the complete test set, we see in Table 3.1 that the best performing functional is optPBE-vdW (MAE 0.2 eV), followed by PBE-dDsC and BEEF-vdW. The best functionals allow us to divide by two the mean error of PBE, although the situation is not perfect, with a MAX error of about 0.5 eV in the worst case. Another aspect is that the statistical error bar for the BEEF-vdW functional can be very large (up to 2 eV for naphthalene) and thus hardly helpful to compare with experimental data.

This global behavior can be nuanced depending on the type of molecules under consideration. For instance, since PBE is sometimes over-bound, the addition of vdW terms in PBE+D type functionals, necessarily stabilizing, does not always yield an improvement with respect to experimental data. For H, ethylidyne, CO and O, PBE-dDsC (and any other functional of that type) deviates even further from experiments than PBE. Then, if we focus on the chemisorbed unsaturated molecules, in absolute value, the chemisorption energies are generally in the order $\text{PBE} = \text{BEEF-vdW} < \text{optPBE-vdW} = \text{PBE-dDsC} < \text{optB86b-vdW}$. The results with BEEF-vdW are more or less similar to the PBE results for the unsaturated molecules despite the inclusion of vdW inter-

actions. One also notices that the PBE-dDsC and optPBE-vdW functionals, although based on a very different approach, give similar adsorption energies (with a maximum difference of 0.25 eV for naphthalene, a case where PBE and optB86b-VdW differ by 2 eV).

3.3.5 Adsorption energies – Performance for each family

Let us now discuss these energy results in more details molecule by molecule, to rationalize the performance of the various functionals under consideration. For interpretation purposes, the fraction of vdW in the adsorption energy of each molecule is provided in Figure 3.4, as obtained with the PBE-dDsC functional.

Basic Fragments

We will start this analysis with the small adsorbates H, CO and O. H shows a small range of change in adsorption energy between functionals. The hcp hollow and top sites are close in energy, and even if for some vdW functionals the top site becomes slightly more stable than the hollow site, we have kept the H atom of the hollow site in this study. For CO, the adsorption energy is markedly overestimated, as well known in the literature. BEEF-vdW decreases this over-binding but it still remains at 15 %. For O, the behavior is rather similar, BEEF-vdW being the best functional at predicting its adsorption energy from $\frac{1}{2}$ O₂.

Saturated hydrocarbons

The cases of methane and ethane contrast with that of the unsaturated molecules (vide infra). PBE gives a weak physisorption (almost absent) while vdW functionals provide a net binding, which is the expected behavior since physisorption is mainly arising through vdW dispersion interactions. optPBE-vdW and optB86b-vdW give similar values, while BEEF-vdW shows a somewhat more moderate adsorption, the experimental

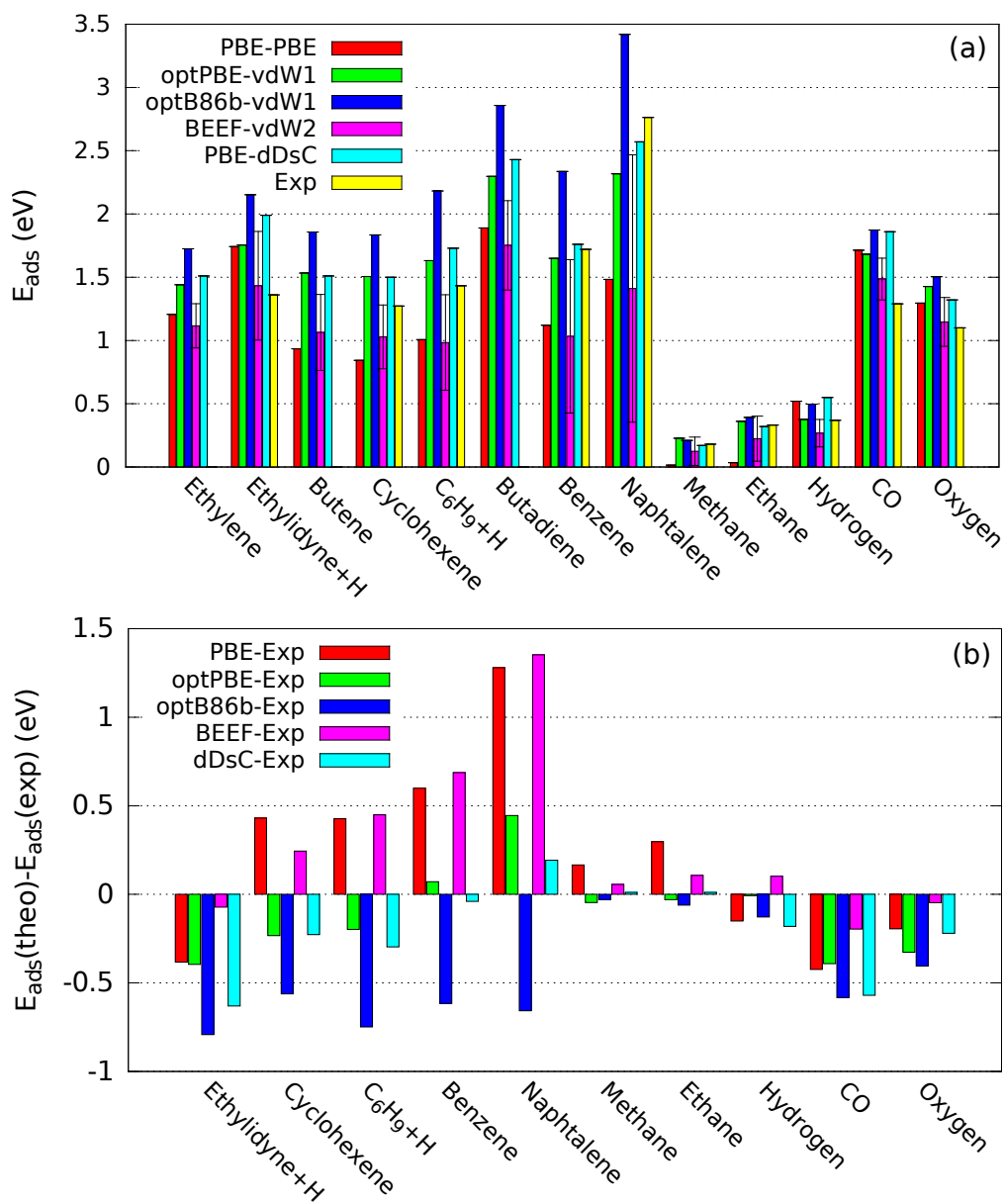


Figure 3.3: (a) Adsorption energy (eV) on Pt(111) at 1/9 ML for the considered systems, calculated with the five considered functionals. The experimental value (see text for evaluation method) is indicated in yellow when available. (b) Deviation of the studied systems on Pt(111) for the five considered functionals

result being in between these values. One can memorize for the following that the vdW interaction between a CH₃ fragment in ethane and the Pt surface is 0.15 eV.

Unsaturated hydrocarbons

The simplest unsaturated molecule is ethylene, and when chemisorbed intact in a di σ mode, one finds, compared to PBE, a marked increase of the energy with vdW functionals (by about 0.23 eV with optPBE-vdW, about 0.3 eV with PBE-dDsC and about 0.5 with optB86b-vdW). BEEF-vdW however, as noted in a general way, provides a smaller adsorption energy value, even smaller than PBE, due to a more repulsive exchange contribution. This form of ethylene is not seen in the experiment at room temperature, since the molecule transforms into ethylidyne plus H. This process is calculated to be exothermic by all functionals (by 0.3-0.5 eV). The influence of the vdW non-local functional on the overall energy of the ethylene dissociative chemisorption in ethylidyne plus H is markedly reduced compared to the flat di σ molecular form (for example the optPBE-vdW energy is almost identical to the PBE value, and BEEF-vdW yields an adsorption energy smaller than PBE by 0.3 eV). The reduction of the dispersion contribution is smaller for the semi-empirical PBE-dDsC functional (only 0.05 eV see Figure 3.3). The behavior of non-local functionals can be explained by two reasons: first since the molecule is standing up, vdW interactions with the surface should be smaller, second the H atom on the surface shows a slightly weaker adsorption energy with vdW functionals (especially with optPBE-vdW: 0.4 eV versus PBE: 0.54 eV). Compared to the experimental value (1.36 eV)², the formation energy of CCH₃ plus H on the surface from C₂H₄ in gas phase appears overestimated by 0.07 eV (BEEF-vdW) to 0.8 eV (optB86b-

²The evaluation of the experimental heat of adsorption requires a comment. We started from Figure 27 of ref 13 which shows the coverage dependent heat of adsorption. The differential heat of adsorption was integrated between zero and 1/9 ML yielding a value of about 185 kJ.mol⁻¹. This value is however incorrect as recognized recently by C. T. Campbell, due to an error in the reflectivity of Pt. A correction of 0.7588 must be applied giving 131 kJ.mol⁻¹ i.e 1.36 eV.

Functional	PBE	optPBE-vdW	optB86b-vdW	BEEF-vdW	PBE-dDsC
MAD (eV)	0.44	0.21	0.46	0.33	0.24
MAPD	45%	18%	37%	25%	23%
MAX (eV)	1.28	0.45	0.79	1.39	0.57

Table 3.1: Overall performance of each functional in predicting the experimental adsorption energy on Pt(111) of a set of selected molecules quantified by the Mean Average Deviation (MAD), the Mean Absolute Percentage Deviation (MAPD) and the maximal deviation (MAX)

vdW). The difference between the calculated and the experimental adsorption energy is graphically shown on Figure 3.3-b.

Going to butene and cyclohexene includes the influence of alkyl substituents on the double bond and of strain from the cyclic form for cyclohexene. Intact chemisorption in the $di\sigma$ mode is first considered for cyclohexene, which is the case for temperatures below 281 K. The PBE adsorption energy shows a marked decrease compared to $di\sigma$ ethylene by up to 0.36 eV for cyclohexene, which can be related to an additional Pauli repulsion between the alkyl substituent and the surface. BEEF-vdW follows this trend with a smaller reduction of adsorption energy (0.1 eV for cyclohexene). In contrast, optPBE-vdW and optB86b-vdW compensate the effect, presumably by an increase of the vdW part of the adsorption from the presence of the alkyl groups. PBE-dDsC shows an accidentally perfect compensation, between the decrease of the PBE exchange-correlation energy component and the additional vdW(dDsC) contribution, with ethylene, butadiene butene and cyclohexene at the same adsorption energy of 1.5 eV. As seen on Figure 3.4, the vdW contribution is roughly doubled between ethylene (0.33 eV) and cyclohexene (0.68 eV) or butene (0.61 eV) and the difference corresponds approximately to the vdW contribution of an ethane molecule (0.28 eV).

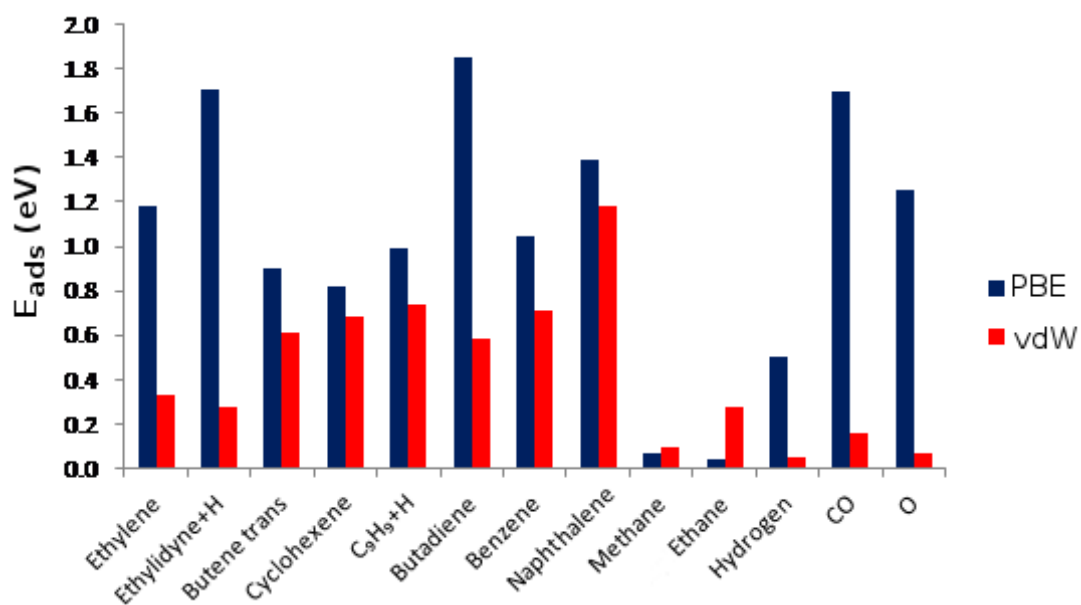


Figure 3.4: Contribution of PBE and the dispersion correction dDsC (denoted as vdW) to the adsorption energy of PBE-dDsC

For the non-local functional, the decomposition of the dispersion component is not straight forward, but one can estimate the effect from methane and ethane physisorption energy. The differential adsorption energy between butene and ethylene amounts to -0.27 , $+0.09$, $+0.13$, -0.05 eV for PBE, optPBE-vdW, optB86b-vdW and BEEF-vdW respectively. Hence the difference between vdW functionals and PBE is $+0.36$, $+0.4$ and $+0.22$ eV for optPBE-vdW, optB86b-vdW and BEEF-vdW, respectively. This value represent the vdW interaction brought by the two substituents on the C=C double bond. This matches well the adsorption energy of ethane (0.36 , 0.39 and 0.22 eV for optPBE-vdW, optB86b-vdW and BEEF-vdW, respectively). Hence when moving from ethylene to butene, the direct chemisorption of the double bond is weakened by 0.27 eV (as seen from the PBE results) but an additional vdW interaction is brought by the two alkyl substituents, which is equivalent to that of the two methyl groups of ethane.

The case of cyclohexene is similar, with a stronger decrease of the direct interaction of the double bond, which can be traced to the constraint of the cycle, and a larger stabilizing effect from vdW contribution of the longer saturated chain. Cyclohexene adsorbs intact at low temperature (100 K) and microcalorimetry gives an accurate coverage dependent heat of adsorption.³² After integration of the data from zero to $1/9$ ML, an adsorption energy value of 1.273 eV is obtained. Compared to this value (Figure 3.3-b), the PBE and the BEEF-vdW calculated adsorption energy are underestimated, while optPBE-vdW, PBE-dDsC and optB86b-vdW overestimate this energy, opt-PBE-vdW and PBE-dDsC giving the best compromise. At temperature above 281 K, cyclohexene looses one H atom that goes on the surface, and microcalorimetry shows that this surface reaction is exothermic by 0.16 eV at $1/9$ ML coverage on Pt(111).³² All functionals give an exothermic transformation, with a value ranging from 0.12 eV (optPBE-vdW) to 0.35 eV (optB86b-vdW), except for BEEF-vdW for which the process is endothermic by 0.05 eV. optPBE-vdW provides the best match with the experimental heat of adsorption for this dissociative adsorption of cyclohexene starting from gas phase (with

1.63 eV versus 1.43 eV in the experiment).

Butadiene extends the unsaturated framework to two C=C bonds. The adsorption energy is hence clearly increased (by a factor of 1.6). The effect is not additive for the two C=C bonds because the two C=C fragments are not independent, both on an electronic (conjugation) and geometric basis. Again, the vdW functional give a contrasted result in comparison with PBE, with a net decrease of the adsorption for BEEF-vdW, and an increase for other functionals, an effect that is amplified compared to case of ethylene. However no experimental data is, unfortunately, available for butadiene.

Aromatics

An interesting case is that of the aromatic benzene molecule, and accurate microcalorimetry data is available.⁵⁹ Benzene does not follow the trend of butadiene, since with six carbon atoms in the unsaturated molecule, its PBE adsorption energy is lower than that of ethylene. It is obvious, however, that benzene is electronically and geometrically very far from the superposition of three ethylene molecules. BEEF-vdW provides a value very similar to PBE, while again a marked increase is found for optPBE-vdW (by 0.47 eV), PBE-dDsC (by 0.64 eV) and optB86b-vdW (by 1.2 eV). The vdW contribution, as evaluated by dDsC, is 0.71 eV, remarkably large compared to the PBE adsorption energy (63 % of it). This surprisingly large influence of dispersion for a strongly chemisorbed molecule like benzene was already underlined using the PBE+vdWsurf approach, where vdW interactions are calculated including the collective response of the substrate.^{49,50} There, the calculated vdW contribution was even larger, 1.15 eV ie 142 % of the PBE energy.

Since benzene on Pt(111) has been considered as a prototype situation in many recent papers, we have decided (vide supra) to extend the number of tested methods in this case, to provide a wider comparison, with the same computational parameters and the same code. The results are given in Table 3.2. The optB88-vdW appears as interme-

Method	PBE	optPBE-vdW	optB86b-vdW	BEEF-vdW	PBE-dDsC
E_{ads}	1.12	1.65	2.34	1.03	1.76
SPD	-35%	-4%	+36%	-39%	+2%

Method	optB88-vdW	PBE-D3	PBE-D3(BJ)	TS	TS with SCS
E_{ads}	1.97	2.16	2.21	2.13	2.23
SPD	+14%	+26%	+28%	+24%	+30%

Table 3.2: Adsorption energy (in eV) and the signed percentage deviation (SPD) to the experimental value (1.72 eV) for benzene at Pt(111) using various functionals

diates between optPBE-vdW and optB86b-vdW, belonging to this same family. The D3 approach, which neglects electronic effects, gives a larger vdW contribution (1.08 eV) than our dDsC correction (0.71 eV). The TS method (with or without self consistent screening) gives a similar result compared to D3, with a vdW contribution of 1.11 eV, in agreement with the previous calculation.^{49,50} The measured heat of adsorption for benzene on Pt(111) (integrated up to a coverage of 1/9ML ML) is 1.72 eV. It was already underlined that PBE calculated values are strongly underestimated with respect to the measured data (in our numbers by -0.6 eV i.e. -35 %). This is obviously even more the case for BEEF-vdW (by -0.68 eV i.e. -39 %). In contrast, optPBE-vdW and PBE-dDsC give an excellent agreement (error -4 % and +2 % respectively), while optB88-vdW and optB86b-vdW more or less severely overestimates the value (+0.25 eV i.e. +14 % and +0.61 eV i.e. +36 %, resp.). The D3 or TS approaches also overestimate the adsorption energy (by ca 25 %).

The largest molecule considered in the set is naphthalene, which condenses two benzene rings in a C10 fused ring system. The relative increase in the adsorption energy from benzene to naphthalene is somewhat functional dependent (32 %, 41 %, 47 %, 36 % and 46 % for PBE, optPBE-vdW, optB86b-vdW, BEEF-vdW and PBE-dDsC respectively)

and is smaller than the relative increase in the number of sp² carbons (66 %). If we now compare with the experimental heat of adsorption, errors are large. PBE and BEEF-vdW almost underestimate the energy by 50 %, and the best result is for PBE-dDsC with an underestimation of 6 %.

3.4 Conclusion

Single crystal adsorption calorimetry has brought us in the recent years a detailed knowledge of the chemisorption energy of molecules on single crystal metal surfaces, as a function of coverage. From this chemisorption energy database, five exchange correlation functionals of different type have been benchmarked in this study. The focus was set on unsaturated hydrocarbons (ethylene, butene, butadiene, benzene, ...) but other simple molecules were also included (CO, O₂, H₂, methane, ethane). If the functionals used provide very similar geometries, and electronic structure as shown by projected density of states, they give strikingly different results for the adsorption energy of unsaturated molecules on Pt(111). The range of calculated adsorption energies is already 0.52 eV for ethylene (BEEF-vdW: 1.12 eV, optB6b-vdW: 1.72 eV) and reaches 1.3 eV for benzene and 2 eV for naphthalene. Such a range of values produced by different functionals is an important fundamental concern and hence great care should be taken for the choice of the functional when modelling processes that depend on chemisorption energy, such as surface coverage, surface reactivity or desorption. Naturally the average deviation between the experimental and the calculated chemisorption energies also strongly depends on the chosen functional. The lowest MAD are obtained with optPBE-vdW and PBE-dDsC (about 0.2 eV) while PBE and optB86b-vdW give twice larger MAD (about 0.45 eV). BEEF-vdW is intermediate with a MAD of 0.33 eV. It is important to underline that “similar” exchange correlation functionals as optPBE-vdW and optB86b-vdW, can yield very different results for the adsorption energy, with for

example a difference of 0.7 eV (i.e. 40 % of the value) for benzene on Pt(111). The adsorption of these molecules indeed results from a compromise between stabilizing and destabilizing interactions. Stabilizing interactions are developed between occupied (resp. vacant) orbitals of the molecules and vacant (resp. occupied) states of the surface, while the interactions between occupied states on both partners lead to destabilizing Pauli interactions. The accurate tuning of exchange and correlation appears crucial for the correct description of this competition and of its consequence on the chemisorption energy compromise. The behaviour of the functionals depends on the type of molecules. For laterally π -bound unsaturated hydrocarbons (cyclohexene, benzene, naphthalene) the GGA PBE functional is severely under-bound, vdW contributions are large and provide a good match with experiments for opt-PBE-vdW and PBE-dDsC, optB86b-vdW being markedly over-bound. BEEF-vdW incorporates a much less repulsive exchange functional so that altogether the adsorption energies are close to PBE, and hence strongly underestimated compared to experiment. Cyclohexene provides data for a surface reaction (first dehydrogenation) and again optPBE-vdW and PBE-dDsC are most accurate for the description of the reaction energy. An extended range of functionals has been tested in the case of benzene on Pt(111), with popular PBE-D3 and PBE-TS. These tend to overestimate the adsorption energy by about 0.4-0.5 eV and hence are less accurate than optPBE-vdW or PBE-dDsC. Vertically bound ethynyl and CO behave differently. They are in contrast over-bound to Pt(111) with PBE. vdW contributions are small and the adsorption energy remains overestimated with the vdW functionals, except for BEEF-vdW that benefits from its less repulsive exchange and provides the best match with experiments.

Based on the existing literature on the general performance and the herein presented benchmarking on adsorption energies, we recommend the use of optPBE-vdW or PBE-dDsC instead of the typical choice of PBE for unsaturated hydrocarbon adsorption and reactivity on Pt(111). These functionals however overestimate CO adsorption by at least

0.4 eV, so that the computational study of co-adsorption and reactivity between unsaturated hydrocarbons and CO remains a challenging task, with no ideal DFT functional seen in this study. The same comment applies for reaction pathways that include both π -bound unsaturated hydrocarbons and upright ethynylidyne. Considering surface coverage, the DFT functionals yield a good behaviour for its influence on adsorption energy⁵⁸, so that the results of this study are expected to remain valid at a different coverage from the value considered here (1/9 ML). For other surfaces of Pt or other metals, very few calorimetric data are available for hydrocarbon molecules. One might expect a similar accuracy of these functionals for sites of metallic coordination close to 9 ((100) surface, steps) for late transition metals. It would be important to harvest experimental data on these systems to check this point in more details. In addition, as underlined earlier, none of the tested exchange-correlation functional is accurate in all cases, so that the search of novel functionals/methods remains an important quest.

Chapter 4

Hydrogen adsorption and coverage dependency on Pt(111) and Sn/Pt-Pt(111)

Contents

4.1	Introduction	56
4.2	Computational details	57
4.2.1	DFT calculations	57
4.2.2	Thermodynamic model	60
4.3	Pt(111): results and discussion	61
4.3.1	Adsorption energy	61
4.3.2	Adsorption structures	66
4.3.3	Electronic structure	68
4.4	Sn/Pt-Pt(111): results and discussion	69
4.4.1	Adsorption energy	69

4.4.2	Adsorption structures	73
4.4.3	Electronic structure	74
4.5	Conclusion	76

4.1 Introduction

Hydrogen has been studied over time since it is involved in many reactions occurring in different fields of chemistry such as fine chemicals production, perfume chemistry and pharmacology.⁶⁰⁻⁶³ Due to its important role in petrochemistry and food industry,¹⁻⁴ hydrogenation has been deeply investigated both experimentally and theoretically.^{64,65} Experimental studies⁶⁶⁻⁶⁸ carried out on close-packed (111) coinage metals in UHV conditions aim at determining the preferential adsorption sites of hydrogen as well as its adsorption energy and give spectroscopic insights on hydrogen adsorption. Theoretical studies Legaré⁶⁹ on Pt(111) and Chizallet et al⁷⁰ on Pd(111) showed in their theoretical studies of hydrogen adsorption that temperature and pressure are two important parameters that need to be taken into account because of their effects on the coverage. This matter is of great importance for hydrogenation reactions as they are carried out under pressure of hydrogen (1 to 10 bar) and at normal temperatures (300-400 K)¹⁻⁴. In this work, we propose a methodology to include the coverage dependency in the theoretical study of hydrogen adsorption on Pt(111) and Sn/Pt-Pt(111) using DFT based calculations. Those two surface catalysts were chosen as they are commonly used for hydrogenation reactions, in particular the surface alloy (Sn/Pt) which has proven to be more selective.^{8,9} Fewer studies are proposed for the adsorption of hydrogen on Sn/Pt-Pt(111).⁷¹

4.2 Computational details

4.2.1 DFT calculations

The calculations were performed within the density functional theory (DFT) framework using the Vienna Ab Initio Simulation Package (VASP)^{6,7} which achieves calculations using periodic boundary conditions based on a plane-wave basis set. The projector augmented wave (PAW) method is used to describe the electron-ion interaction. The generalized gradient approximation (GGA) of Perdew, Burke and Ernzerhof (PBE)¹² has been used. The basis set cut off was set to 400 eV and a second-order Methfessel-Paxton smearing of 0.2 eV was used. A vdW-type functional was also used to compare with PBE results. We chose optPBE¹³ after a first benchmark study as it demonstrated to be accurate for the description of olefins adsorption on a platinum surface. For each system the convergence of the adsorption energy with respect to the thickness of the slab and the Monkhorst-Pack grid was tested to determine the most accurate and computationally efficient set up. The surface was modeled by a two-dimensional slab in a three dimensional periodic cell generated by introducing a vacuum width in the direction perpendicular to the surface (12 Å). The two surface catalysts Pt(111) and Sn/Pt-Pt(111) were modelled by a six-layers slab; for the surface alloy, only the uppermost layer contains tin atoms in a stoichiometry Pt₂Sn with the $(\sqrt{3} \times \sqrt{3})R30^\circ$ structure (see Figure 4.1).⁷² The geometric optimizations were carried out allowing the atoms and the uppermost two layers of the metallic surface to relax with a force criterion of 0.01 eV/Å; the other layers were kept fixed in the bulk geometry. The Pt-Pt distance was initially optimized from Pt bulk calculation. It was found to be 2.814 Å for Pt(111) and 2.821 Å for Sn/Pt-Pt(111). These distances were used for the frozen part of the two different slab.

The coverage of hydrogen (θ_H) given in monolayer (ML) is defined by the ratio of the number of hydrogen atoms adsorbed on the surface (n_H) and the number of atoms

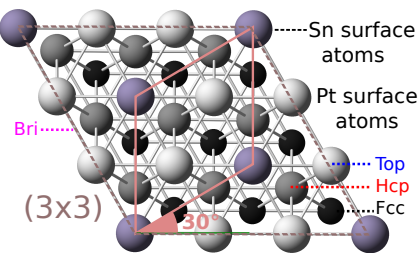


Figure 4.1: Top view of a (3×3) supercell (light brown) of a Sn/Pt-Pt(111) surface in the Pt_2Sn stoichiometry; the pink cell shows the Sn supercell $((\sqrt{3} \times \sqrt{3})R30^\circ)$ structure)

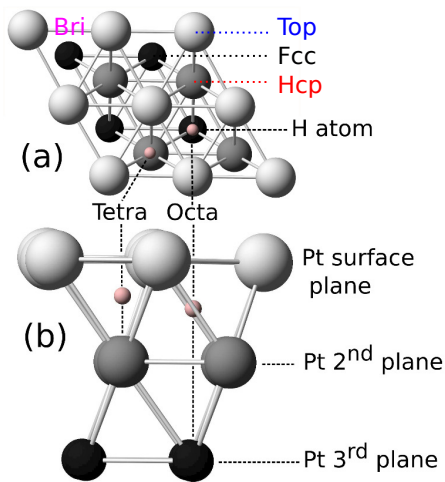


Figure 4.2: Top view of a (2×2) supercell of Pt(111) (a) and side view of the same surface (b); tetra, octa and bri are the tetrahedral, octahedral and bridge adsorption site

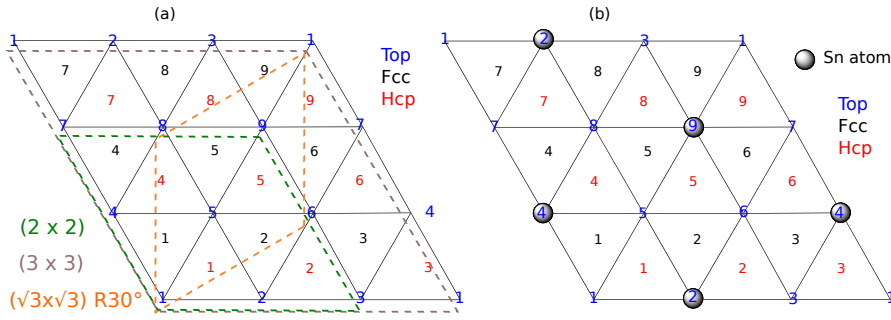


Figure 4.3: Top view of the Pt(111) surface (a) and the Sn/Pt-Pt(111) surface (b); description of the $(\sqrt{3} \times \sqrt{3})$, (2×2) and (3×3) supercells; the numbers are labels given to the different sites of the same nature existing in the (3×3) cell

from the surface ($n_{At,surf}$):

$$\theta_H = \frac{n_H}{n_{At,surf}} \quad (4.1)$$

For example, one hydrogen atom adsorbed on a (3×3) supercell corresponds to a coverage of $\theta=1/9$ ML. "At,surf" can be of different nature, depending on the surface (Pt and/or Sn atoms). In order to find the most stable adsorption configuration, we investigated all the possible configurations; hydrogen atoms can adsorb at fcc, hcp, top and bridge surface sites, but also at tetrahedral and octahedral subsurface sites (see Figure 4.2). In order to explore a large range of coverages on Pt(111), we selected three different supercells: a (2×2) , a $(\sqrt{3} \times \sqrt{3})$ and a (3×3) (see Figure 4.3). The structures were relaxed allowing hydrogen atoms to diffuse on the surface. The 2D Brillouin-zone integration was performed using a $14 \times 14 \times 1$ Monkhorst-Pack grid for the $(\sqrt{3} \times \sqrt{3})$ cell, a $9 \times 9 \times 1$ grid for the (2×2) , and finally, a $5 \times 5 \times 1$ (E_{ads} results) and $7 \times 7 \times 1$ (G_{ads} results) mesh for the (3×3) super-cell. These fine grids are needed to ensure a good accuracy and allow the correct comparison of the adsorption energy on different unit cells.

The adsorption energies (E_{ads}) were calculated at 0 K as follows:

$$E_{ads} = E_{slab+nH} - E_{slab} - \frac{n_H}{2} E_{H_2(g)} \quad (4.2)$$

with $E_{slab+nH}$ being the energy of n_H atoms of hydrogen adsorbed on the slab, E_{slab} being the energy of the slab alone and $E_{H_2(g)}$ the hydrogen gas phase energy; a negative value indicates an exothermic adsorption process.

The adsorption energy per atom (E_{ads}/at) and the differential adsorption energy (E_{ads}^{diff}) are defined as follows:

$$E_{ads}/at = \frac{E_{ads}}{n_H} \quad (4.3)$$

$$E_{ads}^{diff} = E_{ads}((n+1)_H) - E_{ads}(n_H) \quad (4.4)$$

4.2.2 Thermodynamic model

We calculated the Gibbs adsorption free energy of $H_2(g)$ within the ideal gas approximation in order to take into account the entropy of the gas phase. Using the thermodynamic model proposed in Chapter 3 we obtained for the adsorption of n_H atoms :

$$G_{ads}^{n_H}(T, P) = E_{ads}^{n_H} + k_B T \ln[(z_{trans}^{*,H} \times z_{rot}^H)^{n_H}] - n_H k_B T \ln \left[\frac{P^H}{k_B T} \right] \quad (4.5)$$

with the rotational partition functions:

$$z_{rot}(T) = \frac{1}{\sigma_r} \left(\frac{T}{\theta_r} \right) = \frac{1}{2} \left(\frac{8\pi^2 I_H k_B T}{h^2} \right) \quad (4.6)$$

and the translational partition function:

$$z_{trans}^{*,H}(T) = \left(\frac{2\pi m_H k_B T}{h^2} \right)^{3/2} \quad (4.7)$$

Each term of the above equations are given in Chapter 2.

4.3 Pt(111): results and discussion

4.3.1 Adsorption energy

The four possible adsorption sites for hydrogen on Pt(111) are two hollow sites, fcc and hcp, one top site and one bridge site. Their associated adsorption energies calculated with PBE are given in Figure 4.4-b. We can see that fcc is the most stable site at this coverage ($\theta_H = 0.25$ ML) with an adsorption energy of -0.53 eV, followed by hcp with -0.53 eV. The bridge and the top sites are slightly higher in energy with -0.52 eV. The site dependence of the adsorption energy of H on Pt(111) is hence very small with the PBE functional.

The adsorption energies of hydrogen as a function of the coverage on a $(\sqrt{3} \times \sqrt{3})$ and a (2×2) super-cell of Pt(111) are given in Table 4.1. Only the most stable adsorption site for each coverage are reported here, even though all the fcc, hcp, top, tetrahedral and octahedral site were also tested in a (2×2) cell, from 0.25 to 2 ML. The adsorption energies corresponding to those tests are given in Appendix A. PBE was used for all these calculations. In Table 4.1, we can see that fcc is the most stable site from 0.25 to 1 ML. As expected for Pt(111), no stable conformation was found implying subsurface sites (ref16). From 1 to 1.75 ML, we obtained a mix of fcc and top sites and finally, for 2 ML we found a large surface reconstruction. We also noticed that, for $\theta_H = 1.33$ ML, bridge sites were preferred over fcc sites because of symmetry reasons. From 1 to 2 ML, we obtained higher (less favorable) adsorption energies per atom because of the repulsive energy involved in a too crowded cell. None of these high coverage structures are favorable in the range of T and P that we consider. For this reason, we investigated in the following work, only the range of coverages between 0 and 1 ML. We also remark that the adsorption energy per atom decreases when increasing the coverage which illustrates the repulsive interaction between the atoms. Our results are in agreement with former studies of H on Pt^{69,70}. We can however underline that the lateral repulsion is

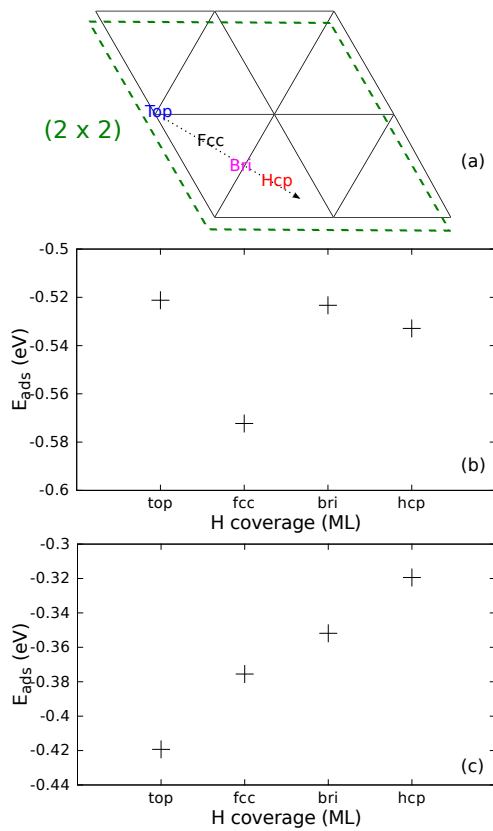


Figure 4.4: Adsorption energies of one atom of hydrogen corresponding to the four existing adsorption sites (fcc, top, hcp and bridge) in a (2×2) cell (a), calculated with PBE (b) and optPBE (c)

weak in the case of H, with a small decrease of the adsorption energy per atom between a coverage of 0.25 and 1 ML.

Using optPBE, the most stable adsorption site is the top site with 0.42 eV, followed by fcc, bridge and hcp (see Figure 4.4-c). We remark that the order of stability of the sites are changed when changing the functional although again the energy difference is small. From this conclusion, all the calculations with optPBE on Pt(111) are done with hydrogen adsorbed on top sites only. As the final aim is to co-adsorb hydrogen and butadiene, the (3×3) cell was chosen to be the best to continue this study on each surface catalysts. Indeed, it is the largest cell which provides a good compromise between calculation time and number of coverages. Moreover, it allows a quite fine study of the evolution of the adsorption energy as a function of the coverage as this cell contains nine Pt atoms, which means that the coverage will increase with steps of 0.11 ML from 0 to 1 ML.

The adsorption energies per atom (E_{ads}/at) and the differential adsorption energies (E_{ads}^{diff}) of hydrogen are given as a function of the coverage of hydrogen (θ_H) in Figure 4.5 for both functionals. We can see that E_{ads}/at varies from -0.54 to -0.46 eV in the case of PBE, while it varies from -0.42 to -0.34 eV for optPBE, both with a regular increase with respect to the coverage. We can note that the range of energy of 0.08 eV for PBE and 0.07 eV for optPBE is quite similar for both functional, and again that it is small. E_{ads}^{diff} shows a quite regular increase using PBE, with a slight jump between 0.11 and 0.22 ML and between 0.33 and 0.44 ML of about 0.03 eV for the last one. This means that the second and the fourth H atoms adsorb less easily than the other atoms. With optPBE, we observe a different behaviour of E_{ads}^{diff} with one plateau between 0.33 and 0.56 ML, and one other between 0.78 and 1 ML. We can conclude that, between the two plateau, from 0.56 to 0.78 ML, hydrogen adsorbs with more difficulty as the energy differences are larger.

The most favourable coverage for H on Pt(111) surface depends on the experimental

θ_H (ML)	Adsorption Site	E_{ads} (eV)	E_{ads}/at (eV)
0.25	1f	-0.53	-0.53
0.33	1f	-0.53	-0.53
0.50	2f	-1.02	-0.51
0.66	2f	-1.00	-0.50
0.75	3f	-1.46	-0.49
1.0	4f	-1.87	-0.47
1.25	4f-1t	-1.72	-0.34
1.33	3bri-1t	-1.36	-0.34
1.5	4f-2t	-1.68	-0.28
1.66	3f-2t	-1.14	-0.23
1.75	4f-3t	-1.32	-0.19
2.0	<i>r</i>	-1.12	-0.14

Table 4.1: Adsorption sites and adsorption energies calculated with PBE and corresponding to different coverages of H on Pt(111) for two different cells: ($\sqrt{3} \times \sqrt{3}$) and (2×2); f, h, t and bri mean fcc, hcp, top and bridge, r means surface reconstruction

conditions of T and P. Figure 4.6 shows the adsorption free energies of hydrogen (G_{ads}) as a function of the temperature. Hydrogen pressure was set to 1 bar. Each line describes one H coverage, and the most stable situation corresponds to the system with the lowest free energy. The lines are not straight because the entropy itself is a function of the temperature. With PBE, hydrogen starts to adsorb at 760 K with a coverage of 0.11 ML which increases gradually until 1 ML when decreasing the temperature until 550 K (see Figure 4.6-a). For optPBE (Figure 4.6-b), we observe a shift of the first adsorption temperature of 110 K towards lower temperatures compared to Figure 4.6-a. This is consistent with the fact that the adsorption energies calculated with optPBE are higher than those calculated with PBE, which means that hydrogen sticks less to the surface. G_{ads} ranges from 0 to -0.82 eV between 570 and 780 K for PBE and to -0.63 eV between 45 and 650 K for optPBE, for coverages from 0 ML to 1 ML. Also, using optPBE, we observe that the configurations $\theta_H = 0.33, 0.44$ and 0.78 ML are never stable as their curves are always above the others.

Figure 4.7 represents the hydrogen coverage corresponding to the most stable configuration for each couple of temperature and pressure. One can first see, for both functionals, a large beige area at relatively low pressure and high temperature which represents the (T, P) domain where hydrogen atoms do not adsorb on the surface ($\theta_H = 0$ ML). In the case of PBE (Figure 4.7-a), we observe a thin domain with different shades of orange. This corresponds to an increase of the coverage step by step when decreasing the temperature and increasing the pressure. With optPBE, the first adsorption is shifted towards lower temperatures of about 150 K and as we saw on Figure 4.6, some intermediate coverage do not exist. Indeed, one passes from 0.22 to 0.56 ML, and from 0.67 to 0.89 ML instead of having a regular increase of the coverage like in the case of PBE. It is important to underline that in the typical conditions for the hydrogenation reaction (T= 300-400 K and $P_{H_2} = 1-10$ bar), the most stable situation corresponds to $\theta_H = 1$ ML using PBE and optPBE. The structures of the configurations of 0.11 and

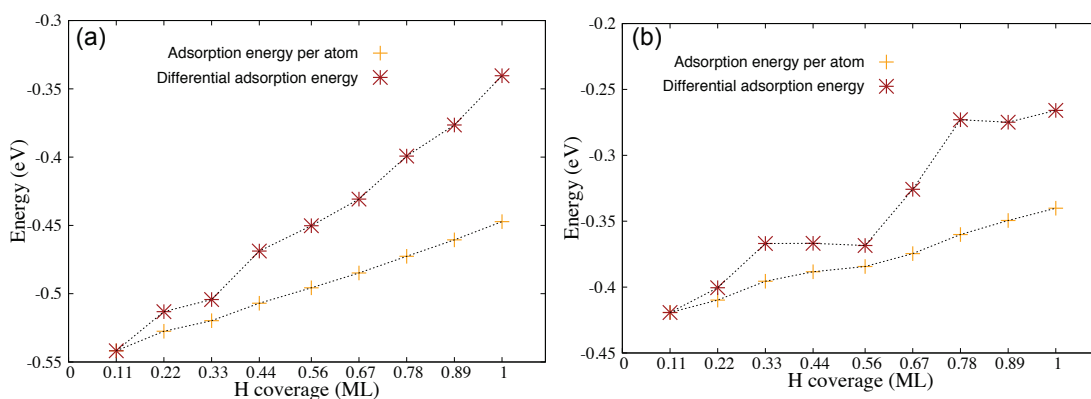


Figure 4.5: Hydrogen adsorption energy per atom (E_{ads}/at) and differential adsorption energy (E_{ads}^{diff}) as a function of the coverage on Pt(111) calculated with PBE functional (a) and optPBE functional (b)

1 ML are given in Figure 4.8 for both functionals.

4.3.2 Adsorption structures

The Figure 4.8 shows the geometric structures of the configurations corresponding to two coverages of hydrogen on Pt: 0.11 and 1 ML. Using PBE or optPBE, one observes almost no surface reconstruction when increasing the coverage from 0.11 ML to 1 ML. With PBE (Figure 4.8-a and b), the (H)-(Pt) distance (the distance between mean planes of H and Pt) is smaller at low coverage compared to high coverage (0.85 vs 0.90 Å). Indeed, nine H atom on the surface interact slightly less than one because of the repulsion between H atoms. At low coverage, we can also see a disparity in Pt-Pt distances as the bulk distance is 2.81 Å and those measured around the adsorption sites are 2.89 Å. The Pt-H interactions weakens the Pt-Pt bond for nearest neighbors. On the contrary, the 1 ML configuration provides equal distances between Pt atoms as it is highly symmetric. With optPBE, the (H)-(Pt) distance follows the same behaviour than with PBE when increasing the coverage but the effect is much weaker (Figure 4.8-c and d). One

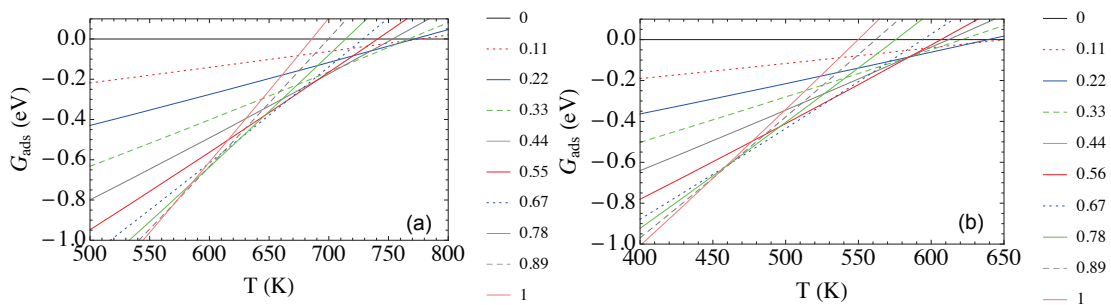


Figure 4.6: Hydrogen adsorption free energy (G_{ads}) as a function of the temperature calculated for $P_{H_2} = P_{But} = 1$ bar, on Pt(111) and for θ_H ranges between 0 and 1 ML; this was calculated with PBE (a) and optPBE (b)

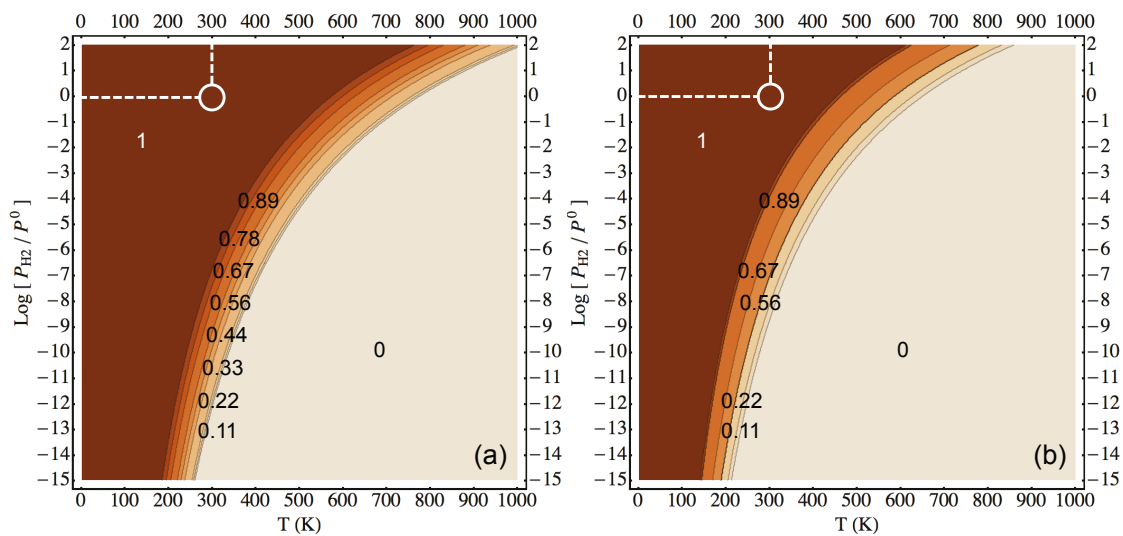


Figure 4.7: Calculated optimal hydrogen coverage given as a function of the pressure of H_2 and the temperature on Pt(111) with the PBE functional (a) and the optPBE functional (b)

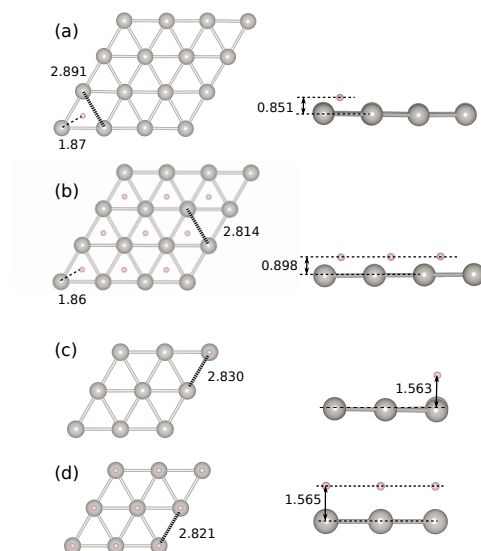


Figure 4.8: Top and side view of a Pt(111) surface covered with 0.11 and 1 ML of hydrogen, calculated with PBE (a and b) and optPBE (c and d); characteristic distances given in Å

H atom adsorbed on top site is already farther from the surface plane because of the intrinsic nature of the site. Thus, the impact on the Pt-Pt distance is very small with 2.830 Å instead of 2.821 Å in the bulk. Then, the add of more atoms on top sites causes a slight repulsion interaction between H atoms which barely extends the (Pt)-(C) distance at 1 ML.

4.3.3 Electronic structure

Only the results obtained with PBE are presented in this part.

Figure 4.9a shows the density of states (DOS) of a bare and partially covered surface of platinum ($\theta_H = 0.11\text{ML}$) projected on the orbitals of the Pt atom bonding with one H atom. We see no differences with the DOS of the bare surface except for the band

appearing at low energies (between -8.5 and -7 eV). This corresponds to the electronic states participating to the bond between H and Pt. One can note that the electronic state of Pt are only affected in this small energy interval, by a mixing between the Pt states and the H1s orbital. The rest of the Pt d band is unaffected. We also compared the DOS of the bare Pt surface to the DOS of the partially covered Pt surface projected on Pt atoms not bonding with the H atom. The comparison confirms that those atoms are not involved in the bond with hydrogen as they do not present states between -8.5 and -7 eV. Figure 4.9b represents the DOS of a bare and a fully covered surface of Pt ($\theta=1$ ML). In the DOS of the fully covered surface, the new peak between -8 and -6.5 eV is now more intense, showing a stronger covalent nature of the Pt-H bond. This peak extends now down to -10 eV. Besides, this novel peak centered on the in-phase bonding combination between H1s and Pt (and confirmed by the projection on H1s), the d band projected on the surface Pt atom is now narrower, from the increase of the distance between first and second Pt layer. This implies also a larger perturbation of the electronic states which is due to the presence of H atoms.

The DOS presented in Figure 4.9 were normalized with respect to the number of atom.

4.4 Sn/Pt-Pt(111): results and discussion

4.4.1 Adsorption energy

We studied the different adsorption sites of hydrogen on Sn/Pt-Pt(111) using a (3×3) cell (see Figure 4.1). Using both functionals, the top site on a Pt atom is the most stable site (0.33 eV with PBE, 0.24 eV with optPBE), and the Pt-Pt bridge site is the only other possible site on this surface structure and is much less stable (0.16 eV with PBE, 0.03 eV with optPBE). The alloy provides different adsorption possibilities compared to the pure metal catalyst because of Sn atoms that have a repulsive interaction with H

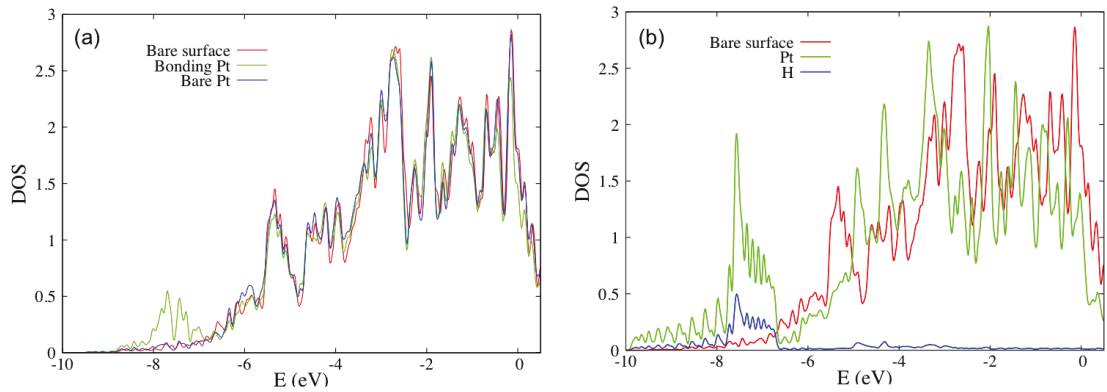


Figure 4.9: (a) Red : density of states (DOS) of the bare surface of Pt(111) projected on all orbitals of one Pt atom. Green : DOS of a partially covered surface of Pt(111) ($\theta_H = 0.11\text{ML}$) projected on all orbitals of three Pt atoms of the top layer forming an fcc site and bonding with an H atom. Blue : DOS of a partially covered surface of Pt(111) ($\theta_H = 0.11\text{ML}$) projected on all orbitals of the six Pt atoms of the top layer not bonding with the hydrogen; (b) Red : density of states (DOS) of the bare surface of Pt(111) projected on all orbitals of one Pt atom. Green : DOS of a covered surface of Pt(111) ($\theta_H = 1\text{ML}$) projected on all orbitals of one Pt atom of the top layer bonding with an H. Blue : DOS of a covered surface of Pt(111) ($\theta_H = 1\text{ML}$) projected on all orbitals of one H atom (blue)

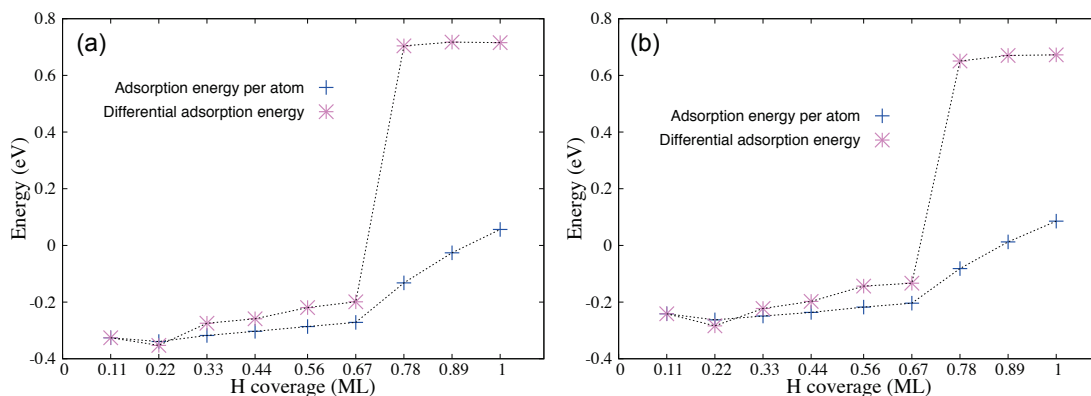


Figure 4.10: Hydrogen adsorption energy (E_{ads}/at) and differential adsorption energy (E_{ads}^{diff}) as a function of the coverage on Sn/Pt-Pt(111) calculated with PBE functional (a) and optPBE functional (b)

atoms. Indeed, on this surface, hollow sites are systematically formed by two Pt and one Sn atom which prevents H to adsorb on it. No Pt₃ site is accessible on the surface. The bridge sites are formed by Pt atoms only which makes them relatively stable. However, they are closer to Sn atoms than top sites, and thus are not the preferred sites. It comes that the coverages between 0.11 and 0.67 ML are composed by top sites only. From 0.78 to 1 ML, we found a mix of top and bridge sites. This is due to the fact that this surface contains six platinum atoms, available for hydrogen to adsorb, and three forbidden tin atoms. We also investigated the subsurface sites and we obtained an adsorption energy of 0.32 eV for the octahedral site and 2.30 for the tetrahedral site which confirmed that they are not conceivable for this surface. The adsorption energies per atom (E_{ads}/at) and the differential adsorption energies (E_{ads}^{diff}) of hydrogen on Sn/Pt are given as a function of the coverage of hydrogen (θ_H) in Figure 4.10.

We observe almost exactly the same behaviour of E_{ads}/at and E_{ads}^{diff} using PBE or optPBE. This system undergoes almost no influence of the functional but presents a very different evolution compared to that of pure Pt surface. The first six adsorptions happen

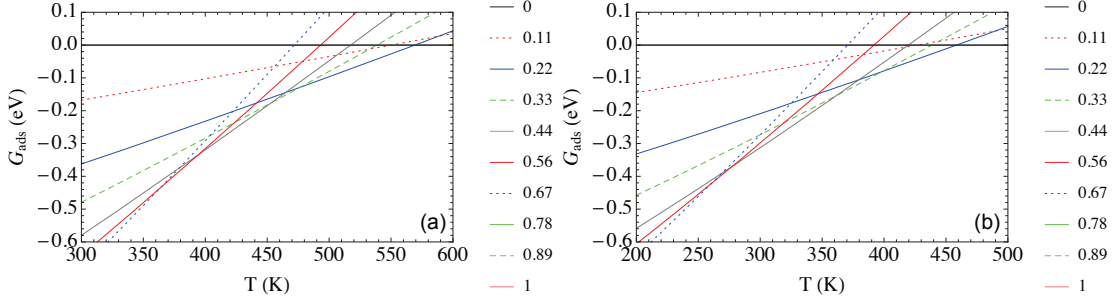


Figure 4.11: Hydrogen adsorption free energy (G_{ads}) as a function of the temperature calculated for $P_{H_2} = 1$ bar, on Sn/Pt-Pt(111) and for $\theta_H = 0$ to 1 ML; this was calculated with PBE (a) and optPBE (b)

quite easily with adsorption energies per atom varying between -0.33 and -0.27 eV. We observe a large jump between the sixth and the seventh adsorption in E_{ads}^{diff} of 0.9 eV which indicates the difficulty for H atoms to adsorb near Sn atom. With optPBE, we can see a similar jump but slightly smaller (0.78 eV). Hence the two functionals favor the same site for H and indicate a favorable adsorption up to six H atoms in the unit cell. The adsorption is markedly weaker on Sn/Pt than on Pt(111).⁷⁴ The adsorption free energies of H (G_{ads}) are given as a function of the temperature in Figure 4.11, for $P_{H_2} = 1$ bar. We observe that, as for Pt, the evolution of G_{ads} when decreasing the temperature is the same using PBE (Figure 4.11-a) or optPBE (Figure 4.11-b). The first adsorption configuration is 0.22 ML which means that 0.11 ML is never enough stable to exist at those T and P conditions. From 0.22 ML to 0.67 ML, all other configurations have a stable domain from 570 to 360 K for PBE, and from 460 to 250 K for optPBE. This difference of temperature is due to the difference in adsorption energies discussed before. Indeed, using optPBE, hydrogen adsorption is weaker than using PBE and thus, H atoms will desorb at lower temperature. Finally, at low temperatures, the most stable configuration stays $\theta_H = 0.67$ ML for both functional. This is consistent with the observations made about the adsorption energies (E_{ads}/at and E_{ads}^{diff}).

Figure 4.12 represents the stability domains of hydrogen for each couple of temperature and pressure, obtained with PBE (a) and optPBE (b). We can remark that the global shape of these thermodynamic diagrams is very similar to those obtained for Pt (see Figure 4.7), with a large area at relatively low pressures and high temperatures corresponding to a clean surface ($\theta = 0$ ML) and another one, at low temperatures and higher pressures, corresponding to the maximal coverage, in this case 0.67 ML. Though, a shift of temperature of 200 K and a smaller amount of intermediate domains are observed when changing the catalyst from Pt to Sn/Pt. We recognize the different domains of coverage existing in the case of Sn/Pt, passing from 0 to 0.22 ML, and after that, from 0.22 to 0.67 ML with a regular increase of H. As explained before, the difference obtained between the two catalysts is due to the presence of Sn atoms which prevent the adsorption of more than six H in the cell. Now if we compare the diagrams with respect to the functionals, we see that all phases are shifted towards lower temperatures, of about 150 K when passing from PBE to optPBE. The influence of the functional, which was first considered as less important in the case of the alloy, has actually a strong impact on the optimal coverage in reaction condition (300 K, 1 bar) as it decreases from 0.67 to 0.44 ML when passing from PBE to optPBE.

4.4.2 Adsorption structures

The geometric structures of the two extreme coverages (0.11 and 0.67 ML for PBE and 0.11 and 0.44 ML for optPBE) are shown in Figure 4.13. We observe a surface relaxation at low coverage. Indeed the Sn-Pt distances depend on the presence or not of one H atom and we can see that Sn atoms are coming out of the surface plane while Pt atoms are going inside the bulk. This is represented in Figure 4.13 by giving the difference between the mean plane height and each Pt and Sn height (blue and red). We can see that the optimal coverage, 0.44 ML, corresponds to a quite irregular structure. Indeed, the fact that not all Pt atoms are covered by H atoms causes a deformation

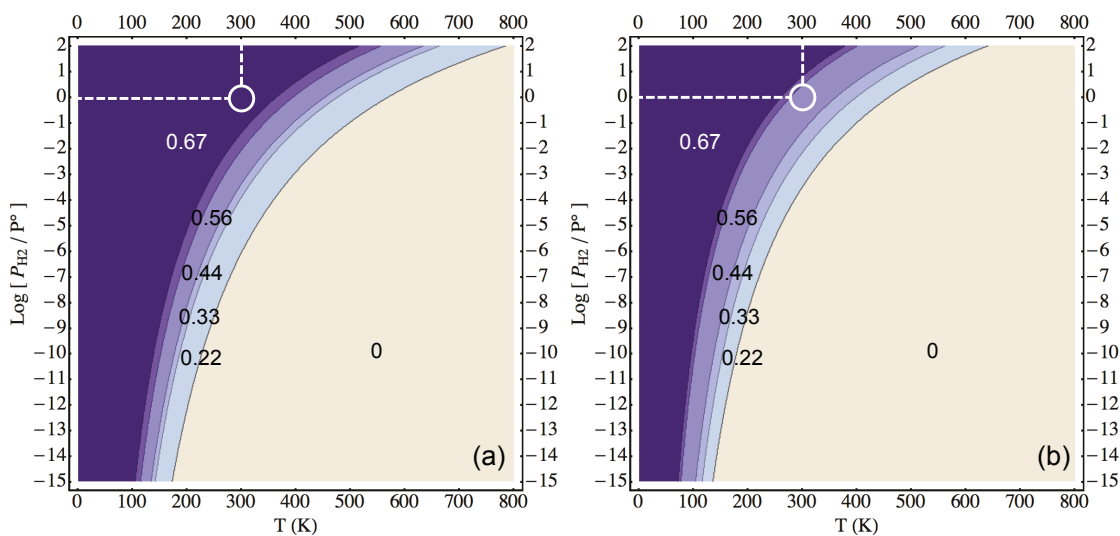


Figure 4.12: Optimal hydrogen coverage as a function of the pressure of H_2 and the temperature on Sn/Pt-Pt(111) calculated with the PBE functional (a) and the optPBE functional (b)

illustrated by the different length of the Sn-Pt distances. However, in the direction perpendicular to the surface, the displacement of the atoms has diminished. We also remark that in this case, the H-Pt distance is longer at low coverage than at high coverage (1.74 vs 1.67 Å) on the contrary of the case of Pt(111).

4.4.3 Electronic structure

The DOS projected on the surface Pt atoms of the Sn/Pt surface alloy are presented in Figure 4.14. The large band between -7 and 0 eV corresponds to the d band states. The projection on the Pt dz2 orbital shows a major peak at -0.5 eV, very close to the Fermi level. This orbital on Sn/Pt is hence a very high-lying reactive orbital, destabilized by the interaction with Sn. If we now look at the Dos of the Sn/Pt surface with one H atom, we see that the dz2 orbital of this atom is strongly shifted to low energy (by 5 eV), by the formation of a strong covalent bond with H. This specific contribution of

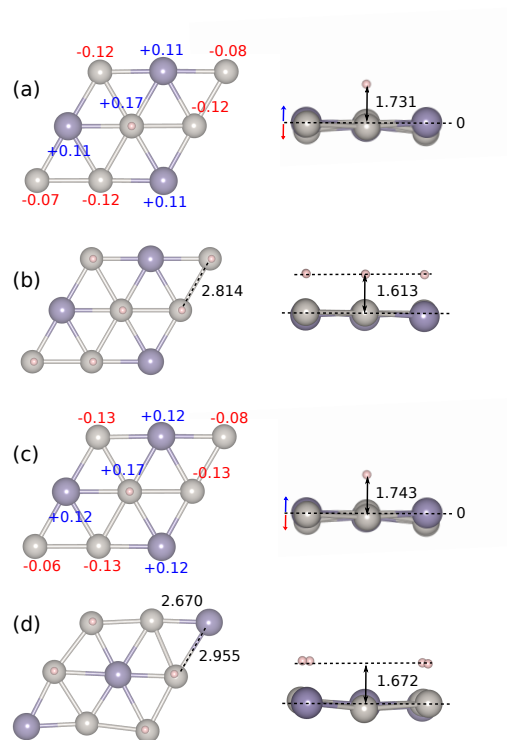


Figure 4.13: Top and side view of a Sn/Pt-Pt(111) surface covered with 0.11 and 0.44 ML of hydrogen, calculated with PBE (a and b) and optPBE (c and d); characteristic distances given in Å (in black)

the dz_2 orbital in the bonding explains the preference for top site on Sn/Pt, in contrast with Pt. On the total DOS of the Pt atom, one sees a shift of the d-band to lower energy. All effects are increased at a high coverage of 6H atoms, with a marked new peak related to the Pt-H interaction at low energy (-5.5 eV). As for Pt, the DOS presented in Figure 4.14 were normalized with respect to the number of atom and correspond to results obtained with PBE only.

4.5 Conclusion

We studied hydrogen adsorption on Pt(111) and Sn/Pt-Pt(111) to understand the impact of the temperature and the pressure on the adsorption configurations on the surface. We confirmed that the fcc site is the most stable one using PBE, while we found out that the top site is the best using optPBE. We calculated the adsorption free energy of hydrogen for a large range of T and P and we saw that under typical reaction conditions (300 K and 1 bar), 1 ML of H atoms is covering the Pt(111) surface, while the Sn/Pt surface alloy is covered by 0.67 ML of H atoms. We explained that the difference obtained on the two catalysts comes from the presence of Sn atoms that do not allow H atoms to adsorb on it. This results were obtained with the usual PBE functional. Using optPBE, we saw that the operating coverage is not changed on Pt, but becomes only 0.44 ML on Sn/Pt. Hydrogen adsorption is less stable using optPBE than using PBE.

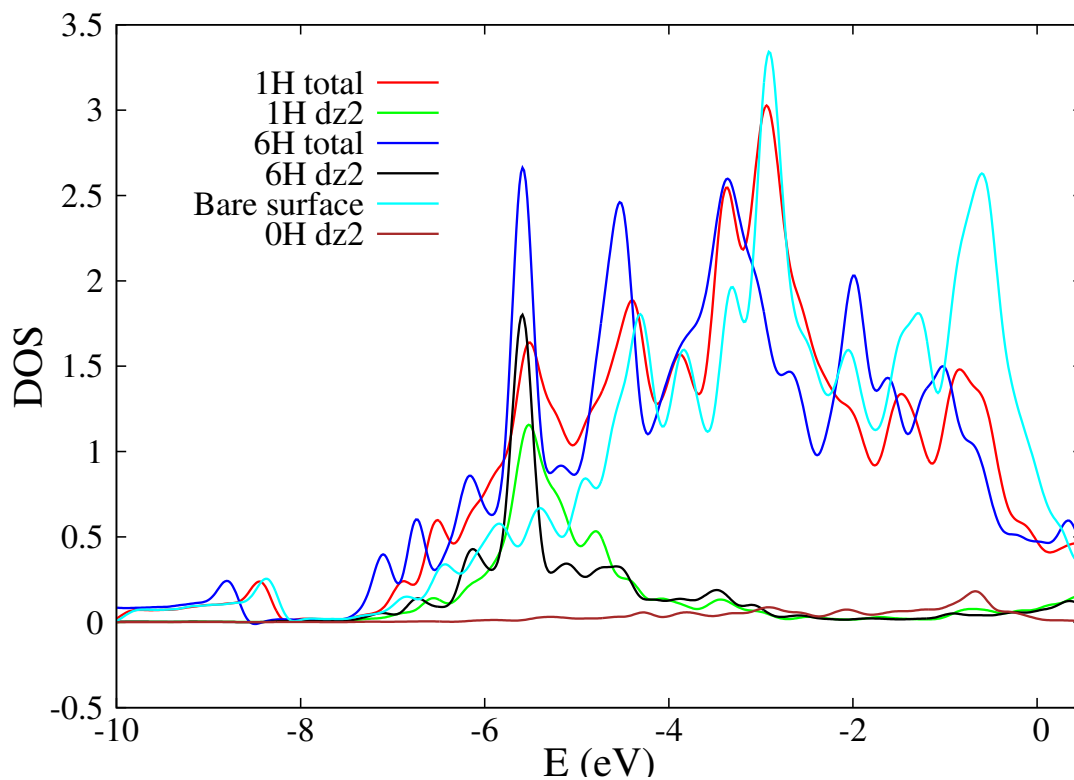


Figure 4.14: Red (*dark blue*) : density of states of a partially covered surface of Sn/Pt-Pt(111) with $\theta_H = 0.11 \text{ ML}$ ($\theta_H = 0.67 \text{ ML}$) projected on all orbitals of one Pt atom of the top layer of the surface forming a bond with an H. Green (*black*) : DOS of a partially covered surface of Sn/Pt-Pt(111) with $\theta_H = 0.11 \text{ ML}$ ($\theta_H = 0.67 \text{ ML}$) projected on the dz2 orbital of one Pt atom of the top layer of the surface forming a bond with an H. Brown : DOS of a partially covered surface of Sn/Pt-Pt(111) with $\theta_H = 0.11 \text{ ML}$ projected on the dz2 orbital of the five Pt atoms not bonding with the hydrogen in brown. Light blue : DOS of the bare surface of Sn/Pt-Pt(111) projected on all orbitals of one Pt atom

Chapter 5

Butadiene and Hydrogen co-adsorption and coverage dependency on Pt(111)

Contents

5.1 Introduction	79
5.2 Computational details	80
5.3 Before co-adsorption, butadiene adsorption on Pt(111)	80
5.4 Screening of the co-adsorption of butadiene with one hydrogen . .	81
5.5 How chemisorbed butadiene modifies the coverage of hydrogen . .	87
5.6 Competitive chemisorption of butadiene and hydrogen	93
5.7 What about butadiene physisorption ?	96
5.8 Conclusion	100

5.1 Introduction

The study of the co-adsorption of hydrogen and butadiene on Pt(111) using PBE and optPBE is presented in this part. As seen in the hydrogen study, the operating con-

ditions (T and P) have a strong influence on the hydrogen coverage^{69,70,73}. At 300 K and $P_{H_2} = 1$ bar the surface is fully covered by hydrogen ($\theta_H = 1$ ML). Thus, before considering butadiene and hydrogen reactivity, it is necessary to investigate their relative stability on the surface. The aim of this part is to elucidate what is the most stable co-adsorption configuration at these conditions and what is the influence of the co-adsorption of hydrogen and butadiene on the hydrogen coverage behaviour obtained previously. Therefore, we report here a thermodynamic study of the co-adsorption of butadiene and hydrogen. We propose a methodology to fully and accurately treat the increase of H coverage around butadiene and for different adsorption sites of butadiene. The coverage of butadiene is always kept at 0.11 ML which means only one molecule of butadiene is adsorbed on the surface (3×3) unit cell. Also, from now on, the pressure of butadiene is set to 1 bar unless otherwise specified.

5.2 Computational details

The DFT calculations were performed in the same conditions than those described in the previous Chapter, but using a four layers slab and a $3 \times 3 \times 1$ k-points mesh for a matter of time. Indeed, because of the number of configurations to test and the bigger size of the system (compared to hydrogen alone), it was necessary to adjust those two computational parameters. The co-adsorption energies and the co-adsorption free energies of hydrogen and butadiene were calculated using Eq.2.22 and 2.35. This is also valid for the Sn/Pt-Pt(111) study.

5.3 Before co-adsorption, butadiene adsorption on Pt(111)

Butadiene adsorption was already studied using standard functionals such as PW91 and has six possible conformations on Pt (see figure 5.1).¹⁰ Their adsorption energies (E_{ads}),

calculated with PBE and optPBE, are reported in Table 5.1. Each adsorption site is named after its type of bond, σ or π and the conformation, cis or trans, of the molecule. It is important to understand that, depending on the site, there is a different number of Pt atoms of the surface involved in the site. The trans-tetra σ butadiene forms four σ bonds with four Pt of the surface and is totally coordinated. The cis-1,4di σ -2,3 π and cis-1,2di σ -3,4 π involve three Pt atoms forming two σ and one π bond, while the trans-di π and the cis-di π involve two Pt atoms forming two π bonds. Finally, the di σ butadiene is partially decoordinated from the surface and forms only two σ bonds with two Pt atoms. In this adsorption site, the molecule has two C atoms that do not bind with atoms of the surface and that point in the gas phase direction.

In table 5.1, we see that the trans-tetra σ is the most stable adsorption site with -1.89 eV using PBE and -2.30 eV using optPBE. One can note that the order of stability of the sites does not depend on the functional. Di σ is the less stable site with -1.02 eV for PBE and does not exist when using optPBE as it falls systematically in the trans-tetra σ mode when optimizing the geometry. As one can observe, optPBE gives stronger adsorption energies than PBE because of the dispersion contribution (see Chapter 3). This means a strong adsorption of the molecule on the surface, also called chemisorption, and this is why the partially decoordinated conformation, di σ , is not stable using optPBE.

5.4 Screening of the co-adsorption of butadiene with one hydrogen

The co-adsorption of butadiene and hydrogen was studied for each adsorption site of butadiene. The adsorption sites of hydrogen, already discussed in Chapter 4 Figure 4.3, are fcc sites when using PBE and top sites when using optPBE.

We started this study by screening of all possible sites for one hydrogen atom to

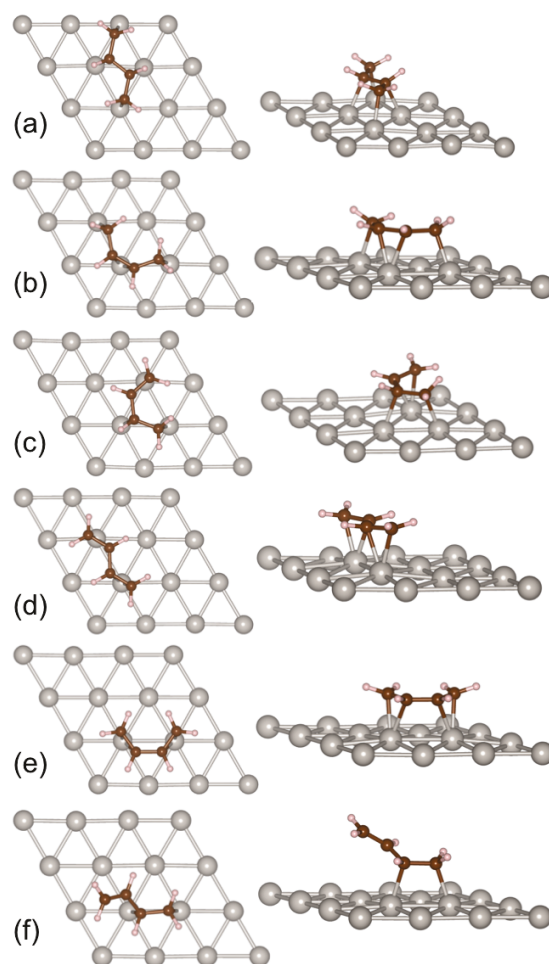


Figure 5.1: Butadiene adsorption conformations on Pt(111) in a (3×3) cell: (a) trans-tetra σ , (b) cis-1,4di σ -2,3 π , (c) cis-1,2di σ -3,4 π , (d) trans-di π , (e) cis-di π , (f) di σ

Adsorption Site	PBE	optPBE
trans-tetra σ	-1.89	-2.30
cis-1, 4di σ -2, 3 π	-1.70	-2.12
cis-1, 2di σ -3, 4 π	-1.64	-2.06
trans-di π	-1.42	-1.84
cis-di π	-1.36	-1.78
di σ	-1.02	fall in trans-tetra σ

Table 5.1: Adsorption sites and adsorption energies (E_{ads} in eV) of butadiene on Pt(111) surface for a (3×3) cell, calculated with PBE and optPBE

adsorb around butadiene in the trans-tetra σ conformation. This allowed us to know which sites would be preferred by hydrogen. For this, we used our previous results that shows that, on Pt(111), the most stable sites for hydrogen alone on the surface are fcc sites using PBE and top sites using optPBE (see Chapter 4). We will see here how the chemisorbed butadiene affects hydrogen adsorption. The nine possible adsorption sites in the (3×3) cell under consideration are not equivalent. Some platinum atoms are already coordinated by C atoms of the butadiene and are expected to be less available for hydrogen adsorption. For instance, the fcc site 5 is composed by two Pt atoms coordinated to one C atom each (see Figure 5.2). In addition, the hydrogen cloud of the butadiene can also destabilize hydrogen adsorption in a neighbouring site as represented in Figure 5.3-a for fcc sites (PBE) and b for top sites (optPBE).

In Table 5.2, we report the adsorption energies of hydrogen ($\theta_H = 0.11$ ML) and butadiene in the trans-tetra σ conformation, on Pt(111) calculated with PBE and optPBE. As expected, the hydrogen preference for a given fcc site with PBE decreases by increasing the number of Pt atoms coordinated to C atoms: in Figure 5.2, the Pt3 site is more stable than the (Pt-C)1-Pt2, itself more stable than the (Pt-C)2-Pt and finally, the

(Pt-C)₃ is the least stable. In other words, the co-adsorption is destabilizing from lateral repulsion mediated by the Pt surface.

Another factor that also decreases the stability of the site is the presence of H atoms of the butadiene molecule near the adsorption site. Indeed, hydrogen will prefer to adsorb on fcc sites that allow a certain distance with the hydrogens of the molecule hence avoiding Pauli repulsion (see Figure 5.3). Finally, the fcc site number 4 that contains two coordinated Pt, does not correspond to a local minimum. That is why, H diffused on the surface towards the site number 6. This last site is the preferred fcc site at the PBE level as it combines a Pt₃ with the maximal distance from the butadiene cloud, which makes it the most stable site.

For optPBE, as the preferred sites are top sites, only one Pt atom is involved in the site and it cannot be coordinated to a C atom. Here, the adsorption of one hydrogen atom on a top site is controlled by the availability of the first Pt neighbour. The top site is more stable if none of the first Pt neighbour are occupied, while it becomes less stable when they are occupied. This effect is still modulated by the steric interaction with butadiene but is lighter in this case than in the PBE case dealing with fcc sites. Indeed, when considering H adsorption sites that are close to the butadiene molecule, the distances between a carbon coordinated Pt atom and a top site is always larger than the distance between a carbon coordinated Pt and an fcc site. As a result, the most stable sites are the top site number 3, 6 and 9 and the less stable are 2 and 7. We can note that the range of stability of top sites is smaller than the one of fcc sites.

This analysis of the sites allows us to know where H atoms would adsorb preferentially around butadiene, using optPBE. We applied this analysis to the five other butadiene conformations to study the co-adsorption at higher coverages. The same study was done for the five other adsorption modes of butadiene and the results are given in Appendix B.

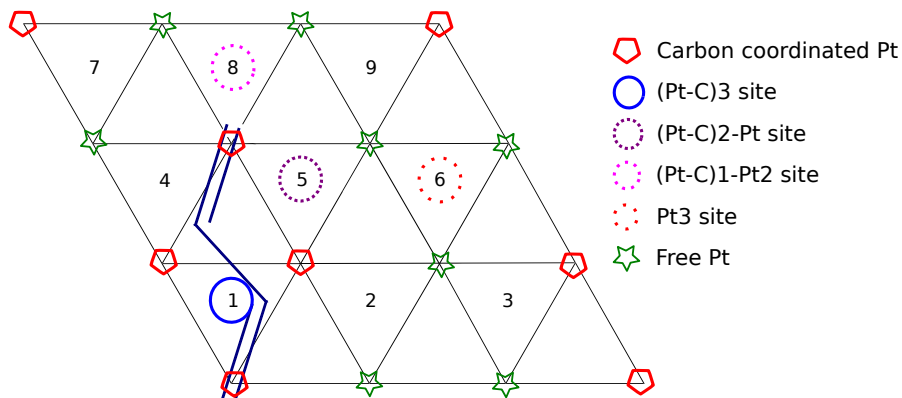


Figure 5.2: Possible fcc adsorption sites for hydrogen in a (3×3) supercell on Pt(111) with one butadiene already adsorbed in the cell in the trans-tetra σ conformation; (Pt-C) x -Pt y gives the number of carbon coordinated Pt (x) and the number of free Pt (y) of the site

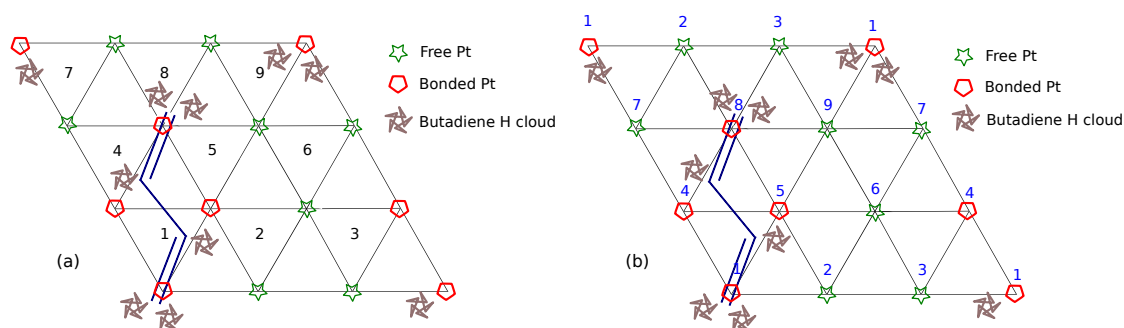


Figure 5.3: Possible adsorption sites for hydrogen in fcc sites (a) and top sites (b) in a (3×3) supercell on Pt(111) with one butadiene already adsorbed in the trans-tetra σ conformation and considering a possible destabilization at the sites by the hydrogen belonging to the molecule

Adsorption Site	E_{ads}^{Tot} PBE	E_{ads}^{But} PBE	Pt-C	E_{ads}^{Tot} optPBE	E_{ads}^{But} optPBE
1	-1.18	-0.67	3	\emptyset	\emptyset
2	-1.96	-1.45	1	-2.37	-2.00
3	-2.02	-1.51	1	-2.43	-2.07
4 => 6	-2.06	-1.55	2 => 0	\emptyset	\emptyset
5	-1.81	-1.30	2	\emptyset	\emptyset
6	-2.05	-1.54	0	-2.43	-2.07
7	-1.83	-1.32	1	-2.37	-2.00
8	-1.96	-1.45	1	\emptyset	\emptyset
9	-1.98	-1.47	1	-2.43	-2.07

Table 5.2: Adsorption energies (in eV) of hydrogen ($\theta_H = 0.11$ ML) and butadiene in the trans-tetra σ conformation on Pt(111) using PBE (with hydrogen on fcc sites) and optPBE (with hydrogen on top sites)

5.5 How chemisorbed butadiene modifies the coverage of hydrogen

We started to increase the coverage of hydrogen around butadiene up to the maximum of atoms in the cell, by taking into account the preferred sites of H, as determined in the low coverage study. The adsorption energies, calculated for each hydrogen coverage and each adsorption conformation of butadiene for PBE, are given in Table 5.3. For optPBE, only the trans-tetra σ and the di σ modes are reported here.

Let us start with the results obtained with PBE. It is important to note that the increase of the coverage does not affect the adsorption site of butadiene, the most stable always staying trans-tetra σ using PBE, unless for 0.89 ML where the di σ mode becomes more stable. This is due to the decoordinated character of the di σ mode which let more space for H adsorption and thus implies less repulsive interaction. We then injected these adsorption energies in the thermodynamic model proposed in Chapter 2 and already used in Chapter 4. With this, we calculated the adsorption free energies of each adsorption site of butadiene for each coverage of hydrogen, as a function of the temperature (T in K) and the pressure of hydrogen (P_{H_2} in bar). This led to six phase diagrams, one for each butadiene adsorption site, given in Figure 5.4. Practically, we force the adsorption of one butadiene as we calculate G_{ads} of co-adsorbed systems, with $\theta_{but} = 0.11$ ML and θ_H ranging from 0 to 1 ML. As a positive adsorption energy of a system means that there is no adsorption on the surface, we summarized such cases by noting " \emptyset " on the diagrams, which implies there is no molecule at all on the surface. This is happening at high temperature and mostly low pressure. Then, the phase where one butadiene alone is adsorbed (with no H atom co-adsorbed) is noted "0". And when increasing the hydrogen pressure and decreasing the temperature, the coverage of hydrogen increases. This is represented by different phases, one for each coverage. One can observe a dark area on the left part at low temperatures and high pressures,

corresponding to the highest hydrogen coverage possible in this range of temperature and pressure. The coverage of hydrogen at $T = 300$ K and $P_{But} = P_{H_2} = 1$ bar (defined as possible operating conditions) noted θ_H^* , depends on the adsorption site of butadiene. Indeed, the trans-tetra σ , the cis-1,4di σ -2,3 π and the cis-1,2di σ -3,4 π sites allow a hydrogen coverage of 0.56 ML, while trans-di π gives 0.44 ML. Cis-di π also allows a coverage of 0.44 ML at the limit of the 0.78 ML phase. Finally, the di σ site, which is partially decoordinated, gives a higher optimal coverage of 0.67 ML as it binds with only two Pt atoms and thus, leaves more space on the surface for H to adsorb. One can note that θ_H^* decreased as compared to 1 ML which is the one obtained when only hydrogen is adsorbed on the surface. Figure 5.5-a and b shows the geometrical structures of the trans-tetra σ and the di σ modes at θ_H^* of each site. Figure 5.6-a gives the relative stability of the six adsorption sites of butadiene in the situation θ_H^* for each site. It shows that the trans-tetra σ adsorption mode always stays the most stable.

We focused our interest on the totally coordinated most stable adsorption mode (trans-tetra σ) and the partially decoordinated one (di σ). Their adsorption energies are given in Table 5.3. One can see that with optPBE, the trans-tetra σ site does not exist for θ_H higher than 0.67 ML, neither the di σ mode for $\theta_H = 0.78$ ML. This is due to the adsorption sites of hydrogen that are top sites when using optPBE. The trans-tetra σ mode requires four free Pt atoms to chemisorb on the surface whereas the di σ site requires only two free Pt atoms. In the same way than for PBE, we calculated the adsorption free energies of those two systems with optPBE (see Figure 5.5-c for trans-tetra σ and 5.5-d for di σ). By comparing with Figure 5.4-a and f, we can see that the change of the functional affects the behaviour of hydrogen coverage. For the trans-tetra σ mode, θ_H^* stays the same, 0.56 ML, but the maximal coverage changes from 0.89 ML with PBE to 0.56 ML with optPBE. This is due to a different relative stability between H atoms and butadiene when changing the functional. For the di σ mode, as it does not exist without hydrogen on the surface, we observe a direct jump from no species on the surface

θ_H	0.11	0.22	0.33	0.44	0.56	0.67	0.78	0.89
PBE								
trans-tetra σ	-2.06	-2.42	-2.72	-2.97	-3.16	-3.25	-3.28	-2.91
cis-1,4di σ -2,3 π	-1.87	-2.22	-2.53	-2.84	-3.06	-3.13	-3.12	-3.25
cis-1,2di σ -3,4 π	-1.83	-2.20	-2.53	-2.77	-3.06	-3.05	-3.28	-3.24
trans-di π	-1.64	-2.01	-2.37	-2.65	-2.77	-2.83	-2.87	-2.80
cis-di π	-1.77	-1.79	-2.00	-2.33	-2.37	-2.61	-2.79	-2.87
di σ	-1.31	-1.71	-2.10	-2.47	-2.78	-3.04	-3.18	-3.30
optPBE								
trans-tetra σ	-2.43	-2.74	-2.99	-3.13	-3.24	\emptyset	\emptyset	\emptyset
di σ	-1.74	-1.98	-2.28	-2.61	-2.76	-2.87	-2.90	\emptyset

Table 5.3: Total adsorption energies (eV) of hydrogen and butadiene on Pt(111) for the six possible conformations of butadiene and from $\theta_H = 0.11$ to 0.89 ML, calculated with PBE and optPBE (the most stable are in bold letters)

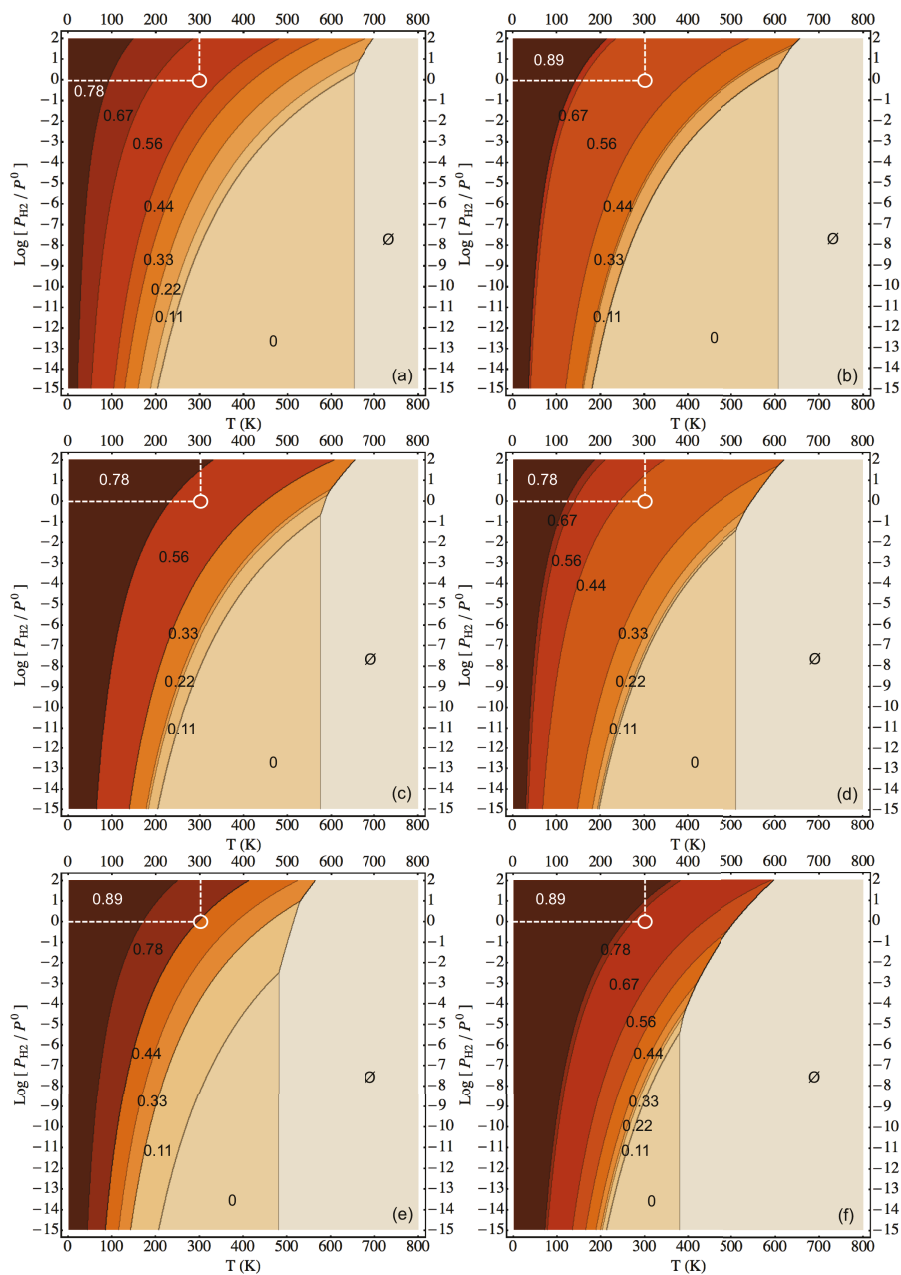


Figure 5.4: Hydrogen coverage on a surface of Pt(111) precovered with one butadiene in the trans-tetra σ (a), cis-1,4di σ -2,3 π (b), cis-1,2di σ -3,4 π (c), trans-di π (d), ciq-di π (e) and di σ (f) conformations, obtained with PBE

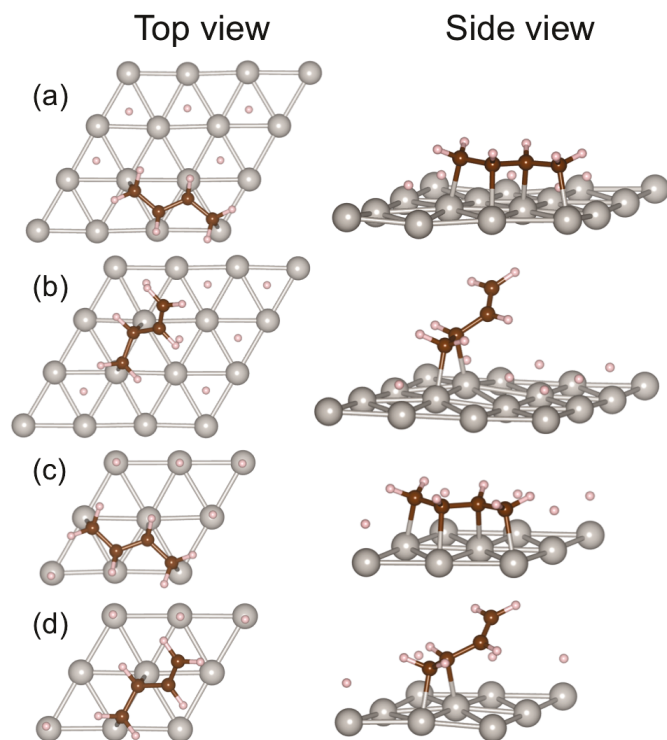


Figure 5.5: Geometrical structures of the trans-tetra σ and the di σ mode at their optimal coverage on Pt(111), calculated with PBE (a: $\theta_H = 0.56$ ML, b: $\theta_H = 0.67$ ML), and with optPBE (c: $\theta_H = 0.56$ ML, d: $\theta_H = 0.44$ ML)

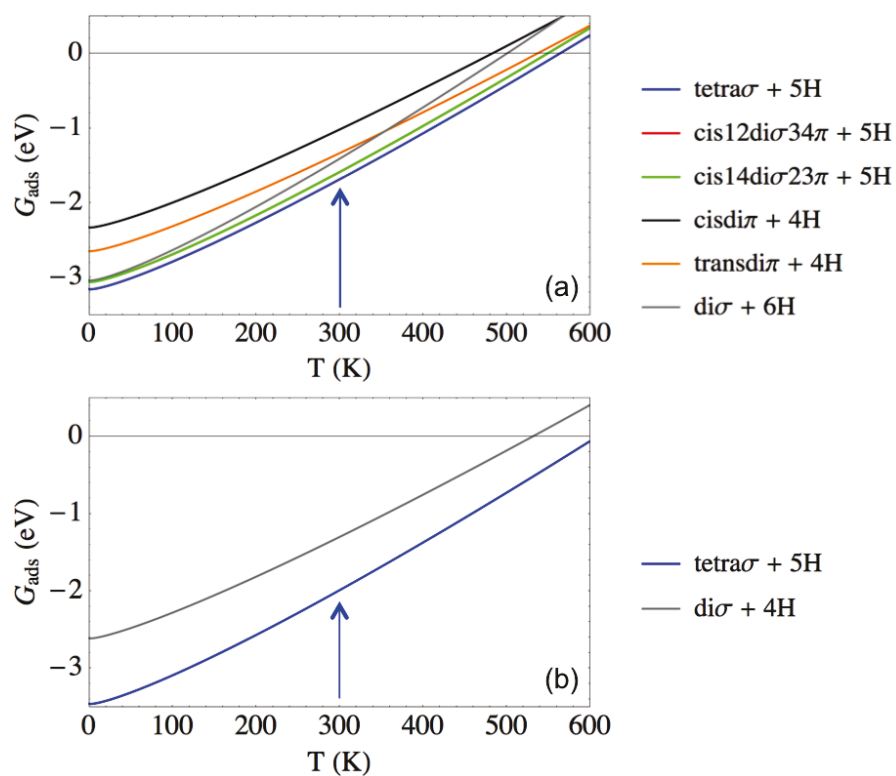


Figure 5.6: Adsorption free energies of the six possible adsorption modes of butadiene calculated with PBE (a) and of the trans-tetra σ and the di σ mode calculated with optPBE (b) on Pt(111), for $P_{H_2} = P_{But} = 1$ bar and as a function of the temperature

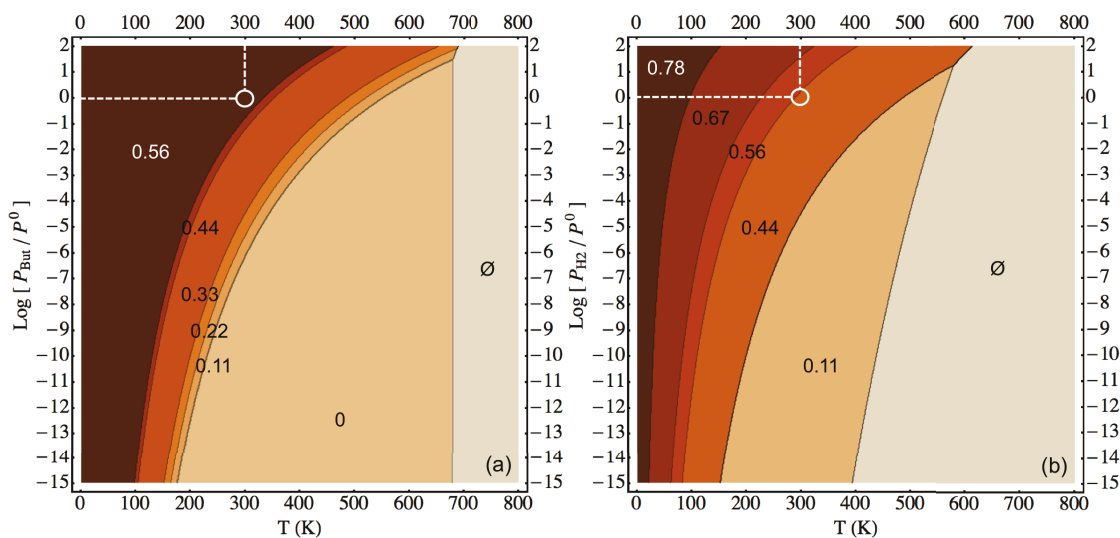


Figure 5.7: Hydrogen coverage on a surface of Pt(111) precovered with one butadiene in the trans-tetra σ (a) and the di σ (b) conformations, obtained with optPBE

(\emptyset) to a co-adsorption of butadiene with one hydrogen ($\theta_H = 0.11$ ML). Also, θ_H^* is changed from 0.67 ML with PBE to 0.44 ML with optPBE and the maximal coverage becomes 0.78 ML as hydrogen is destabilized when using optPBE. Finally, Figure 5.6-b shows that the trans-tetra σ mode is always more stable than the di σ mode at $P_{But} = P_{H_2} = 1$ bar.

5.6 Competitive chemisorption of butadiene and hydrogen

The adsorption configurations of the diagrams of Figure 5.4 and Figure 5.5 correspond to calculations where we force butadiene adsorption on the surface. Indeed, the only inputs of the thermodynamic model are the energies of the co-adsorbed systems (butadiene + hydrogen). In order to understand what is the composition of the surface at the thermodynamic equilibrium, we compare the thermodynamics of the co-adsorbed

system to hydrogen alone on the surface, for the trans-tetra σ and di σ mode. Figure 5.8 represents the most stable conformation found for each couple of pressure and temperature as in Figure 5.4. However, the co-adsorption of butadiene and hydrogen is now compared to the adsorption of hydrogen alone. In the case of the trans-tetra σ (Figure 5.8-a and b), one can see that the PBE functional gives a smaller window of stability for the co-adsorbed system (green) compared to optPBE. Indeed, with PBE, the orange phase (where hydrogen is more stable) is localized at extreme temperatures (more than 600 K and less than 100 K) and at high pressures of H (above 1 bar). With optPBE, the adsorption of H alone is reduced to the zone starting after 680 K, where the co-adsorption of butadiene and hydrogen gives rise to positive adsorption free energies (\emptyset in Figure 5.5-a). However, this phase corresponds to no hydrogen on the surface (see Figure 4.7-b of Chapter 4). One can note that for PBE, the optimal conformation at 300 K and $P_{H_2} = 1$ bar corresponds to 1 ML of hydrogen alone, while for optPBE, it corresponds to butadiene and $\theta_H = 0.56$ ML. For the di σ mode, we see that the phase corresponding to hydrogen alone (orange) is larger when using PBE than when using optPBE as observed in the case of trans-tetra σ . In fact, for PBE, the co-adsorbed system with the di σ site never exist in this range of temperature and pressure. The optimal conformation at 300 K and $P_{H_2} = 1$ bar is $\theta_H = 1$ ML with PBE (as for diagram a), and for optPBE, it corresponds to the co-adsorbed conformation with $\theta = 0.44$ ML. We also note that the di σ adsorption site has a smaller window of stability (green) than the trans-tetra σ mode.

Thanks to this comparison of the species on the surface we know that with PBE and at the thermodynamic equilibrium, the totally hydrogenated surface is the most stable configuration at $T = 300$ K and $P_{But} = P_{H_2} = 1$ bar. Using optPBE and in the same conditions, the partially hydrogenated surface (0.56 ML) covered with 0.11 ML of butadiene in its trans-tetra σ mode is the most stable system.

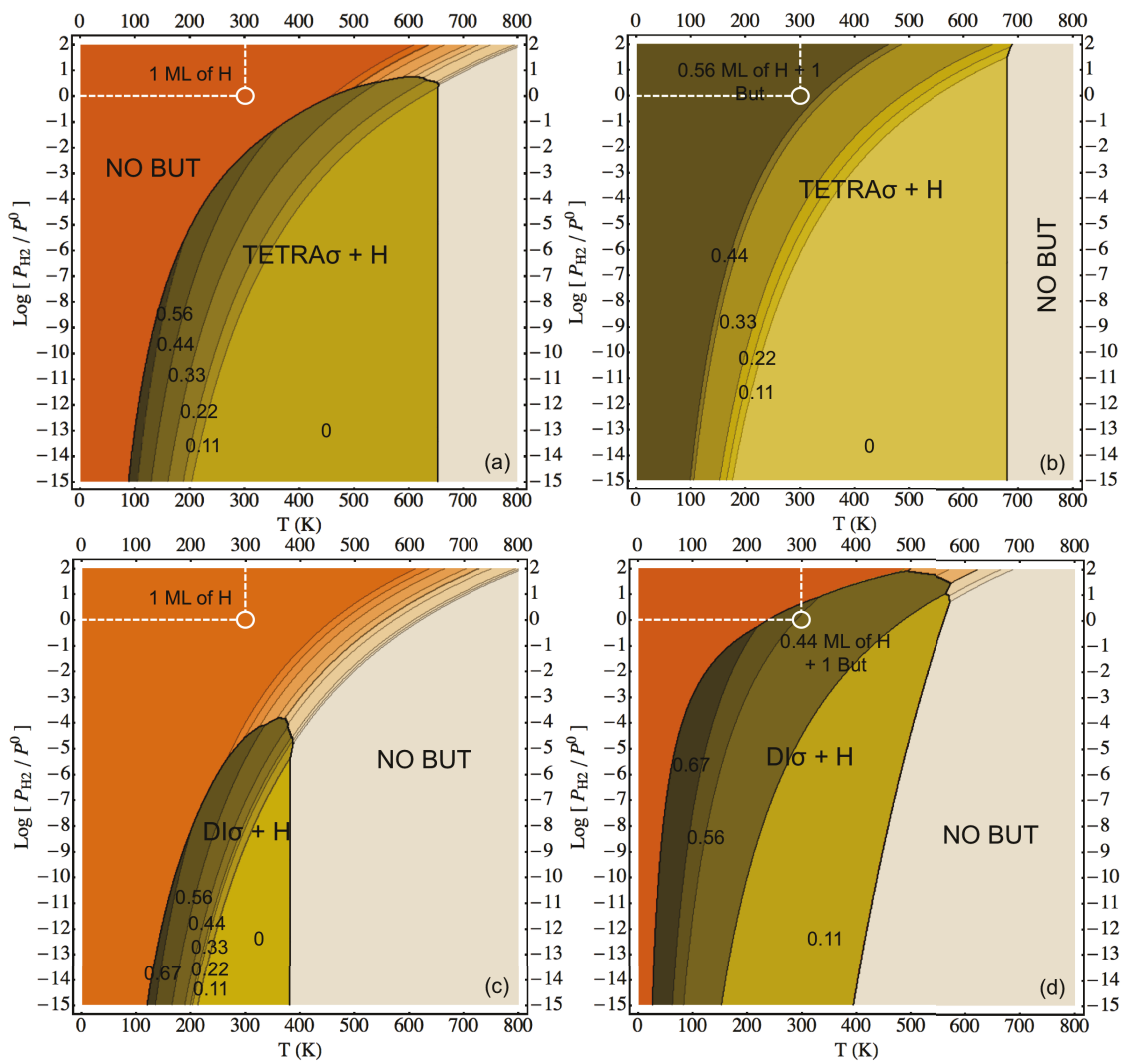


Figure 5.8: Thermodynamic diagram showing the most stable conformation as a function of T and P when comparing the co-adsorption of hydrogen and butadiene (green) to the adsorption of pure hydrogen (orange) on Pt(111) for two butadiene modes : the trans-tetra σ mode calculated with PBE (a) and optPBE (b), and the di σ mode calculated with PBE (c) and optPBE (d)

5.7 What about butadiene physisorption ?

However, until now, we only considered strong interactions between butadiene and the catalyst when studying the chemisorption (χ) of the molecule on the surface. As we are interested in the behaviour of butadiene adsorption at high coverage, we also investigated the possible physisorption (ϕ) configurations of butadiene on a hydrogenated surface. The adsorption energies of hydrogen and butadiene are given in Table 5.4 with their structures in Figure 5.9 for both functionals. One can note that the type of adsorption of butadiene (χ or ϕ) depends on the coverage of hydrogen, which is fixing the free space in the cell for butadiene to adsorb. It depends also on the hydrogen sites; indeed, using PBE, H atoms adsorb on fcc sites, which allows to increase θ_H up to 0.89 ML around butadiene and still consider a chemisorption (see Figure 5.9-a). With optPBE, chemisorption takes place until a maximal coverage of only 0.67 ML. This is due to the fact that H atoms adsorb on top sites which are not available anymore for the molecule to adsorb (see Figure 5.9-a', b' and c'). We can remark that for $\theta_H = 0.89$ ML using PBE, the two situations exist but the physisorbed state is more stable of 0.42 eV than the chemisorbed one. Also, the distance between the molecule and the surface is shorter when using optPBE (4.06 Å) than when using PBE (4.12 Å). In Table 5.5, we reported the adsorption free energies of the same system. We also calculated G_{ads} for the physisorbed systems, to which we added a two dimensional translation component for butadiene in the calculation of the entropy (ϕ 2D) in Eq.2.36 of Chapter 2. Instead of considering the molecule fixed on the surface, we authorize a partial translation in the two directions of the surface, but not in the direction perpendicular to the surface. Indeed, as the molecule is weakly bonded to the surface, it may translate, leading to the following equation:

θ_H (ML)	PBE χ	PBE ϕ	optPBE χ	optPBE ϕ
0.11	-2.06	\emptyset	-2.43	\emptyset
0.22	-2.42	\emptyset	-2.74	\emptyset
0.33	-2.72	\emptyset	-2.99	\emptyset
0.44	-2.97	\emptyset	-3.13	\emptyset
0.56	-3.16	\emptyset	-3.24	\emptyset
0.67	-3.25	\emptyset	-2.67	\emptyset
0.78	-3.28	\emptyset	\emptyset	-2.75
0.89	-2.91	-3.33	\emptyset	-2.88
1	\emptyset	-3.65	\emptyset	-3.17

Table 5.4: Total adsorption energies (E_{ads} in eV) of hydrogen and butadiene in the trans-tetra σ mode when chemisorbed (χ) and in trans gas phase conformation when physisorbed (ϕ), on Pt(111); \emptyset means no structure found

$$\begin{aligned}
G_{ads}^{Tot}(T, P) = & E_{ads}^{Tot} + k_B T \sum_{i=1}^x \ln[(z_{trans}^{*,i})^{1/3} \times z_{rot}^i]^{n_i} \\
& - k_B T \sum_{i=1}^x n_i \ln \left[\left(\frac{P^i}{k_B T} \right)^{1/3} \right]
\end{aligned} \tag{5.1}$$

Each term of eq 5.1 is explicitly defined in Chapter 2. With this hypothesis, we can see that the physisorbed systems are stabilized of about 0.28 eV compared to the chemisorbed systems (Table 5.5). It is then required to compare these physisorbed states to the hydrogenated surface alone to know if physisorbed butadiene is more stable or at least competitive to hydrogen alone.

Figure 5.10 and Figure 5.11 show the results for both functionals. Using PBE, the totally hydrogenated surface (9H) is more stable than any system involving butadiene as it has the lowest adsorption free energies between 0 and 680 K, after which the species desorb as we enter the positive adsorption energies. Using optPBE, the co-adsorption

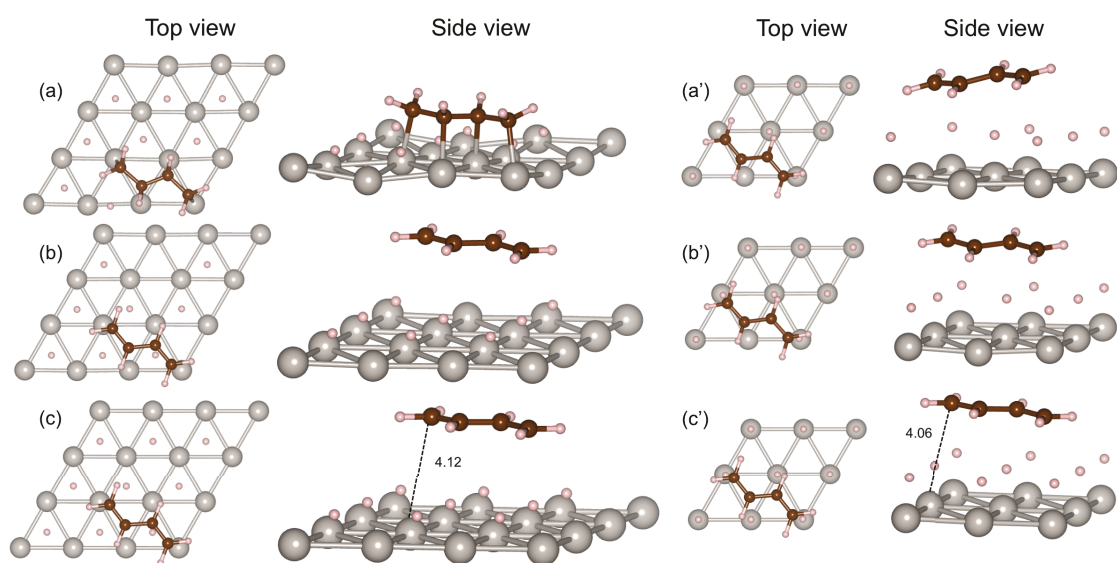


Figure 5.9: Top and side view of $8\text{H}+\text{But}_\chi$ (a) $8\text{H}+\text{But}_\phi$ (b) and $9\text{H}+\text{But}_\phi$ (c) obtained with PBE and of $7\text{H}+\text{But}_\phi$ (a') $8\text{H}+\text{But}_\phi$ (b') and $9\text{H}+\text{But}_\phi$ (c') obtained with optPBE, on Pt(111)

θ_H (ML)	PBE χ	PBE ϕ	PBE ϕ 2D	optPBE χ	optPBE ϕ	optPBE ϕ 2D
0.11	-1.21	\emptyset	\emptyset	-1.64	\emptyset	\emptyset
0.22	-1.42	\emptyset	\emptyset	-1.80	\emptyset	\emptyset
0.33	-1.57	\emptyset	\emptyset	-1.93	\emptyset	\emptyset
0.44	-1.65	\emptyset	\emptyset	-1.97	\emptyset	\emptyset
0.56	-1.69	\emptyset	\emptyset	-1.99	\emptyset	\emptyset
0.67	-1.62	\emptyset	\emptyset	-1.16	\emptyset	\emptyset
0.78	-1.40	\emptyset	\emptyset	\emptyset	-1.06	-1.35
0.89	-0.96	-1.38	-1.67	\emptyset	-1.12	-1.41
1	\emptyset	-1.55	-1.84	\emptyset	-1.17	-1.45

Table 5.5: Total adsorption free energies (G_{ads} in eV at $T = 300$ K and $P_{But} = P_{H_2} = 1$ bar) of hydrogen and butadiene in the trans-tetra σ mode when chemisorbed (χ) and in trans gas phase conformation when physisorbed (ϕ), on Pt(111); \emptyset means no structure found; 2D means that a two dimensional component of the translation is taken into account in the calculation of the entropy

of butadiene and five hydrogen (5H+But χ) is the most stable configuration as it has the lowest curve (black). We decreased the pressure of hydrogen to decrease the ratio P_{H_2}/P_{But} to 10^{-3} and see the effects on the relative stability of these systems (Figure 5.10-b for PBE and Figure 5.11-b for optPBE). For PBE, we can see that the difference in energy between 9H and the other systems is decreased of about half, but not enough to see a crossing of the curves. The simple adsorption of hydrogen stays the most stable configuration and the order of stability of the other configurations are hardly changed; we observe a larger range of stability of the 9H+But ϕ 2D conformation over the 5H+But χ . For optPBE, we also see a reduction of the distance between the black curve representing 5H+But χ and the group the other curves representing the other systems (9H, 9H+But ϕ and 9H+But ϕ 2D). As for PBE, a lower pressure of hydrogen did not change the relative stability of the most stable configuration and the others.

5.8 Conclusion

We can conclude that at the chosen conditions, PBE favours the adsorption of hydrogen only and does not allow a stable adsorption of butadiene on the platinum catalyst. The physisorbed state is metastable but more stable than the chemisorbed state. Physisorption of butadiene is thus favoured on the surface and this could lead to an Eley-Rideal type mechanism for the first hydrogenation (see Figure 5.12). Indeed, this mechanism implies one reactant adsorbed on the surface (H) and one other molecule reacting directly from the gas phase before any adsorption (butadiene). On the contrary, optPBE favours the adsorption of butadiene in a chemisorbed state with an intermediate coverage of hydrogen of 0.56 ML. This leads more likely to the Langmuir-Hinshelwood mechanism for the hydrogenation reaction which requires the reactants to be adsorbed on the surface before reacting (see Figure 5.12).

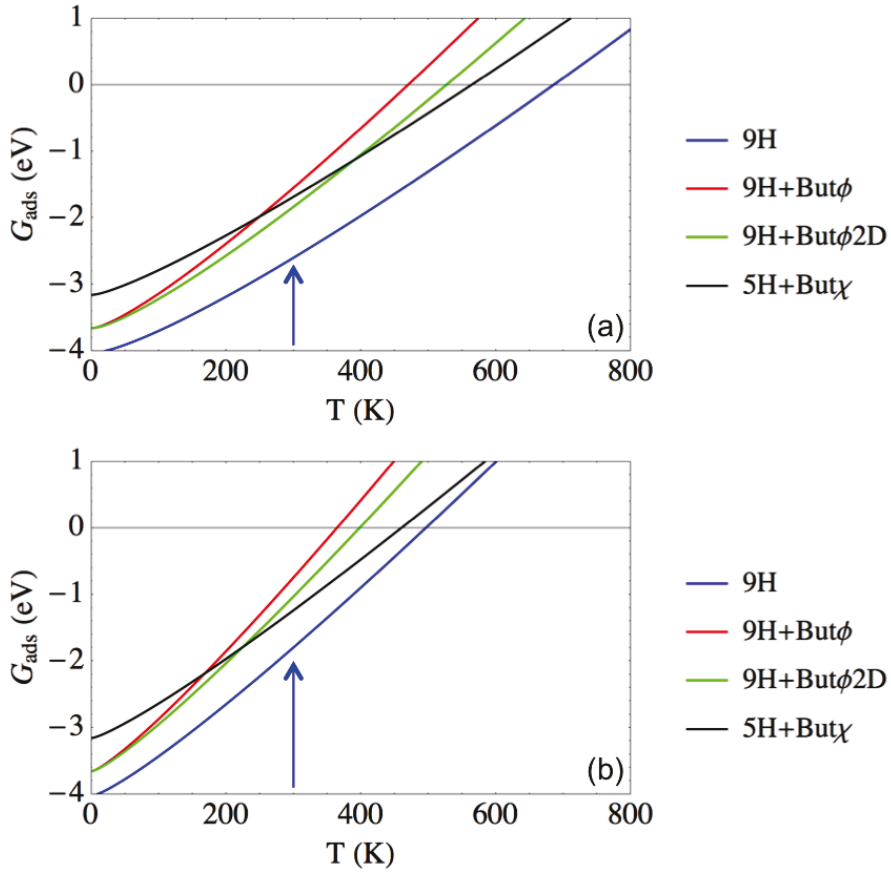


Figure 5.10: Relative stability of different systems on Pt(111) calculated with PBE: hydrogen with $\theta_H = 1$ ML (9H), butadiene physisorbed on a hydrogenated surface (9H+But ϕ) and with a two dimensional translation authorized (9H+But ϕ 2D), and butadiene chemisorbed in the trans-tetra σ mode on a partially hydrogenated surface (5H+But χ); we propose two pressure ratio: $P_{H_2}/P_{But} = 1$ (a) and $P_{H_2}/P_{But} = 10^{-3}$ (b)

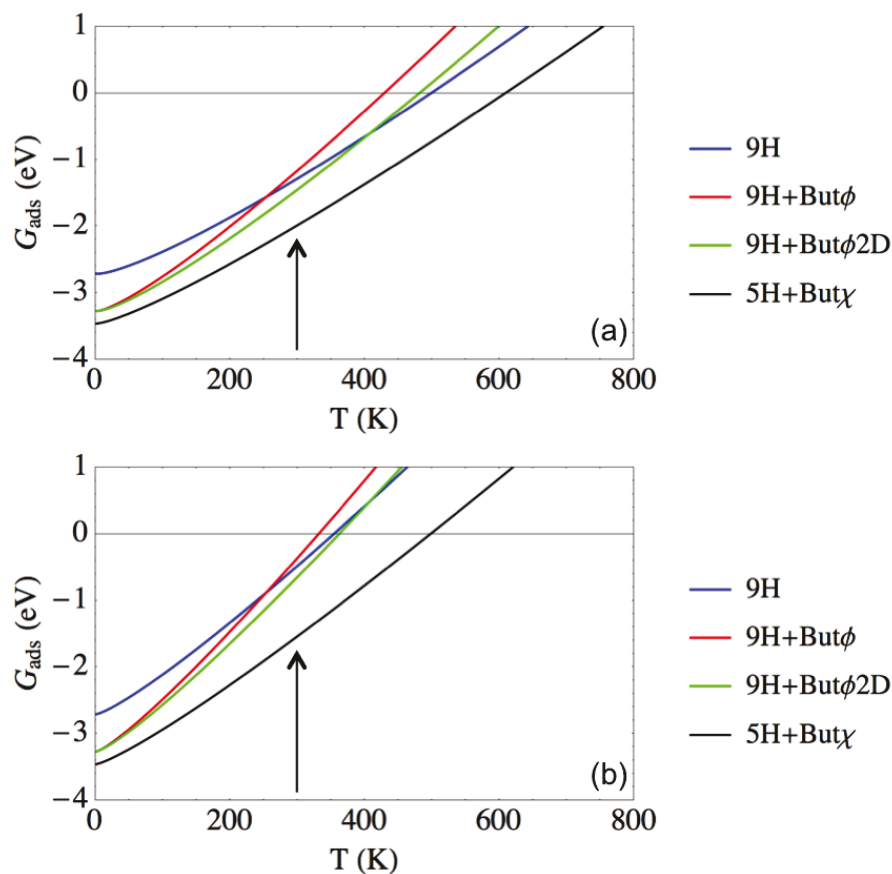


Figure 5.11: Relative stability of different systems on Pt(111) calculated with optPBE: hydrogen with $\theta_H = 1$ ML (9H), butadiene physisorbed on a hydrogenated surface (9H+But ϕ) and with a two dimensional translation authorized (9H+But ϕ 2D), and butadiene chemisorbed in the trans-tetra σ mode on a partially hydrogenated surface (5H+But χ); we propose two pressure ratio: $P_{\text{H}_2}/P_{\text{But}} = 1$ (a) and $P_{\text{H}_2}/P_{\text{But}} = 10^{-3}$ (b)

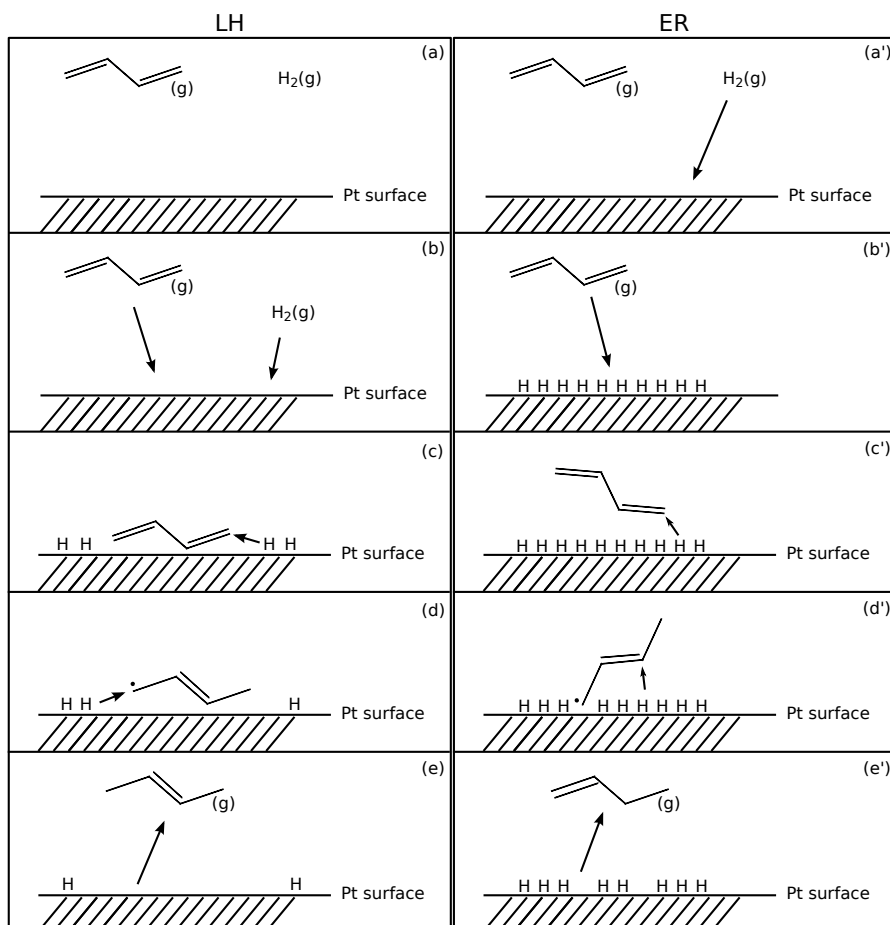


Figure 5.12: Langmuir-Hinshelwood (LH) mechanism illustration: (a) reactants in the gas phase, (b) adsorption of the reactants on the surface, (c) first hydrogenation, (d) second hydrogenation, (e) desorption of the product. Eley-Rideal (ER) mechanism illustration: (a') reactants in the gas phase, (b') adsorption of one reactant on the surface, (c') physisorption of the second reactant and first hydrogenation, (d') second hydrogenation, (e') desorption of the product

Chapter 6

Butadiene and Hydrogen co-adsorption and coverage dependency on Sn/Pt-Pt(111)

Contents

6.1 Introduction	106
6.2 Before co-adsorption, butadiene adsorption on Sn/Pt-Pt(111) . . .	106
6.3 Screening of the co-adsorption of butadiene with one hydrogen . .	108
6.4 How chemisorbed butadiene modifies the coverage of hydrogen . .	109
6.5 Competitive chemisorption of butadiene and hydrogen	116
6.6 What about butadiene physisorption ?	116
6.7 Conclusion	120

6.1 Introduction

We applied the method developed on Pt(111) to the surface alloy Sn/Pt-Pt(111) and present the results in this part. The computational details are the same than those presented for Pt(111).

6.2 Before co-adsorption, butadiene adsorption on Sn/Pt-Pt(111)

As for Pt(111), butadiene adsorption has already been studied using standard functionals such as PW91.⁷⁴ Only five different adsorption sites exist on Sn/Pt-Pt(111) due to the presence of tin atoms that decrease the number of adsorption sites (see Figure 6.1). Indeed, the surface alloy has different electronic properties than the pure metallic surface, and because of the electronic structure of Sn atom, no bond can be formed between those atoms and any adsorbate.^{8,9} Their adsorption energies (E_{ads}), calculated with PBE and optPBE, are reported in table 6.1. We can see that the cis-1,4di σ -2,3 π is the most stable one with -0.82 eV for PBE and -1.23 eV for optPBE. As for Pt, the less stable sites is di σ with -0.40 eV for PBE and -0.98 eV for optPBE. As in the case of Pt(111), the order of stability between the different adsorption modes is the same for both functional.

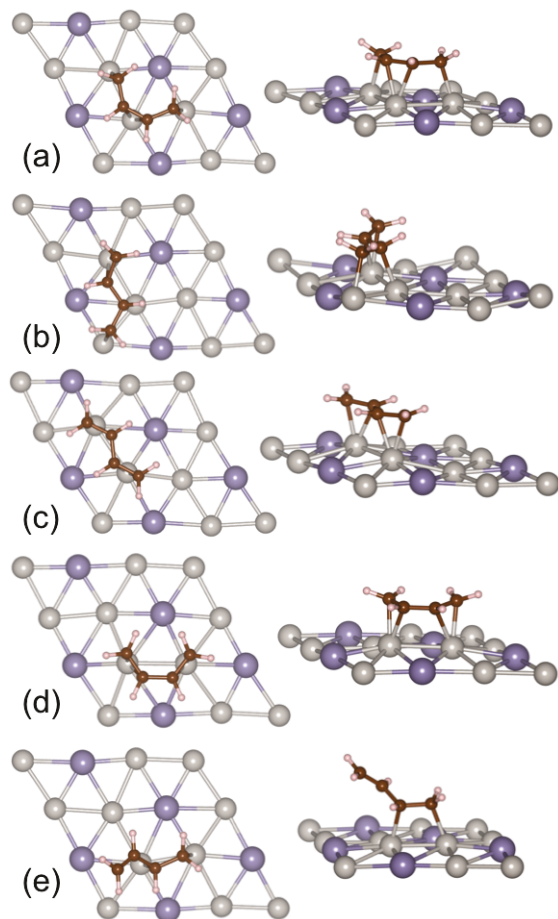


Figure 6.1: Butadiene adsorption conformations on Sn/Pt-Pt(111) in a (3×3) cell : (a) cis-1,4di σ -2,3 π , (b) trans-1,2di σ -3,4 π , (c) trans-di π , (d) cis-di π , (e) di σ

Adsorption Site	PBE	optPBE
cis-1, 4di σ -2, 3 π	0.82	-1.23
trans-1, 2di σ -3, 4 π	-0.68	-1.09
trans-di π	-0.65	-0.86
cis-di π	-0.56	-1.08
di σ	-0.40	-0.98

Table 6.1: Adsorption sites and adsorption energies (E_{ads} in eV) of butadiene on Sn/Pt-Pt(111) surface for a (3×3) cell, calculated with PBE and optPBE functional

6.3 Screening of the co-adsorption of butadiene with one hydrogen

The co-adsorption of butadiene and hydrogen was studied for each adsorption site of butadiene. The adsorption sites of hydrogen on Sn/Pt, already discussed in Figure 4.3 of Chapter 4, are top sites for both functionals.

As for Pt(111), we evaluated the best sites by screening of all possible sites for one hydrogen to adsorb around butadiene in the cis-1, 4di σ -2, 3 π adsorption mode. This allowed us to know which sites would be preferred by hydrogen. For this, we used our previous results that shows that, on Sn/Pt-Pt(111), the most stable sites for hydrogen alone on the surface are top sites using PBE as well as optPBE (see Chapter 4).

The adsorption energies of hydrogen adsorbed on top sites are reported in Table 6.2 for PBE and optPBE. When using PBE, the site number 1 is the most stable with -1.07 eV, followed by the number 3 of -1.03 eV, and the number 7 with -1.01 eV. A first remark is that the differences in energy between those three sites are quite small (0.02 to 0.04 eV) compared to those observed in the case of pure Pt (0.63 to 0.87 eV). We can see that the sites 3 and 7 are both near Pt atoms that are σ bonding with each

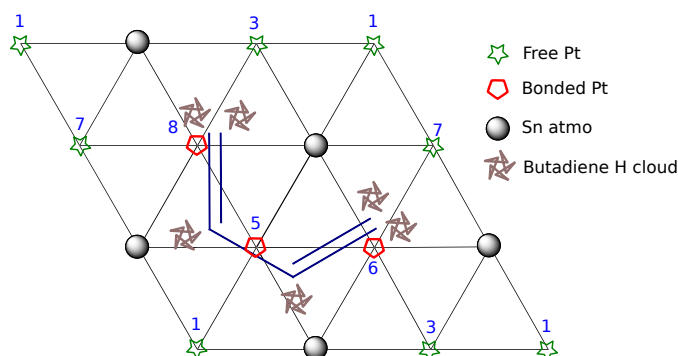


Figure 6.2: Possible adsorption sites for hydrogen in a (3×3) supercell on Sn/Pt-Pt(111) with one butadiene already adsorbed in the cell in the *cis*-1, 4*di* σ -2, 3 π conformation

terminal carbon atom of the chain. Because of that, H atoms of butadiene are pointing in their direction which causes a small destabilization (see Figure 6.2). The Pt number 1 is adjacent to a Pt forming a π bond with the two C inside the chain. As can be seen on Figure 6.2, H atoms of the molecule are pointing towards the Sn atoms and do not interfere with the hydrogen adsorbed on this site which can explain the slightly larger stability. To conclude, we consider that the site 3 and 7 are equivalent but different from the site number 1 which is the most stable one. With the optPBE functional, we found the same order in stability for the H sites, with a stronger total adsorption energy, which is expected for butadiene when passing from PBE to optPBE.

6.4 How chemisorbed butadiene modifies the coverage of hydrogen

We increased the coverage of hydrogen around butadiene up to the maximum of atoms in the cell, by taking into account the preferred sites of H, as determined in Chapter 4. The adsorption energies of each butadiene conformation at each coverage are given in Table 6.3. For optPBE, only the *cis*-1, 4*di* σ -2, 3 π and the *di* σ modes are reported here.

Adsorption site	E_{ads}^{Tot} PBE	E_{ads}^{But} PBE	E_{ads}^{Tot} optPBE	E_{ads}^{But} optPBE
1	-1.07	-0.78	-1.44	-1.21
3	-1.03	-0.73	-1.40	-1.17
7	-1.01	-0.72	-1.38	-1.15

Table 6.2: Adsorption energies (in eV) of hydrogen ($\theta_H = 0.11$ ML) and butadiene in the cis-1, 4di σ -2, 3 π conformation on Sn/Pt-Pt(111) for PBE and optPBE, with hydrogen on top sites

Starting with the results obtained with PBE, we can see that unlike for Pt, adding H atoms did impact the preferred adsorption site on Sn/Pt. From 0.11 ML to 0.33 ML the order in stability stays the same than for butadiene alone on the surface, cis-1, 4di σ -2, 3 π being the most stable followed by trans-di π , trans-1, 2di σ -3, 4 π , cis-di π and the less stable, di σ . From 0.44 ML, the order is changed and is different for each coverage. With this, we calculated the adsorption free energies of each coverage and for each adsorption site of hydrogen and butadiene as a function of the temperature (T in K) and the pressure of hydrogen (P_{H_2} in bar). This leads to five phase diagrams, one for each butadiene adsorption site, given in Figure 6.3. These stability diagrams are similar to those obtained on Pt(111) in Figure 5.4 which means that we force the adsorption of butadiene, and report here the evolution of the coverage of H for T between 0 and 800 K, and with P_{H_2} ranging from 10^{-15} to 10^2 bar. We can observe a large clear area on the right part of the diagrams at high temperature, which corresponds to the clean surface, which is larger in the case of Sn/Pt than in the case of Pt. This means that one has to work at lower temperatures to adsorb butadiene on the alloy. We then find phases corresponding to the intermediate coverages when decreasing the temperature. Finally, we observe a darker area on the left part for low temperatures, corresponding to the highest coverage possible in this range of temperature and pressure. In this case,

	0.11	0.22	0.33	0.44	0.56	0.67
PBE						
cis-1, 4di σ -2, 3 π	-1.07	-1.32	-1.62	-1.49	-1.14	-1.04
trans-1, 2di σ -3, 4 π	-0.94	-1.18	-1.41	-1.51	-1.24	-1.00
trans-di π	-0.89	-1.16	-1.38	-1.32	-1.05	-0.82
cis-di π	-0.82	-1.11	-1.28	-1.38	-1.13	-1.38
di σ	-0.61	-0.89	-1.09	-1.29	-1.27	-1.15
optPBE						
cis-1, 4di σ -2, 3 π	-1.44	-1.67	-1.96	-1.72	-1.23	-0.93
di σ	-1.02	-1.26	-1.44	-1.57	-1.43	-1.18

Table 6.3: Total adsorption energies (eV) of hydrogen and butadiene on Sn/Pt-Pt(111) for the five possible conformations of butadiene and for coverages of hydrogen between 0.11 and 0.67 ML, calculated with PBE (the most stable are in bold letters)

the optimal coverage of hydrogen at $T = 300$ K and $P_{But} = P_{H_2} = 1$ bar is 0.33 ML for the first four conformations, and becomes 0.44 ML for the di σ site even though we are at the limit of no adsorption at all. As already mentioned before, this conformation is partially decoordinated, which leaves more space on the surface for H to adsorb and thus, gives rise to a higher optimal coverage. The structures of the cis-1, 4di σ -2, 3 π and di σ modes at their optimal coverages are given in Figure 6.4. Figure 6.5-a shows that the cis-1, 4di σ -2, 3 π adsorption site, with $\theta_H = 0.33$ ML, is the most stable one when compared to the other adsorption modes. As for Pt(111), we can see in Figure 6.5-b that the change of functional does not affect the order of stability of the adsorption modes; the cis-1, 4di σ -2, 3 π site with $\theta_H = 0.33$ ML stays the most stable between 0 and 600 K using optPBE, and for the chosen conditions.

As for platinum, we further investigated the co-adsorption of butadiene and hydrogen concentrating on the totally coordinated most stable mode, namely cis-1, 4di σ -

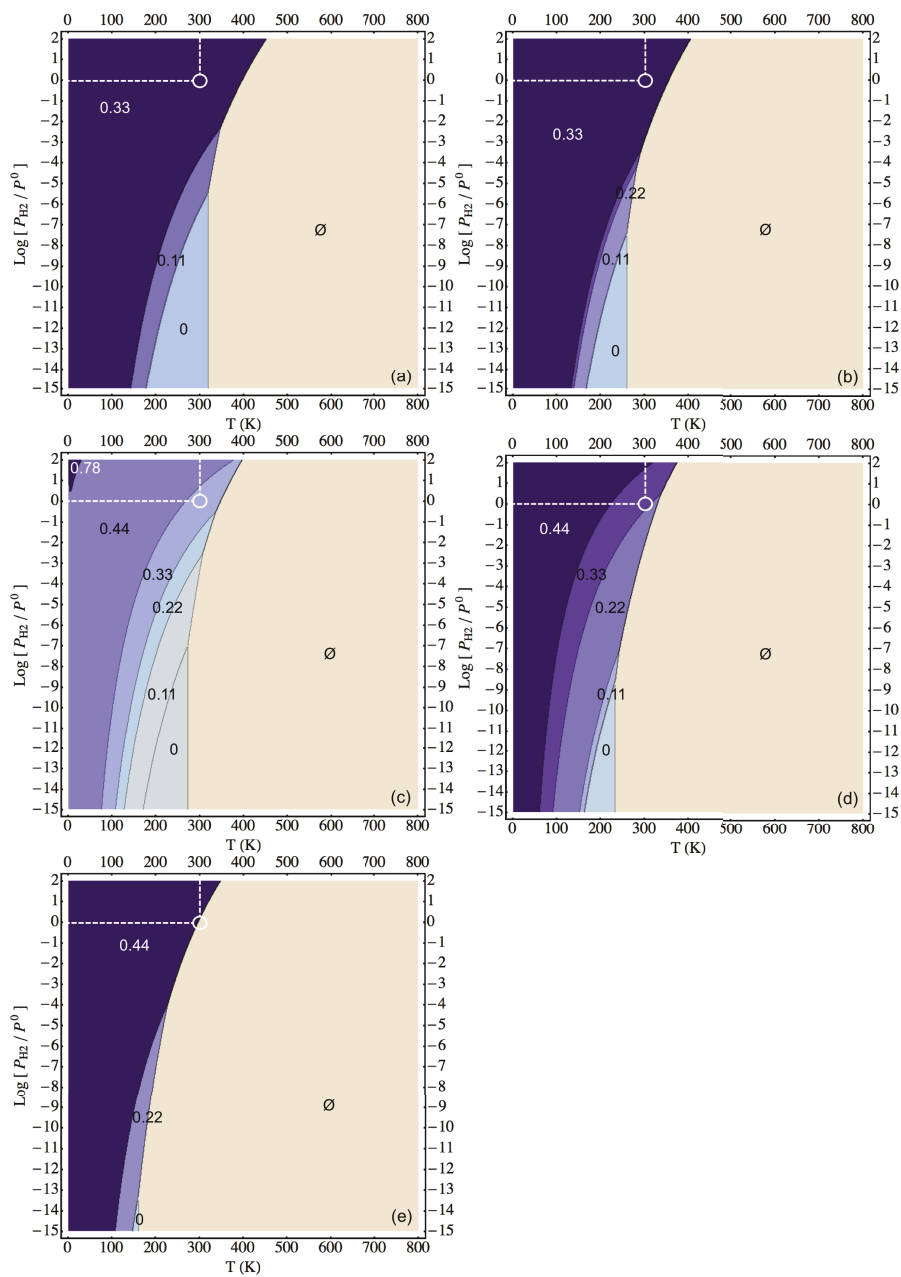


Figure 6.3: Hydrogen coverage on a surface of Sn/Pt-Pt(111) precovered with one butadiene in the cis-1, 4di σ -2, 3 π , trans-1, 2di σ -3, 4 π (b), trans-di π (c), cis-di π (d), di σ (e) conformations, obtained with PBE

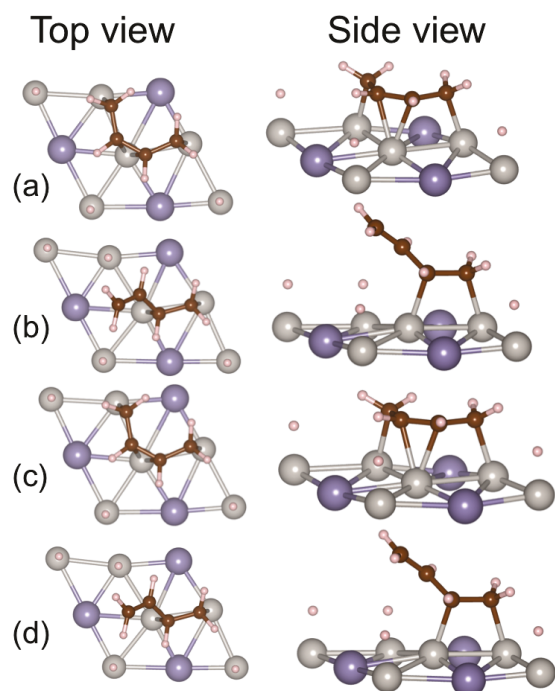


Figure 6.4: Geometrical structures of the cis-1,4di σ -2,3 π and the di σ mode at their optimal coverage on Sn/Pt-Pt(111), calculated with PBE (a: $\theta_H = 0.33$ ML, b: $\theta_H = 0.44$ ML), and with optPBE (c: $\theta_H = 0.33$ ML, d: $\theta_H = 0.33$ ML)

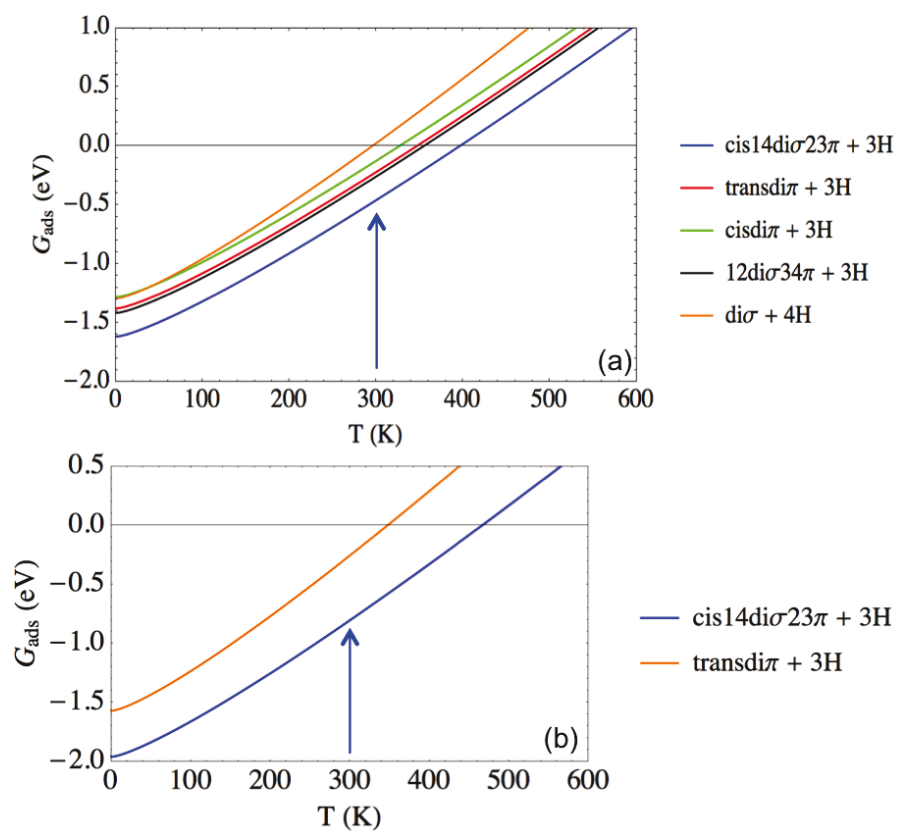


Figure 6.5: Adsorption free energies of the five possible adsorption modes of butadiene calculated with PBE (a) and of the $\text{cis-1,4di}\sigma\text{-2,3}\pi$ and the $\text{di}\sigma$ mode calculated with optPBE (b) on Sn/Pt-Pt(111), for $P_{\text{H}_2} = P_{\text{But}} = 1$ bar

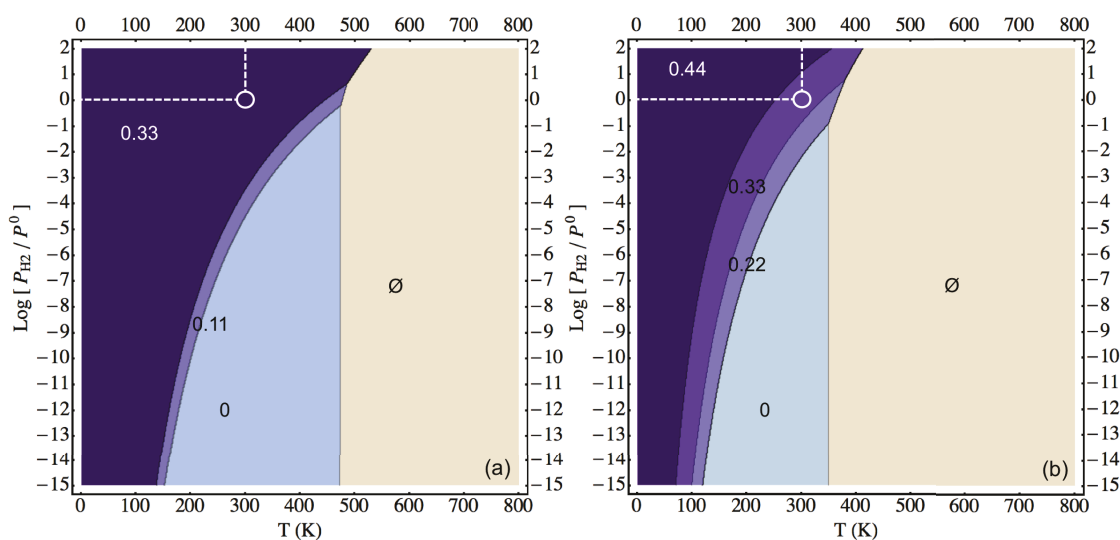


Figure 6.6: Hydrogen coverage on a surface of Sn/Pt-Pt(111) precovered with one butadiene in the *cis*-1, 4*di* σ -2, 3 π (a), and *di* σ (b) conformations, obtained with optPBE

2, 3 π , and the partially decoordinated mode, *di* σ . The results obtained with optPBE are given in Figure 6.6. One can see that the optimal coverage of the first mode stays the same when changing the functional, while it changes for the second one and becomes 0.33 ML. The *di* σ diagram is the most strongly affected by the change of functional as a new phase appears for $\theta_H = 0.33$ ML. Also, we can remark that the purple area, corresponding to the adsorption of the molecules, is larger when using optPBE compared to PBE. Indeed the adsorption starts at about 530 K for the *cis*-1, 4*di* σ -2, 3 π mode and 410 K for the *di* σ one with optPBE instead of 450 and 350 K with PBE. This is to correlate to the fact that optPBE gives stronger adsorption energies than PBE.

6.5 Competitive chemisorption of butadiene and hydrogen

In order to understand what surface species are present on the surface as a function of the temperature and the pressure, we compare the co-adsorption of hydrogen and butadiene to the adsorption of hydrogen alone, as done for Pt(111). The results of this comparison are shown in Figure 6.7. The first striking information that we extract from this figure is that the co-adsorption of hydrogen and butadiene in its $di\sigma$ adsorption mode is never more stable than hydrogen alone on the surface in these range of T and P. Indeed, one can see that the panel c corresponds entirely to the phase diagram of hydrogen alone seen in Chapter 4. When we switch the functional and use optPBE (panel d), the $di\sigma$ co-adsorption phase limit (red) is adjacent to restrained area of the chosen conditions ($T=300$ K and $P_{H_2} = P_{But} = 1$ bar). Thus, the optimal conformation is composed by hydrogen only, with a coverage of 0.44 ML. In contrast, the $cis-1, 4di\sigma-2, 3\pi$ adsorption site has a stability phase using both functional and is the most stable conformation together with 0.33 ML of hydrogen at the optimal conditions when using optPBE. However, with PBE, the optimal configuration stays 1 ML of hydrogen alone.

To conclude, this stability diagrams show that with PBE, 9H atoms in the cell are more stable than any co-adsorption configuration while with optPBE, the co-adsorption with butadiene in the $cis-1, 4di\sigma-2, 3\pi$ mode and 3H atoms is the most stable configuration. In any case, the $di\sigma$ adsorption site does not adsorb strongly enough to exist within this range of T and P.

6.6 What about butadiene physisorption ?

Because of the previous results, we also studied the physisorption of butadiene on a partially hydrogenated surface of Sn/Pt (see Table 6.4). At first we can see that physisorbed

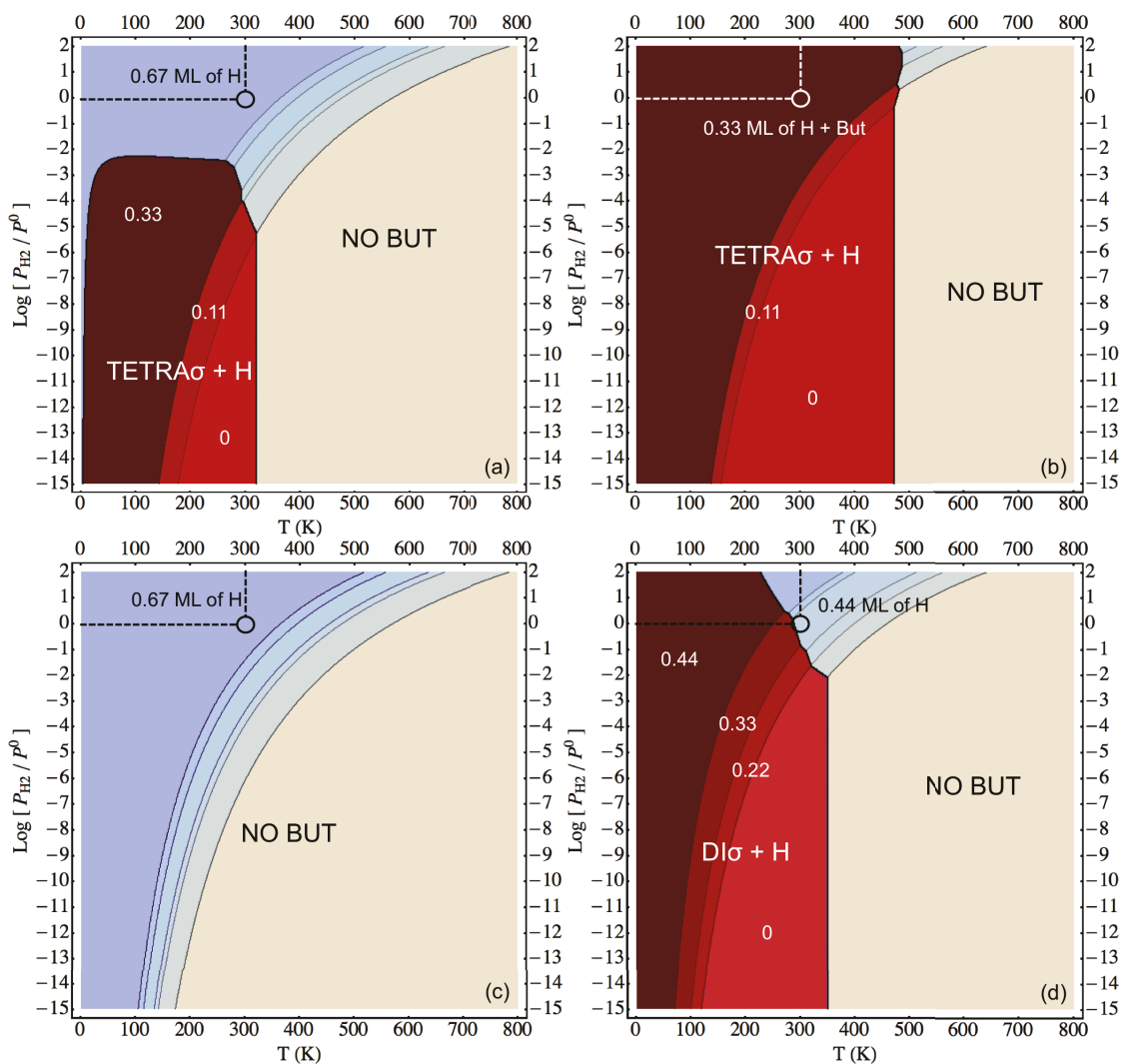


Figure 6.7: Thermodynamic diagram showing the most stable conformation as a function of T and P when comparing the co-adsorption of hydrogen and butadiene (red) to the adsorption of pure hydrogen (light blue and beige) on Sn/Pt-Pt(111) for two butadiene modes : the $\text{cis-1, 4di}\sigma\text{-2, 3}\pi$ calculated with PBE (a) and optPBE (b), and the $\text{di}\sigma$ calculated with PBE (c) and optPBE (d)

states exist from 0.44 to 0.67 ML using both functionals. For both cases, the physisorbed states in presence of 4H in the cell is less stable than the chemisorbed one, while for 5 and 6H, it is more stable. Their structures given in Figure 6.8 show that, using PBE, butadiene is farther to the surface with Pt-C distance of 4.60 Å compared to optPBE that gives a distance of 4.33 Å. This structural consequence of the functional is larger in this case than when using the Pt catalyst. The main difference is that here, the adsorption sites of H do not change with the functional whereas on Pt(111), they change from fcc with PBE to top with optPBE. Even though the molecule interacts more strongly when using optPBE, the higher distance between H atoms in top positions and Pt atoms increases the distance between the molecule and the surface. With H in fcc sites, lower than top sites, the distance between the surface and butadiene is decreased which softens the effect of functional on the Pt-C distance. The Table 6.5, presents the adsorption free energies of the same structures. As we did for Pt(111), we also corrected the entropy of butadiene with a two dimensional translation term (see Eq.5.1 of Chapter 5). This contribution stabilizes the physisorbed states of about 0.29 eV and is independent of the functional, the coverage and the surface catalyst.

Now we know that at certain conditions, the hydrogenated surface is more stable than the system composed by chemisorbed butadiene co-adsorbed with hydrogen, we investigated the relative stability of this hydrogenated surface and physisorbed butadiene.

Figure 6.9 and Figure 6.10 show the adsorption free energies of the different possible adsorption states (χ or ϕ) for PBE and for optPBE. In the case of PBE (Figure 6.9), we can see that 6H atoms alone on the surface are more stable than the co-adsorption of hydrogen and butadiene with $\theta_H = 0.33$ ML. In panel b, we decreased the ratio P_{H_2}/P_{But} to 10^{-3} and this causes a shift of the blue curve (6H) towards higher energies. The system 3H+But χ has become more stable than H alone. Unlike in the case of Pt(111), we see here that this change of pressure ratio affects the relative stability of

θ_H (ML)	PBE χ	PBE ϕ	optPBE χ	optPBE ϕ
0.11	-1.07	\emptyset	-1.44	\emptyset
0.22	-1.32	\emptyset	-1.67	\emptyset
0.33	-1.62	\emptyset	-1.96	\emptyset
0.44	-1.49	-0.90	-1.72	-1.20
0.56	-1.14	-1.15	-1.23	-1.35
0.67	-1.04	-1.37	-0.93	-1.52

Table 6.4: Total adsorption energies (E_{ads} in eV) of hydrogen and butadiene in the cis-1, 4di σ -2, 3 π mode when chemisorbed (χ) and in cis gas phase conformation when physisorbed (ϕ), on Sn/Pt-Pt(111); \emptyset means no structure found

θ_H (ML)	PBE χ	PBE ϕ	PBE ϕ 2D	optPBE χ	optPBE ϕ	optPBE ϕ 2D
0.11	-0.24	\emptyset	\emptyset	-0.60	\emptyset	\emptyset
0.22	-0.33	\emptyset	\emptyset	-0.67	\emptyset	\emptyset
0.33	-0.46	\emptyset	\emptyset	-0.81	\emptyset	\emptyset
0.44	-0.18	0.42	0.13	-0.41	0.11	-0.18
0.56	0.33	0.32	0.03	0.23	0.12	-0.17
0.67	0.59	0.25	-0.03	0.69	0.11	-0.18

Table 6.5: Total adsorption free energies (G_{ads} in eV at T= 300 K and $P_{But} = P_{H_2} = 1$ bar) of hydrogen and butadiene in the cis-1, 4di σ -2, 3 π mode when chemisorbed (χ) and in cis gas phase conformation when physisorbed (ϕ), on Sn/Pt-Pt(111); \emptyset means no structure found; 2D means that a two dimensional component of the translation is taken into account in the calculation of the entropy

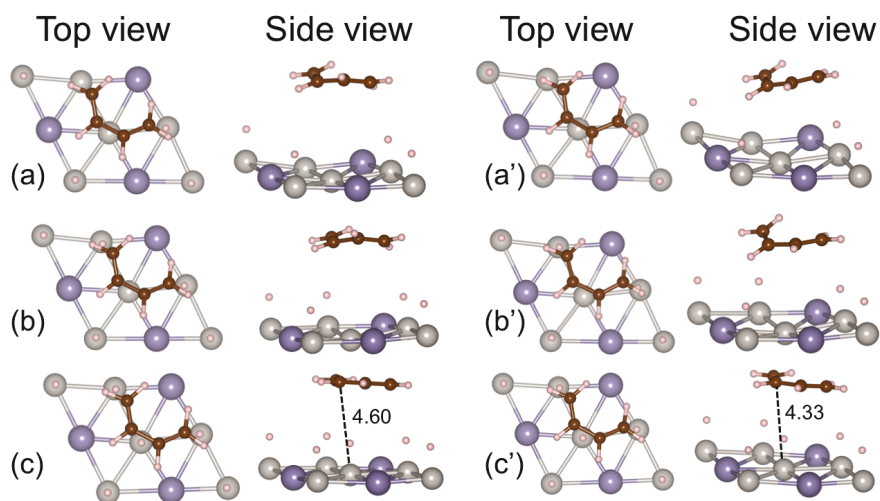


Figure 6.8: Top and side view of the structures of $4\text{H}+\text{But}\phi$ (a), $5\text{H}+\text{But}\phi$ (b) and $6\text{H}+\text{But}\phi$ (c) on Sn/Pt-Pt(111) obtained with PBE and optPBE (a', b', c')

these systems. Using optPBE (Figure 6.10), we see that the chemisorbed state in presence of 3H is always lower in energy. In panel b, we increased the hydrogen pressure to obtain a pressure ration of 10^3 . The physisorbed states remain less stable for both ration (a and b) and the 4H curve (blue) crosses the co-adsorbed system curve (red) at the limit of the desorption of the species.

6.7 Conclusion

From this we conclude that at the optimal conditions ($T=300\text{ K}$ and $P_{H_2} = P_{But} = 1\text{ bar}$), PBE favours the adsorption of hydrogen over the co-adsorption. In this case, the Eley-Rideal mechanism would be preferred for the first hydrogenation, involving physisorbed butadiene (see Figure 5.12). On the contrary, using optPBE, the composition of the surface would lead to a Langmuir-Hinshelwood mechanism with strongly adsorbed reactants (see Figure 5.12). The study of the behaviour of hydrogen and buta-

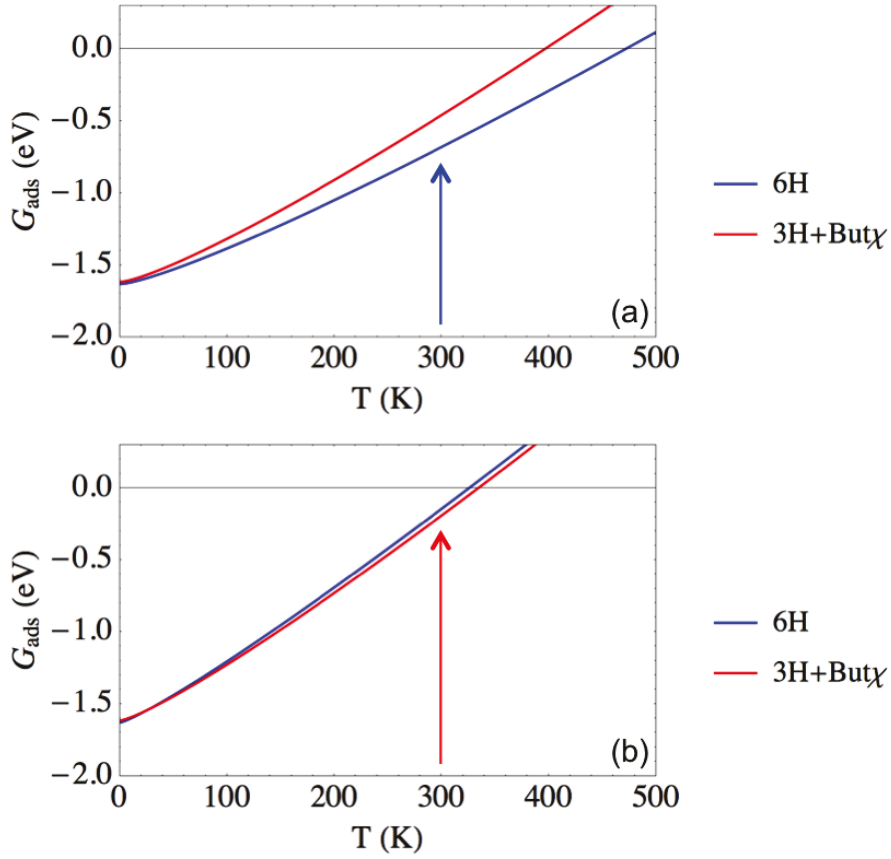


Figure 6.9: Relative stability of two systems on Sn/Pt-Pt(111) calculated with PBE: hydrogen with $\theta_H = 0.67$ ML (6H), and butadiene chemisorbed on a partially hydrogenated surface (3H+But χ); we propose two pressure ratio: $P_{H_2}/P_{But} = 1$ (a) and $P_{H_2}/P_{But} = 10^{-3}$ (b)

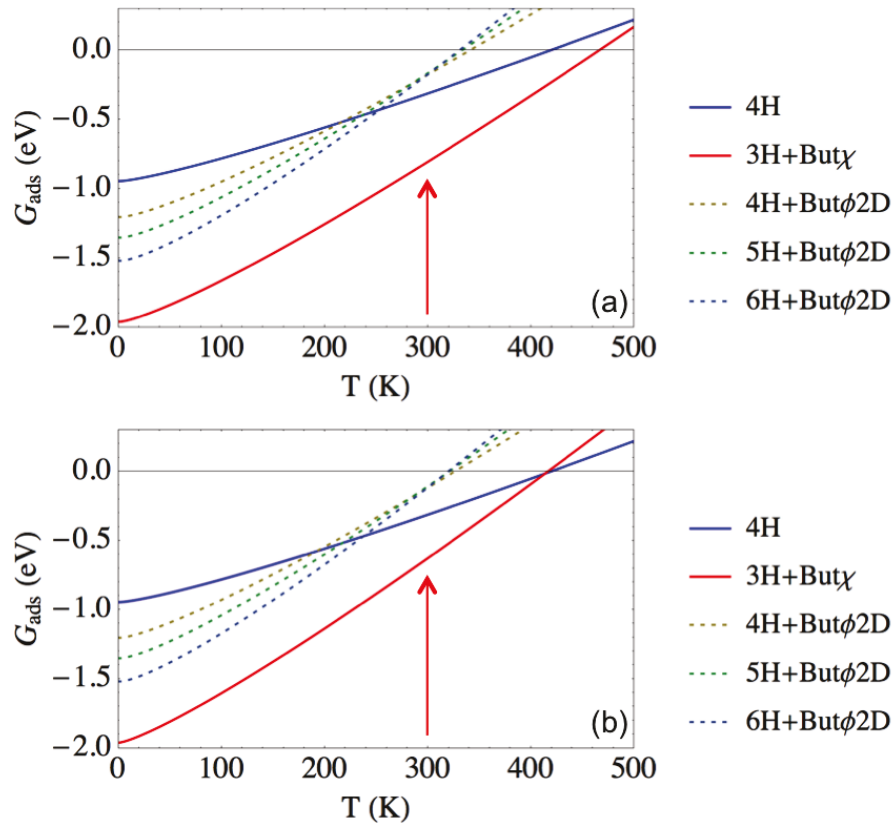


Figure 6.10: Relative stability of different systems on Sn/Pt-Pt(111) calculated with optPBE: hydrogen with $\theta_H = 0.44$ ML (6H), butadiene chemisorbed on a partially hydrogenated surface (3H+But χ), butadiene physisorbed on a partially hydrogenated surface (4H+But ϕ , 5H+But ϕ and 6H+But ϕ); we propose two pressure ratio: $P_{\text{H}_2}/P_{\text{But}} = 1$ (a) and $P_{\text{H}_2}/P_{\text{But}} = 10^{-3}$ (b)

diene adsorption and co-adsorption on Pt(111) and Sn/Pt-Pt(111) bring to similar conclusions with respect to the influence of the functional. This brought new insights on the thermodynamics of these systems, which were necessary to set up the following kinetic study of butadiene hydrogenation at high coverage of hydrogen.

Chapter 7

Butadiene hydrogenation as a function of the coverage on Pt(111) and Sn/Pt-Pt(111)

Contents

7.1 Introduction	126
7.2 Pt(111)	128
7.2.1 Low coverage	128
7.2.2 Intermediate coverage	132
7.2.3 High coverage	145
7.2.4 Conclusion	150
7.3 Sn/Pt-Pt(111)	150
7.3.1 Low coverage	151
7.3.2 Intermediate coverage	152
7.3.3 Conclusion. Comparison with Pt(111)	160

7.1 Introduction

The Horiuti-Polanyi reaction scheme of butadiene hydrogenation is given in Figure 7.1. One can see that there are many pathways to form butane out of butadiene. For a matter of time, we focused our interest in the first two steps of the hydrogenation reaction, which means from butadiene to 1-butene, 2-butene and radical. The radical intermediate butan-1,4-diyl (B14R) was found high in energy and thus not taken into account. Previous results obtained in our laboratory on the hydrogenation of butadiene on Pt(111) and Sn/Pt-Pt(111) describe the reaction mechanisms at low coverage, e.g. at $\theta_H = 0.11$ ML.^{4,74} The Langmuir-Hinshelwood mechanism is occurring in this case as there are few molecules on the surface and enough free sites for them to adsorb before reacting (see Figure 5.12 of Chapter 5). At this coverage, the only H atom present on the surface is consumed by butadiene during the first hydrogenation. To realize the second hydrogenation we consider the adsorption of a "new" H atom coming from the gas phase ($\frac{1}{2}H_2$), on a site that allows to obtain the most stable system (see Chapter 5). This model implies to keep the hydrogen coverage constant during the hydrogenation reaction. We apply this approach to the studies of higher coverages. Our aim is develop a solid method to investigate the impact of the coverage on the hydrogenation barriers and on the selectivity of this reaction, on Pt(111) and Sn/Pt-Pt(111). As explained before, we used two different functionals; the standard PBE functional allows to compare our results with previous studies while the optPBE vdW-type functional takes into account the long range interactions existing between butadiene and the surface. The results obtained with both functionals are presented for each coverage of our interest and on both catalyst. In order to approach realistic conditions, the pathways presented here result from the calculations of the free energy of the different species (given in $\text{kJ}\cdot\text{mol}^{-1}$) at $T = 300$ K and $P_{But} = P_{H_2} = 1$ bar (see Chapter 2). As mentioned before, the coverage of butadiene is always kept at 0.11 ML. Using PBE, we saw in Chapter 5 that, when the thermodynamic equilibrium is reached, butadiene remains in the gas phase. Hence,

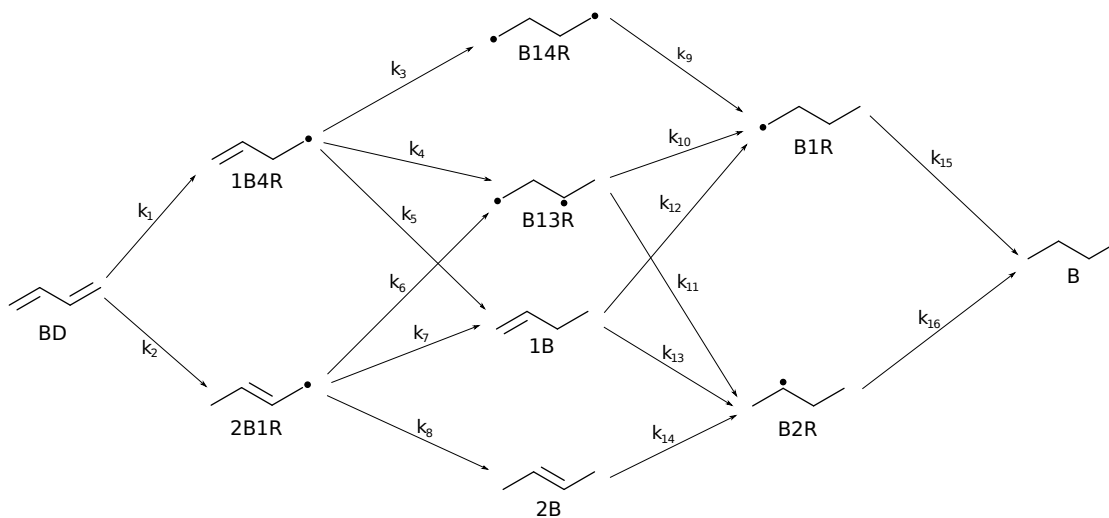


Figure 7.1: Horiuti-Polanyi reaction scheme of butadiene hydrogenation (BD: butadiene, 1B: 1-butene, 2B: 2-butene, B: butane)

the hypothesis of a low coverage of butadiene is certainly valid. Using optPBE, this hypothesis becomes more debatable as this functional reverses the relative stability of butadiene and hydrogen compared to PBE, and describes a strong adsorption of butadiene. One could imagine to obtain higher coverages of butadiene at the thermodynamic equilibrium. However, a (3×3) cell does not allow to adsorb two molecules of butadiene on the same adsorption site without having the molecules share a Pt atom which would be very unfavoured. We could extend the size of the cell to study higher coverages of butadiene but this would be very time consuming. Thus we considered the hypothesis of $\theta_{But} = 0.11$ ML accurate enough for this stage of our work.

The computational details are the same than those described in Chapter 5.

7.2 Pt(111)

7.2.1 Low coverage

The only adsorption mode of butadiene considered at low coverage is the most stable one e.g. the trans-tetra σ mode.

PBE

Figure 7.2-a shows the first two steps of the hydrogenation pathway of butadiene with a constant coverage of 0.11 ML. As we saw in Chapter 5, this coverage does not correspond to the thermodynamic equilibrium at $T = 300$ K and $P_{H_2} = 1$ bar. However, to understand the effects of H coverage on the reaction pathway, it is necessary to start the study at low coverage. The sum of the energy of the partially hydrogenated surface ($\theta_H = 0.11$ ML) and the energy of butadiene in the gas phase was taken as a reference, and thus was set at 0 kJ.mol⁻¹. We can see that butadiene (BD) adsorbs very easily (-88 kJ.mol⁻¹) before the first hydrogenation barrier of 88 kJ.mol⁻¹. As already known, the two first transition states (TS) are very close in energy.⁴ TS1 corresponds to the attack of H on C₂, while TS2 corresponds to the attack on C₁. As you can see in Figure 7.3-a and b, the TS are composed of a three-center Pt-C-H unit. They lead to two intermediates, 1buten-4yl (1B4R) and 2buten-1yl (2B1R) that are radical species and stick quite strongly on the surface (see Figure 7.4-a and b). After the first hydrogenation, the coverage is 0 ML as the only hydrogen adsorbed was consumed by the molecule. We assume that one dihydrogen molecule dissociates which provides a "new" hydrogen atom in the cell. This is an exothermic process as the surface is not saturated and thus allows stabilizing adsorption of H. With this, the coverage is back to 0.11 ML. From the two intermediates, the second hydrogenation occurs with different possibilities for H to attack⁴ which leads to five TS, corresponding to k_4 , k_5 , k_6 , k_7 and k_8 of Figure 7.1. Their geometry are given in Figure 7.3-c to e. As noted earlier,

B14R is not very stable and hence, the TS leading to it was not taken into account in this work. The products obtained on the surface are 1-butene (1B), 2-butene (2B) and the radical butan-1, 3-diyl (B13R). Their structures are shown in Figure 7.4. TS4 and TS5 are the transition states obtained when hydrogenating 1B4R into B13R and 1B respectively (purple in Figure 7.2). TS6, TS7 and TS8 are formed from 2B1R and lead to B13R, 1B and 2B respectively. We remark that the barrier leading to TS1 and TS2 is the limiting step of this path. The selectivity towards butene is controlled by the second barrier. The lowest TS, TS6 and TS7, are close in energy with 5 kJ.mol⁻¹ of difference. TS6, the lowest, leads to the radical B13R, while TS7 allows to form 1B. As the desorption barrier of 1B is slightly exothermic, this process is most likely to happen. Also, the further hydrogenation of B13R is limited by the next barrier. Even though it is not shown here, we expect this hydrogenation barrier to be of at least about 70-80 kJ.mol⁻¹, which would favour the desorption process. We note that the desorption of 2B is also slightly endothermic but its formation on the surface is unfavoured as TS8 is higher than TS6 and TS7 of about 15 kJ.mol⁻¹.

optPBE

Figure 7.2-b shows the same two first steps of butadiene hydrogenation at low coverage but calculated with optPBE. We can see that the global appearance of this diagram is close to the one obtained with PBE. For example, the hydrogenation barriers corresponding to TS1 and TS8 are of 90 and 103 kJ.mol⁻¹, to compare to 88 and 95 kJ.mol⁻¹ with PBE. However, we can see that butadiene adsorption free energy is larger with 134 kJ.mol⁻¹ instead of 88 with PBE. This is no surprise as we saw in Chapter 5 that optPBE gives stronger adsorption energies for butadiene than PBE. A second effect of the change of functional is the energy cost to desorb butene; for 1-butene, we pass from 15 with PBE to 70 kJ.mol⁻¹ with optPBE. The conclusion is that optPBE stabilizes the adsorbed species of about 50 kJ.mol⁻¹ compared to PBE. The geometrical structures of

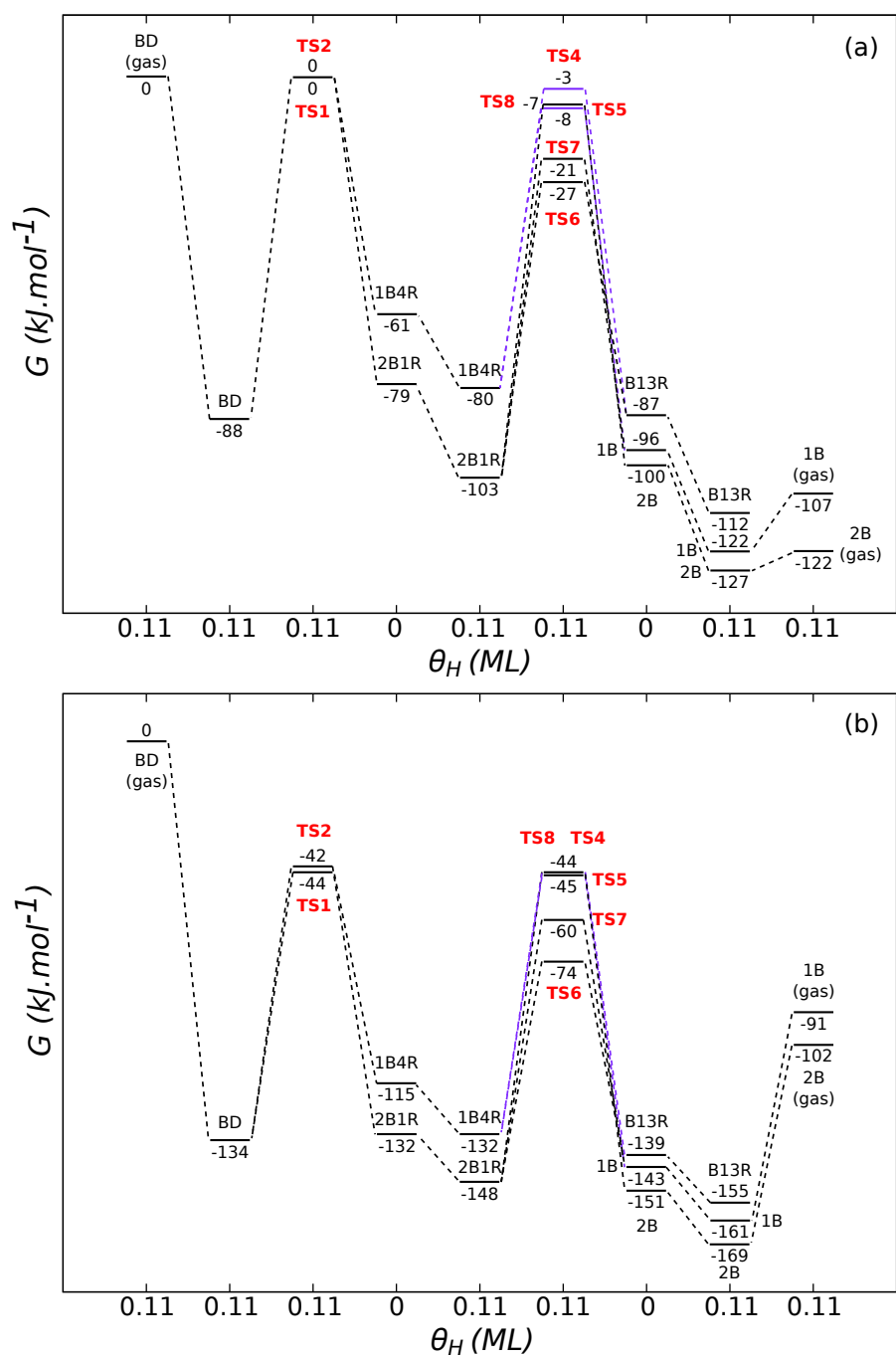


Figure 7.2: Butadiene hydrogenation pathway calculated with PBE (a) and optPBE (b) on Pt(111) for $\theta_H = 0.11$ ML; the purple path corresponds to the hydrogenation of 1B4R into 1B and B13R

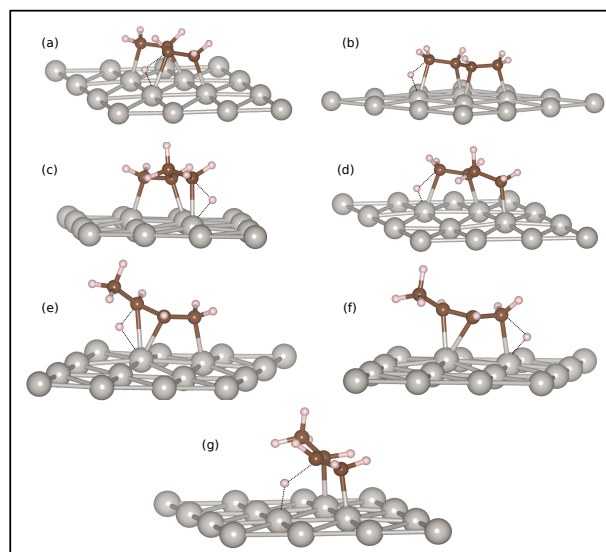


Figure 7.3: Geometrical structures of TS1 (a), TS2 (b), TS5 (c), TS4 (d), TS7 (e), TS8 (f) and TS6 (g) corresponding to the reaction pathway of $\theta_H = 0.11$ ML on Pt(111), calculated with PBE

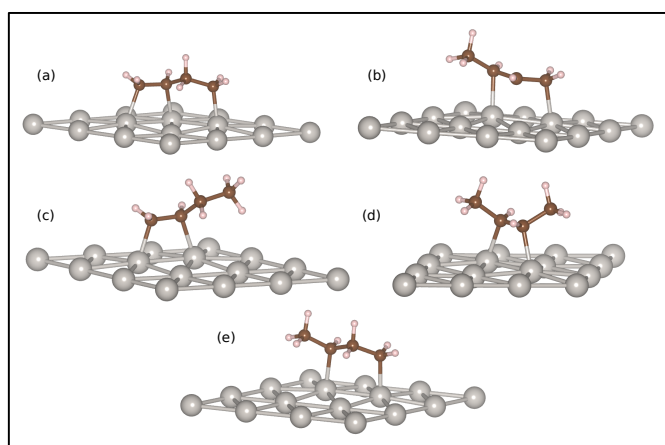


Figure 7.4: Geometrical structures of 1B4R (a), 2B1R (b), 1B (c), 2B (d) and B13R (e) corresponding to the reaction pathway of $\theta_H = 0$ ML on Pt(111), calculated with PBE

the transition states are almost exactly the same as those obtained with PBE. Indeed we saw in Chapter 3 and 5 that the change of functional did not impact the structures of butadiene apart from a small shorten of the Pt-C distance with optPBE. It did impact on the preferred site of hydrogen but as we are at low coverage in this case, the structures presented in Figure 7.3 are accurate enough to describe the species obtained with optPBE. Finally, using optPBE, the second hydrogenation TS stay in the same relative order of stability than when using PBE, with TS6 leading to B13R still being the lowest. However, the desorption barriers of 1B and 2B are higher (70 and 65 kJ.mol⁻¹) which implies a stronger competition between the desorption and the further hydrogenation of B13R. With this, we conclude that the use of optPBE impacts on the selectivity of the reaction.

7.2.2 Intermediate coverage

We investigated the hydrogenation pathways of this reaction at intermediate coverages as we saw with the co-adsorption results that the thermodynamic equilibrium at T= 300 K and $P_{H_2} = P_{But} = 1$ bar is reached at 0.56 ML with PBE and optPBE, when considering a fully coordinated mode (trans-tetra σ). As we are also interested in the di σ mode that is partially decoordinated, we explored its reaction pathway at $\theta_H = 0.67$ ML for PBE and 0.44 ML for optPBE, which corresponds to the optimal coverage of H at 300 K and 1 bar (θ_H^*) for this adsorption site.

trans-tetra σ

Figure 7.5-a shows the hydrogenation pathway of butadiene in its trans-tetra σ conformation on a partially hydrogenated surface with $\theta_H = 0.56$ ML and calculated with PBE. The adsorption free energy of butadiene is only of 32 kJ.mol⁻¹ because of the five H atoms adsorbed in the cell. This creates a quite strong repulsive interaction between the molecule and H atoms and between H atoms themselves which destabilizes

the system. The first hydrogenation barrier is of 75 kJ.mol^{-1} for TS1 and the second is of 70 kJ.mol^{-1} for TS8, instead of 88 and 95 kJ.mol^{-1} at low coverage. Thus, a second effect of the increase of the coverage is a decrease of the barriers, which is illustrated by these two examples, with -13 kJ.mol^{-1} for the first and -25 kJ.mol^{-1} for the second. We can remark that the intermediates are not stabilized anymore by the arrival of one more H in the cell, as they were in the case at low coverage. Indeed, 1B4R and 2B1R are almost not affected by the adsorption of an additional H atom. This is due to the fact that we are close to the thermodynamic equilibrium. On the contrary, the add of one H atom to obtain 0.56 ML on the surface causes a change in the order of stability of the products. The radical B13R becomes more stable than 1B with a slightly exothermic process, while 1B becomes 19 kJ.mol^{-1} less stable than it was at 0.44 ML. This could be due to the positions of H atoms in the cell. For this case, other combination of hydrogen adsorption around butadiene must be tested. Also, the formation of 2B undergoes an exothermic process of 16 kJ.mol^{-1} when increasing the coverage. Finally, the desorption of butene has become exothermic at this coverage instead of the endothermic process observed at low coverage. Now if we look at the relative order of the second barrier TS, we remark an inversion of TS7 and TS6, which implies the formation of 1B to be more likely with a barrier of 57 kJ.mol^{-1} instead of 82 at low coverage. Also adding the decrease of the barrier of TS8 leading to 2B, we can conclude that the selectivity of this reaction is affected by the increase of hydrogen coverage as the barriers are lowered and the desorption process is favoured over the hydrogenation of B13R. The structures of the transition states are shown in Figure 7.6-a and b. They did not change drastically with the increase of coverage as we recognize the three-center units composed of one Pt, one C and the H atom attacking the molecule.

Figure 7.5-b shows the hydrogenation pathway of butadiene in the trans-tetra σ mode, calculated with optPBE and for the intermediate coverage of 0.56 ML. As already observed at low coverage, the change of functional causes a stabilization of about

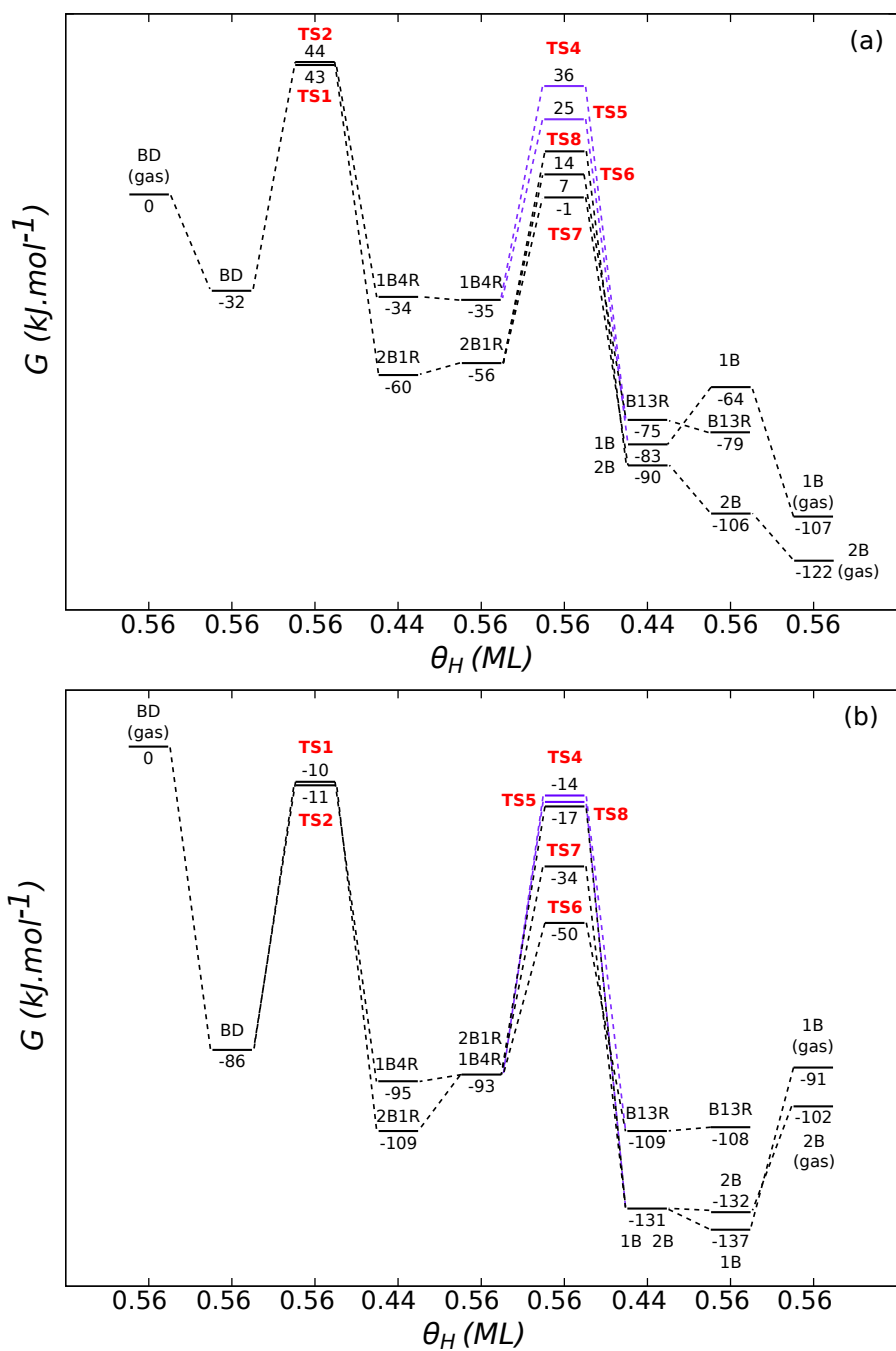


Figure 7.5: Butadiene hydrogenation pathway calculated with PBE (a) and optPBE (b) on Pt(111) for $\theta_H = 0.56$ ML; the purple path corresponds to the hydrogenation of 1B4R into 1B and B13R

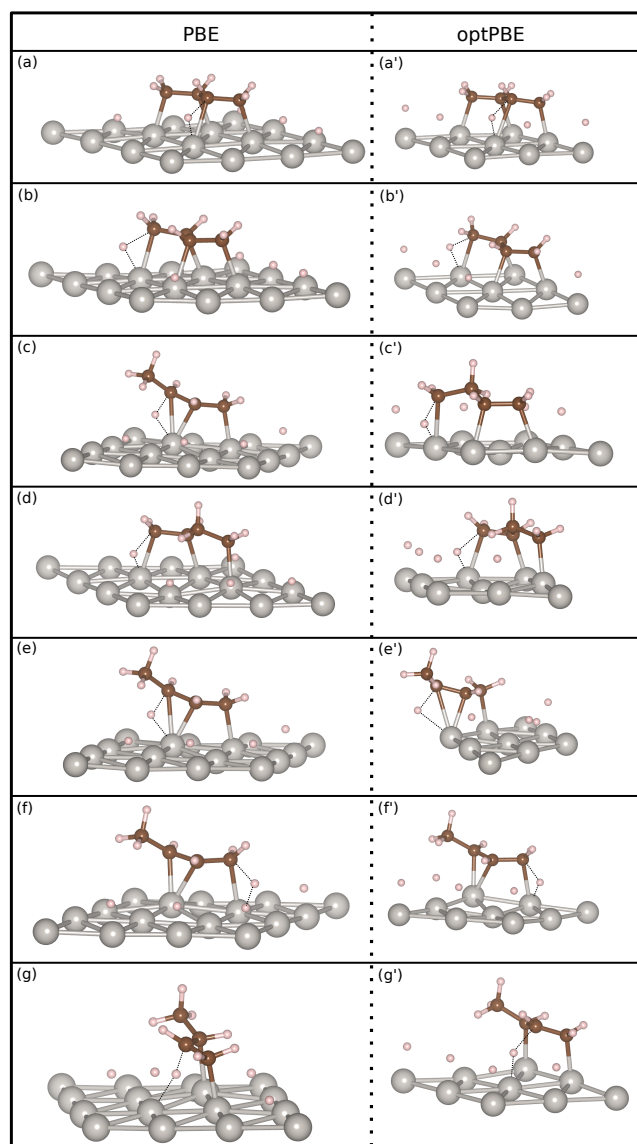


Figure 7.6: Geometrical structures of TS1 (a and a'), TS2 (b and b'), TS5 (c and c'), TS4 (d and d'), TS7 (e and e'), TS8 (f and f') and TS6 (g and g') corresponding to the reaction pathway of $\theta_H = 0.56$ ML on Pt(111), calculated with PBE and optPBE (')

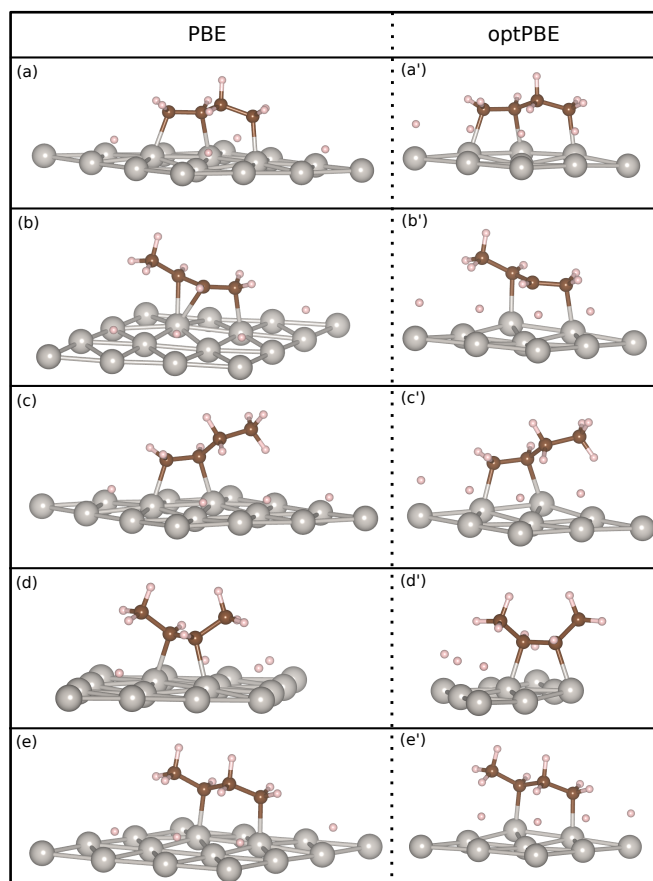


Figure 7.7: Geometrical structures of 1B4R (a and a'), 2B1R (b and b'), 1B (c and c'), 2B (d and d') and B13R (e and e') corresponding to the reaction pathway of $\theta_H = 0.44$ ML on Pt(111), calculated with PBE and optPBE (')

50 kJ.mol⁻¹ which gives an adsorption free energy of BD of -86 kJ.mol⁻¹ instead of -32 kJ.mol⁻¹ with PBE. We also remark that the increase of the coverage from 0.44 to 0.56 ML causes a larger destabilization of 2B1R when using optPBE compared to PBE while 1B4R is not affected. The desorption barrier of 1B and 2B are smaller than at low coverage but remain an endothermic process (+46 and +35 kJ.mol⁻¹). However, B13R is now too high to allow the further hydrogenation to compete with the desorption process. We also observe that the relative order of the TS is now almost the same than the one obtained at low coverage. The inversion of TS6 and TS7 observed in the case of PBE is not occurring using optPBE. The barriers are lower with 40 and 60 kJ.mol⁻¹ instead of 74 and 72 kJ.mol⁻¹ at low coverage but TS6 being quite lower than TS7, the formation of B13R is more likely than the formation of 1B. However, at low coverage, the desorption barriers did suggest a strong competition between the further hydrogenation of the radical and the desorption of butene while at 0.56 ML, the desorption is favoured. We can conclude that using optPBE, the increase of hydrogen coverage has an impact on the selectivity of the reaction even though it is less important than when using PBE. Figure 7.6 shows the TS of this pathway. One can see that they are very close to those obtained using PBE but the hydrogen atoms are now on top sites instead of fcc sites.

di σ

The pathway of this reaction starting from butadiene in its di σ mode (BD-2) is given in Figure 7.8-a at a hydrogen coverage of 0.67 ML and calculated with PBE. This coverage corresponds to the thermodynamic equilibrium at 300 K and $P_{But} = P_{H_2} = 1$ bar. We first see that this conformation implies an endothermic adsorption of 17 kJ.mol⁻¹ and then provides relatively low barriers of 39 and 50 kJ.mol⁻¹ for the first hydrogenation. The two first TS (cisTS2 and trTS2 in Figure 7.9-a and b) both correspond to the transfer of one H atom from the surface to the terminal carbon of the chain (C₁), which is not

coordinated to the surface. This leads to the allyl 2B1R. As demonstrated by Vigné et al.⁷⁴, the attack at C₂ implies the bonding of C₁ with the surface which involves high constraints, and thus is highly unfavoured. For this reason, we reported here only the intermediate species resulting from the attack at C₁ (2B1R) and only the three TS corresponding to the hydrogenation of 2B1R (TS6,TS7 and TS8). We can see that TS7 is still lower than TS6 at this coverage, and the distance between the energies of these two TS is even larger with 16 kJ.mol⁻¹ instead of 8 at 0.56 ML. As for the totally coordinated mode at 0.56 ML, we remark that the desorption of the products is exothermic. The increase of the coverage from 0.56 to 0.67 ML has almost no influence on the products as their energies are almost not affected. This shows that 0.56 and 0.67 ML correspond to situations both very close to the thermodynamic equilibrium. Also, 2B is now lower than B13R of 27 kJ.mol⁻¹ which starts to be significant and suggest the desorption of the molecule to be more likely than the further hydrogenation towards butane. We conclude that the selectivity of the reaction did not change from the one observed at 0.56 ML and strongly favours the formation of gaseous butene. It is important to note that the structures of cisTS2 and trTS2 are quite different from those totally coordinated (TS2) as it is shown in Figure 7.9-a' and b'; instead of the three-center Pt-C-H unit, they form a six-center unit containing two Pt atoms, three C atoms and one H atom. These structures were obtained at low coverage on Sn/Pt where the presence of Sn atoms causes a weaker adsorption of butadiene, and thus favours the diσ conformation. As we saw in Chapter 5, this adsorption mode also exists at low coverage on Pt(111) but it is of about 70 kJ.mol⁻¹ less stable than the coordinated mode (see Table 5.3 for T=0 K as an indication). For this reason we did not consider the possibility of hydrogenating butadiene from this mode at $\theta_H = 0.11$ ML.

Figure 7.8-b shows the first hydrogenation step calculated with PBE for two different conformations: the trans-tetraσ mode co-adsorbed with $\theta_H = 0.56$ ML in black, and the diσ conformation with $\theta_H = 0.67$ ML in blue. The most hydrogenated surface

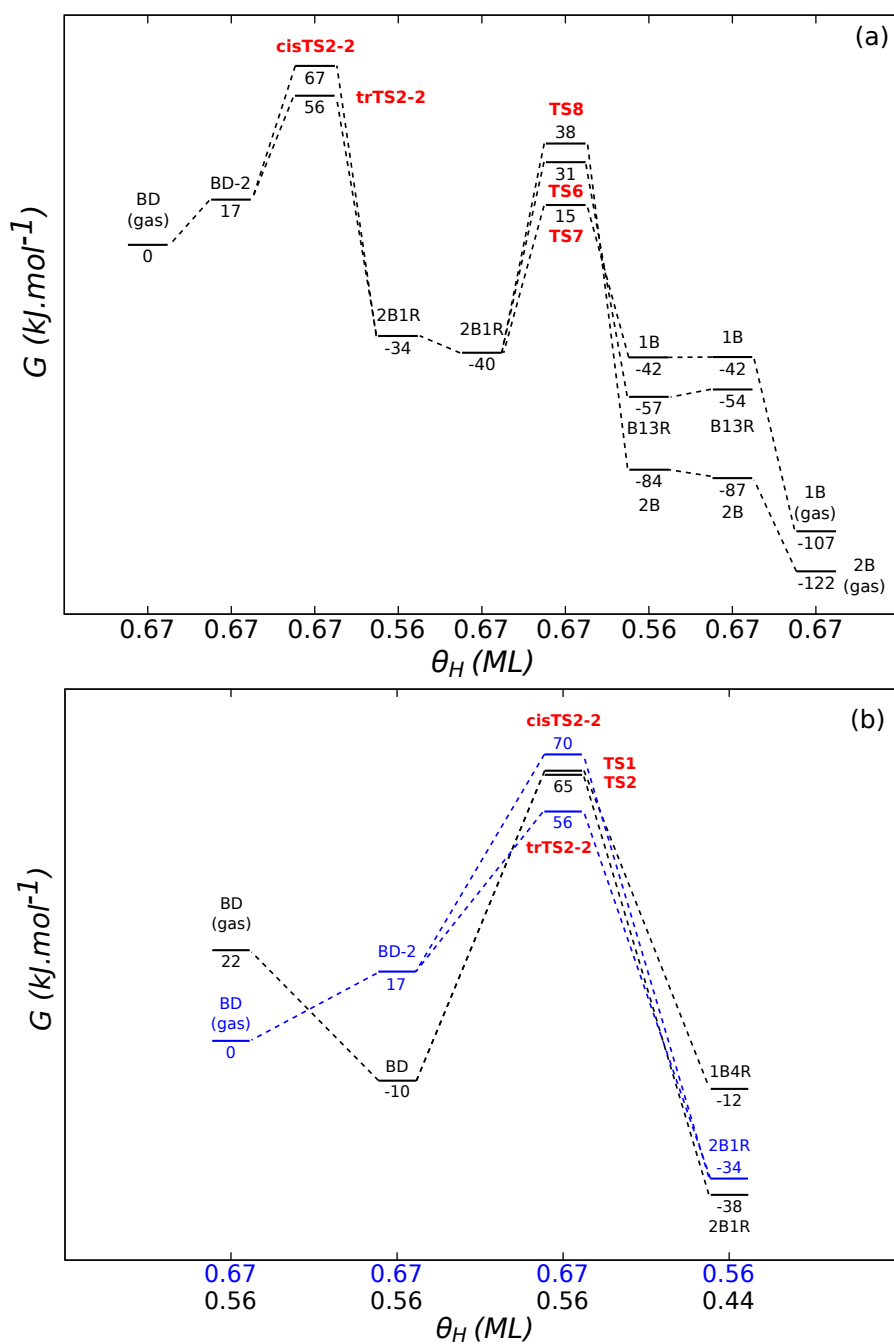


Figure 7.8: Butadiene hydrogenation pathway calculated on Pt(111) with PBE for $\theta_H = 0.67$ ML with butadiene adsorbed in the $\text{di}\sigma$ mode (BD-2) (a); comparison of the first step of this pathway (blue) with the one of the $\text{trans-tetra}\sigma$ mode (black) with $\theta_H = 0.56$ ML (b)

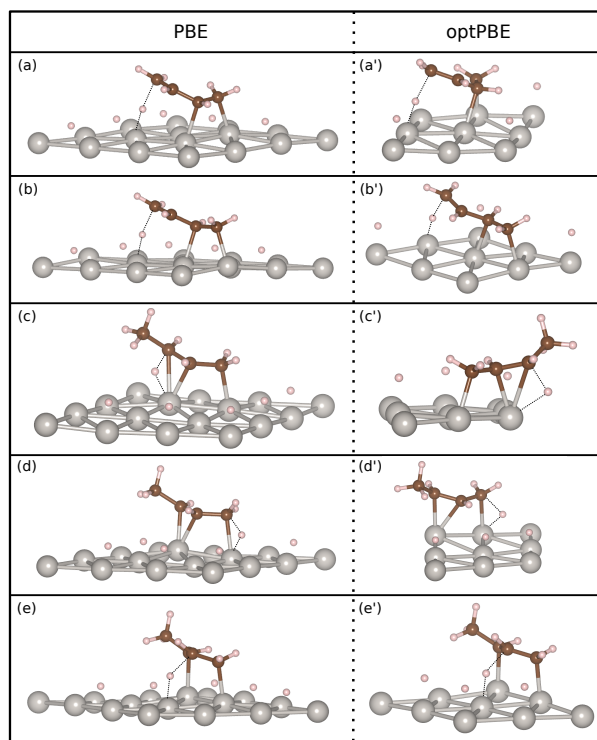


Figure 7.9: Geometrical structures of trTS2 (a and a'), cisTS2 (b and b'), TS7 (c and c'), TS8 (d and d') and TS6 (e and e') corresponding to the reaction pathway of $\theta_H = 0.67$ ML for PBE and $\theta_H = 0.44$ ML for optPBE (') on Pt(111)

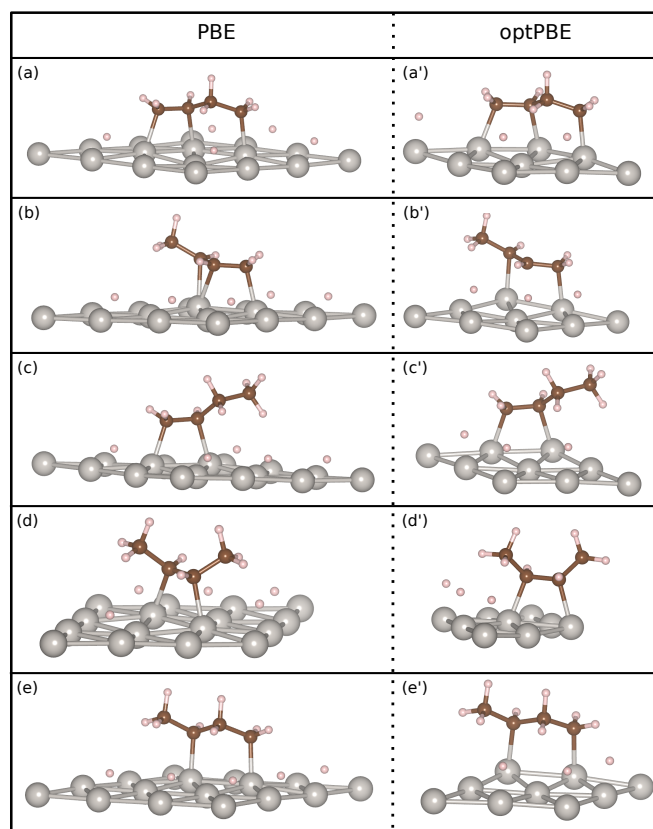


Figure 7.10: Geometrical structures of 1B4R (a and a'), 2B1R (b and b'), 1B (c and c'), 2B (d and d') and B13R (e and e') corresponding to the reaction pathway of $\theta_H = 0.56$ ML for PBE and $\theta_H = 0.44$ ML for optPBE (') on Pt(111)

(0.67 ML) was set as the reference and thus is lower of 37 kJ.mol^{-1} than the less hydrogenated one (0.56 ML). Even though the blue path requires an endothermic adsorption whereas the black one allows a stable adsorption, it crosses the black path because the blue barriers are small enough to give rise lower TS of about 25 kJ.mol^{-1} . It hence provides a less activated pathway. In Chapter 5, we saw that the thermodynamics predicted the $\text{di}\sigma$ adsorption site to be less stable than the $\text{trans-tetra}\sigma$ one. However the pathway study shows that this route is actually favoured when using PBE.

Figure 7.11-a presents the reaction pathway starting from the $\text{di}\sigma$ mode calculated with optPBE, hence at $\theta_H^* = 0.44 \text{ ML}$. As seen in Figure 5.4-f of Chapter 5, the optimal coverage at 300 K and 1 bar is 0.44 ML but the limit with the next phase (0.56 ML) is very close to that point. For this limit case, it seems needed to investigate other possible adsorption sites for H atoms, and to increase the accuracy of our calculations. Indeed, we expected this partially decoordinated mode to allow a higher amount of H atoms in the cell than the totally coordinated one, as this is observed with the PBE functional. Because of the great number of situations studied and presented in this work, an exhaustive investigation of the adsorption sites was not possible, and may be the reason of this curious behaviour. However, PBE and optPBE provide a reverse relative stability of hydrogen and butadiene. This can explain why, in this case, the decoordination is not enough to allow a higher coverage.

The structures of trTS2 and cisTS2 of Figure 7.11-a are given in Figure 7.9-a' and b'. The first large difference between this diagram and the one obtained with PBE (see Figure 7.8) is that the adsorption of butadiene is now exothermic. The second is that the desorption of the products is endothermic. This effects are due to the use of optPBE which stabilizes butadiene adsorption, in this case of about 70 kJ.mol^{-1} instead of 50 kJ.mol^{-1} observed before. The decrease of hydrogen coverage between these two diagrams (0.67 to 0.44 ML) can explain this higher stabilization. Indeed, the lower hydrogen coverage clearly results in a smaller lateral interaction with butadiene. It is

also possible that the change of site impacts on this stabilization. The first hydrogenation barriers of the cis and trans conformations are reduced to 21 and 27 kJ.mol⁻¹ instead of 39 and 50 kJ.mol⁻¹ with PBE. However, the second hydrogenation barrier slightly increased passing from PBE to optPBE, with 61 kJ.mol⁻¹ instead of 55 for TS6. The decrease of hydrogen coverage did not change the relative order of the TS, and thus, the selectivity of the reaction remains close to the one obtained for the trans-tetra σ conformation at 0.56 ML and already discussed above.

We can see in Figure 7.11-b that the exothermic adsorption of the di σ mode and the decrease of the first hydrogenation barriers, both due to optPBE, are not enough to cause a crossing of the blue (di σ) and the black (trans-tetra σ) pathways. The TS belonging to both pathways are very close (5 to 10 kJ.mol⁻¹). However, in this case, the trans-tetra σ adsorption site is more stable than the di σ one of 28 kJ.mol⁻¹, and thus is dictating the reaction route. Using optPBE and at the thermodynamic equilibrium, butadiene hydrogenation occurs with higher probabilities through the totally coordinated mode.

This first part treated the possible hydrogenation routes when considering the Langmuir-Hinshelwood (LH) mechanism at a low and intermediate coverage. However, the conclusions of the co-adsorption study opened to a different mechanism, the Eley-Rideal (ER) mechanism, that proposes a reaction between adsorbed species and weakly adsorbed molecule (see Figure 5.12 of Chapter 5). Indeed, using PBE, the 1 ML hydrogenated surface was found to be the most stable system at the thermodynamic equilibrium chosen at T= 300 K and $P_{H_2} = P_{But} = 1$ bar. As illustrated with the kinetic studies described above, the thermodynamics of a system are not enough to predict which state of the reactant will actually bring to the less expensive pathway. This is why it is necessary to investigate the kinetics of the reaction occurring between physisorbed butadiene and adsorbed hydrogen.

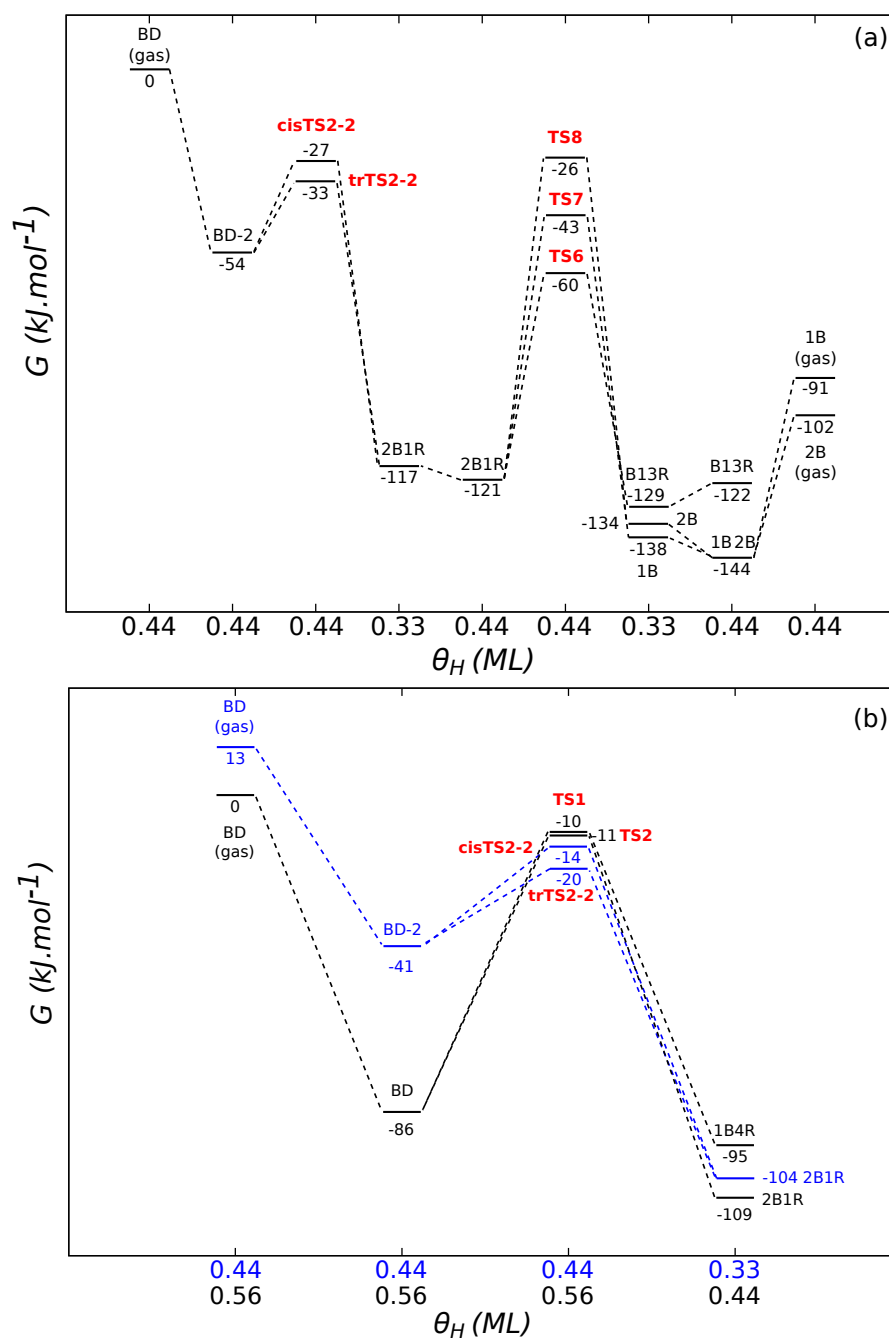


Figure 7.11: Butadiene hydrogenation pathway calculated on Pt(111) with optPBE for $\theta_H = 0.44$ ML with butadiene adsorbed in the di σ mode (BD-2) (a); superposition of the first step of this pathway (blue) with the one of the trans-tetra σ mode (black) with $\theta_H = 0.56$ ML (b)

7.2.3 High coverage

PBE

Figure 7.12-a shows the hydrogenation pathway starting from a physisorbed structure of butadiene calculated with PBE. It can be noticed that TS2 was not found yet and thus is not reported here. The structure of BDphy is shown in Figure 5.9-c of Chapter 5 and the structure of TS1 is shown in Figure 7.13. One can first see that the physisorption is a quite expensive endothermic process (64 kJ.mol^{-1}). The first barrier, of 71 kJ.mol^{-1} , is lower than the one obtained at low coverage (88 kJ.mol^{-1}) and equivalent to the intermediate coverage one (70 kJ.mol^{-1}). The delicate point at that coverage is the co-adsorption of the intermediate and eight H atoms in the cell. Indeed, one cannot consider a physisorbed state for the radical intermediate because it interacts strongly with the surface. We can see that 1B4R is largely destabilized when passing from 0.89 to 1 ML while 2B1R is almost not affected. This different behaviour can be explained by the structures (see Figure 7.14); 1B4R requires more space on the surface as it bonds with four Pt atoms while 2B1R needs only three Pt atoms and is partially decoordinated, leaving more space to H atoms and thus less repulsive interaction. Finally, the second hydrogenation barriers range from 105 to 200 kJ.mol^{-1} and will hardly be overcome to produce butene. This means that this hydrogenation pathway cannot be considered to explain the hydrogenation mechanism.

The entropic loss when physisorbing butadiene can be reduced by the 2D translation correction proposed in Chapter 5. Indeed, the system is stabilized when allowing two degrees of freedom in both directions of the surface to the translational movement. A comparison of the adsorption free energies corresponding to three different approaches are given in Figure 7.12-b. We present here the co-adsorbed system with, on one hand $\theta_H = 0.56 \text{ ML}$, butadiene in the trans-tetra σ mode, on the other hand $\theta_H = 0.67 \text{ ML}$ with the di σ mode, and finally the physisorbed system, with and without the 2D transla-

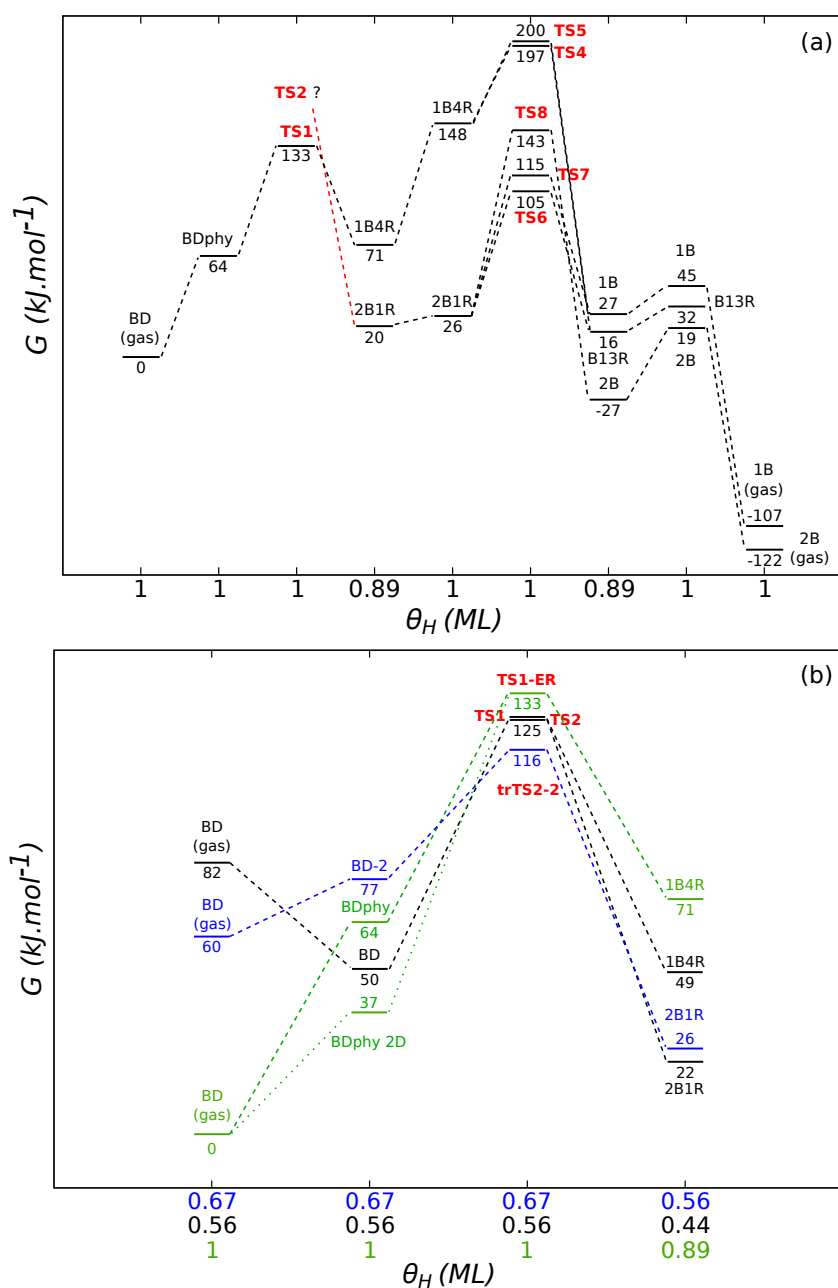


Figure 7.12: Butadiene hydrogenation pathway calculated with PBE on Pt(111) for $\theta_H = 1$ ML with physisorbed butadiene (a); superposition of the first step of this pathway (green) with the one of the trans-tetra σ with $\theta_H = 0.56$ ML (black), and with the one of the di σ with $\theta_H = 0.67$ ML (blue)

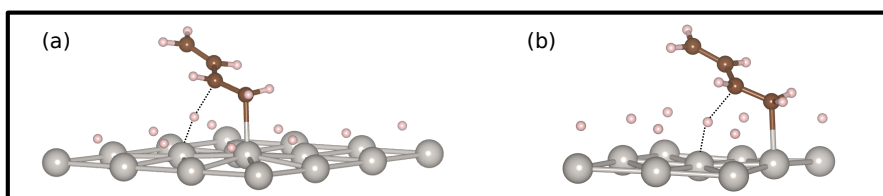


Figure 7.13: Geometrical structure of TS1 at $\theta_H = 1$ ML calculated with PBE (a) and optPBE (b)

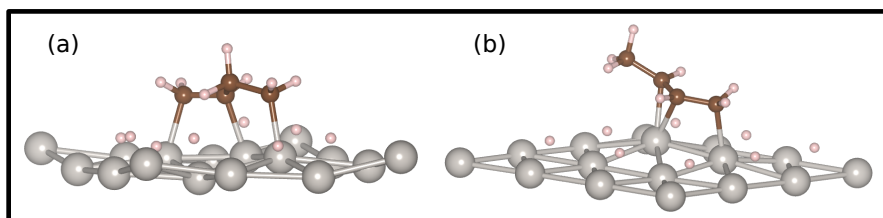


Figure 7.14: Geometrical structure of 1B4R (a) and 2B1R at $\theta_H = 0.89$ ML calculated with PBE

tion correction. The fully hydrogenated surface, which was found to be the most stable system thanks to the thermodynamic study, was set at 0 as the reference. The striking information given here is that, even with an entropic loss of 64 kJ.mol^{-1} , the physisorbed conformation leads to the lowest barrier which is still quite high with 133 kJ.mol^{-1} . Both chemisorbed systems are too unfavoured by the thermodynamics to be competitive with the Eley-Rideal type TS. Indeed, their barrier are much higher than the ER barrier with 162 and 186 kJ.mol^{-1} . One can note that the 2D correction stabilizes the reactant (see Chapter 5) but has no effect on the barrier as the TS is a fixed species and thus loses its three degrees of freedom and cannot translate.

optPBE

The structure of physisorbed butadiene found with optPBE changes from the PBE one as the molecule lies flat above 1 ML of hydrogen adsorbed on top sites instead of fcc sites (see Figure 5.9-c and c' of Chapter 5). As in the case of the PBE study, only the TS1 is presented here and its structure, given in Figure 7.13, is very similar to the one obtained with PBE, with H atoms on top sites instead of fcc sites. The two reaction intermediates (1B4R and 2B1) could not be isolated in this case; as they are radical species, they tend to react very easily to form the products. As H atoms are on top sites and numerous ($\theta_H = 0.89 \text{ ML}$) they are even more accessible in this case than in the case of PBE where they are located on fcc sites. At this coverage, one needs to consider a double and concerted hydrogenation, leading directly to B13R or to butene.

The first step of the reaction pathway is shown in Figure 7.15 for the three different butadiene conformations (trans-tetra σ , di σ and physisorbed) and at the thermodynamic equilibrium. We can see that the consideration of a possible 2D translation stabilizes the physisorbed reactant, but not enough to become more stable than the chemisorbed one. However, the barrier that must be overcome to hydrogenate BD is very high with 118 kJ.mol^{-1} . The blue path corresponding to the partially decoordinated species is of

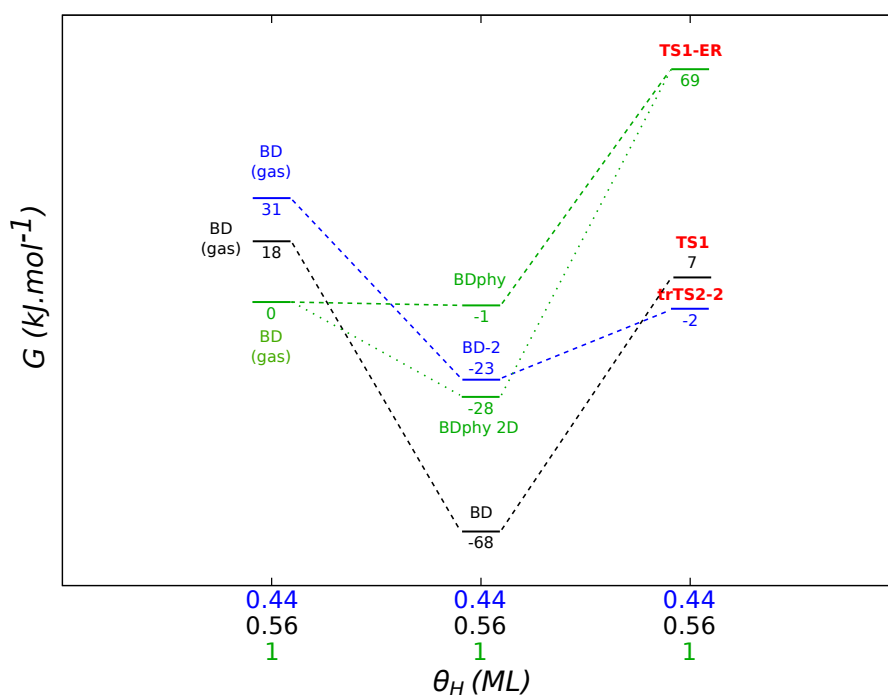


Figure 7.15: Partial butadiene hydrogenation pathway calculated with optPBE on Pt(111) with $\theta_H = 0.56$ ML for butadiene adsorbed in the trans-tetra σ mode (BD, black), with $\theta_H = 0.44$ ML for the di σ mode (BD-2, blue) and with $\theta_H = 1$ ML for the physisorbed state (BDphy, green and dashed green for the 2D contribution)

great interest as it follows a low endothermic barrier of 31 kJ.mol^{-1} to first desorb five H atoms, and then, thanks to a very low hydrogenation barrier of 22 kJ.mol^{-1} , it crosses the black path corresponding to the totally coordinated mode to become the most favourable path. The route obtained through the physisorbed states is very unfavourable with a barrier of 70 kJ.mol^{-1} when considering a fixed physisorbed species, and 98 kJ.mol^{-1} when allowing the species to translate.

7.2.4 Conclusion

We saw that on Pt(111), the PBE functional favours a high selectivity towards the formation of butene at low coverage (0.11 ML) and this effect is stronger when the coverage is increases until 0.56 and 0.67 ML as we observe a stabilization of TS7 which leads to 1B. The use of optPBE decreases the selectivity of the reaction because of the stabilization of the adsorbed species that it induces, and this at both low and intermediate coverage. We conclude the increase of hydrogen coverage has, on one hand, a quantitative effect on the pathway. Indeed, the path obtained at 0.56 ML is very close to the one obtained at 0.11 ML, the TS structures are very similar, but the barriers are lowered and the selectivity is affected in the case of PBE. On the other hand, we also observe a qualitative effect of the increase of θ_H as we saw that it opens new routes, through a partially decoordinated mode ($di\sigma$) or a physisorbed state (BDphy). These new routes are kinetically favoured over the pathways obtained from a totally coordinated mode ($trans-tetra\sigma$). However, the possibility for the reaction to occur through those new pathways depends on the functional. Using PBE avoids to pay the energetic cost of the creation of holes on the totally hydrogenating surface by allowing the ER mechanism through the physisorption of butadiene. The use of optPBE, does not favour a physisorbed state but allows to follow the route opened by the partially decoordinated precursor for a total energetic cost of 31 kJ.mol^{-1} .

7.3 Sn/Pt-Pt(111)

The low coverage mechanism of butadiene hydrogenation on Sn/Pt-Pt(111) was already studied using the PW91 functional.⁷⁴ However, the effect of vdW functionals such as optPBE on the hydrogenation pathway have to be determined. For this reason, we present first in this part the kinetics of butadiene hydrogenation on Sn/Pt-Pt(111) at low coverage. We saw in the Pt study that the thermodynamics predictions needed to

be completed with the kinetic study in order to know what mechanism would occur during the reaction. We present in a second part the pathways obtained at intermediate coverage which were determined at the thermodynamic equilibrium (θ_H^*).

7.3.1 Low coverage

Figure 7.16-a shows the reaction pathway of butadiene at low coverage calculated with PBE. The TS names were chosen to correspond to the TS published in the paper of Vigné et al.⁷⁴. The intermediate species are the same than those found on pure Pt. The cis-1, 4di σ -2, 3 π (BD) and the di σ (BD-2) adsorption modes are considered in this path. One can note that the TS12 leading to 1-butene is missing because it was not obtained yet with these functionals. The green path also leads to 1-butene but contains a very high barrier (TS1, 130 kJ.mol⁻¹) and thus cannot produce 1-butene. This corresponds to the attack on C₂, as one can see in Figure 7.17-b. This is less favourable than the attack on the terminal carbon of the chain, as in the case of Pt(111). We can remark that BD and BD-2 require both a metastable adsorption of 10 and 35 kJ.mol⁻¹ respectively. However, the last mode leads to the lowest TS, TS4-2 which corresponds to an attack on C₁ and gives a six member-unit TS (Figure 7.17-c). The 1-buten-3-yl intermediate (2B1R) is much more stable than 3-buten-1-yl (1B4R) because it requires only two Pt atoms to adsorb instead of three for the second (see Figure 7.18-a).⁷⁴ 2B1R leads to TS8, 9, and 13 shown in Figure 7.17-d, e and f, which themselves lead to 2B, B13R and 2B, the last one having the lowest barrier. The structures of the products are given in Figure 7.18. The desorption of 1B and 2B is strongly exothermic with -107 and -122 kJ.mol⁻¹. We can see that, as for Pt(111), the increase of the coverage from 0 to 0.11 ML after each hydrogenation, stabilizes the system of about 11 kJ.mol⁻¹.

When changing the functional, we observe a stabilization of 61 kJ.mol⁻¹ for BD, and of 45 kJ.mol⁻¹ for BD-2 as you can see in Figure 7.16-b. The TS1 is lower using optPBE than using PBE, but has a higher effective barrier of 147 kJ.mol⁻¹. The rest of

the path is very similar to the one obtained with PBE, apart from the desorption of the products, that is now slightly endothermic because of the stabilization of the adsorbed species brought by the use of optPBE. The structures obtained at low coverage with optPBE are not shown as their are very similar to those obtained with PBE. We remark that changing the functional does not affect the best hydrogenation route which still starts from the BD-2 conformation.

It is difficult to discuss the selectivity of the reaction as the TS12, leading to 1B, is missing. However, we know from previous results obtained with PW91⁷⁴, that this TS is lower than the others and is responsible for the formation of 1B. As the order of relative stability of the other TS of this path is not changed when passing from PBE to optPBE, one can believe that it is also the case for TS12. What we can conclude is that the change of functional does not affect the selectivity of the reaction at low coverage as the desorption process, even slightly endothermic, is still favoured over the further hydrogenation process that implies the next hydrogenation barrier to be at least of 70 kJ.mol⁻¹.

7.3.2 Intermediate coverage

We saw in Chapter 6 that $\theta_H^* = 0.33$ ML for butadiene adsorbed in its cis-1,4di σ -2,3 π mode. The reaction pathway starting from this configuration calculated with PBE is given in Figure 7.19-a and the structures of the surface species along the path are shown in Figure 7.20 for the TS and Figure 7.21 for the intermediates and products. Only the structures calculated with PBE are given here because in the case of Sn/Pt, no change of site is observed for H atoms. Thus, the geometries found with each functional remain very close to each other. The global shape of the pathway is the same of that found at low coverage. However, the adsorption of BD is now stable with -12 kJ.mol⁻¹. Also, the stabilization of the intermediates and the products brought by the increase of the coverage is lower than at low coverage (about 7 kJ.mol⁻¹). As we saw in the case of

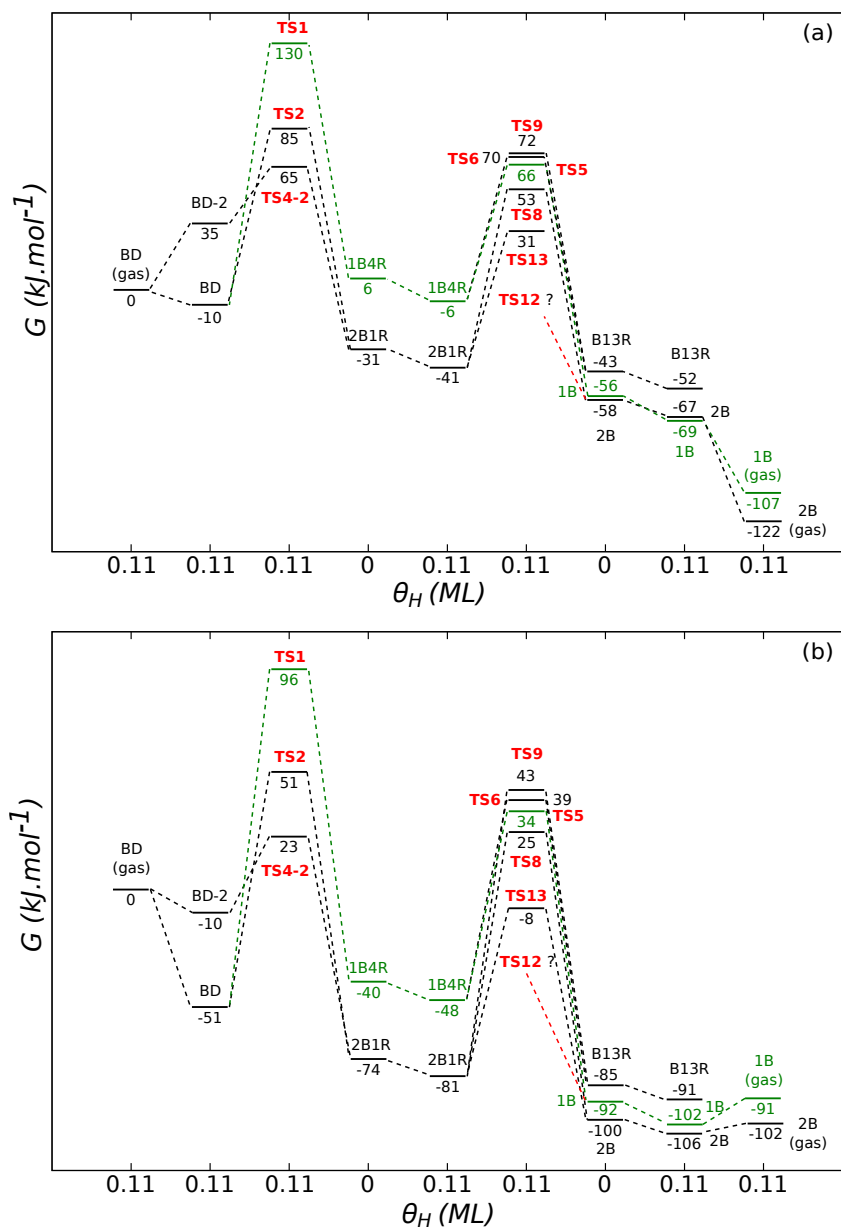


Figure 7.16: Butadiene hydrogenation pathway calculated with PBE (a) and optPBE (b) on $\text{Sn}/\text{Pt-Pt}(111)$ for $\theta_H = 0.11 \text{ ML}$; the green path shows the less favourable path to produce 1-butene

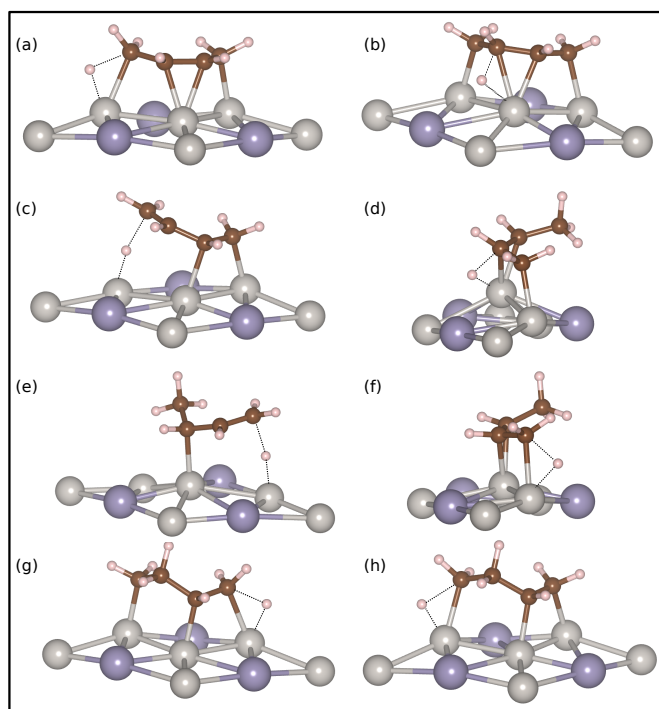


Figure 7.17: Geometrical structures of TS1 (a), TS2 (b), TS4-2 (c), TS9 (d), TS13 (e), TS8 (f), TS6 (g) and TS5 (h) corresponding to the reaction pathway of $\theta_H = 0.11$ ML on Sn/Pt-Pt(111), calculated with PBE

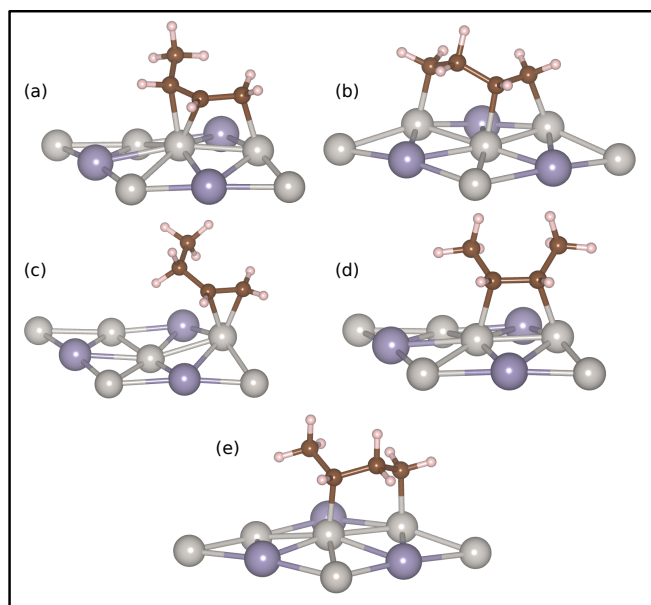


Figure 7.18: Geometrical structures of 2B1R (a), 1B4R (b), 1B (c), 2B (d) and B13R (e) corresponding to the reaction pathway of $\theta_H = 0.11$ ML on Sn/Pt-Pt(111), calculated with PBE

Pt, when we work at conditions close to the thermodynamic equilibrium, the add of one H atom in the cell does not affect strongly the energy of the system. We remark that TS6 and TS9, very close at low coverage, have undergone an inversion at intermediate coverage, bringing the TS9 lower than the 6. However, they are the highest in energy and both form a radical, which does not influence much the selectivity. The other TS are not affected by the increase of coverage as their barriers remain almost exactly at the same level.

Figure 7.19-b shows the reaction pathway through the partially decoordinated mode at θ_H^* , namely 0.44 ML. The adsorption of butadiene is metastable, as for the low coverage situation, and the first barrier is slightly favoured with 60 kJ.mol⁻¹ instead of 65 at low coverage. The stabilization of 2B1R when passing from 0.33 to 0.44 ML is a bit larger with 13 kJ.mol⁻¹ instead of 10 at low coverage. Here we compare the co-adsorption of butadiene and three H atoms to the equilibrium co-adsorption (four H atom), while at low coverage we compare two situations both far from the thermodynamic equilibrium which explains a smaller difference in energy for the low coverage path. The increase of the coverage from 0.11 to 0.44 ML did not change much the second hydrogenation barriers. However, it did affect the barriers of the products when adding one H atom before the desorption. Indeed, it seems that the radical and the two butene molecules co-adsorbed with three H atoms are situations already close to the equilibrium as we observe almost no influence on the energies when adding one more H atom in the cell. The desorption of the butenes is slightly more exothermic than at low coverage, which keeps the reaction selective towards the formation of gaseous butene.

We note that the increase of H coverage from low to an intermediate value does not affect the hydrogenation pathway.

The comparison of the paths corresponding to the coordinated butadiene at 0.33 ML and the decoordinated one at 0.44 ML is given in Figure 7.22. As already seen, the adsorption of butadiene in the cis-1, 4di σ -2, 3 π mode is stabilizing the system while the

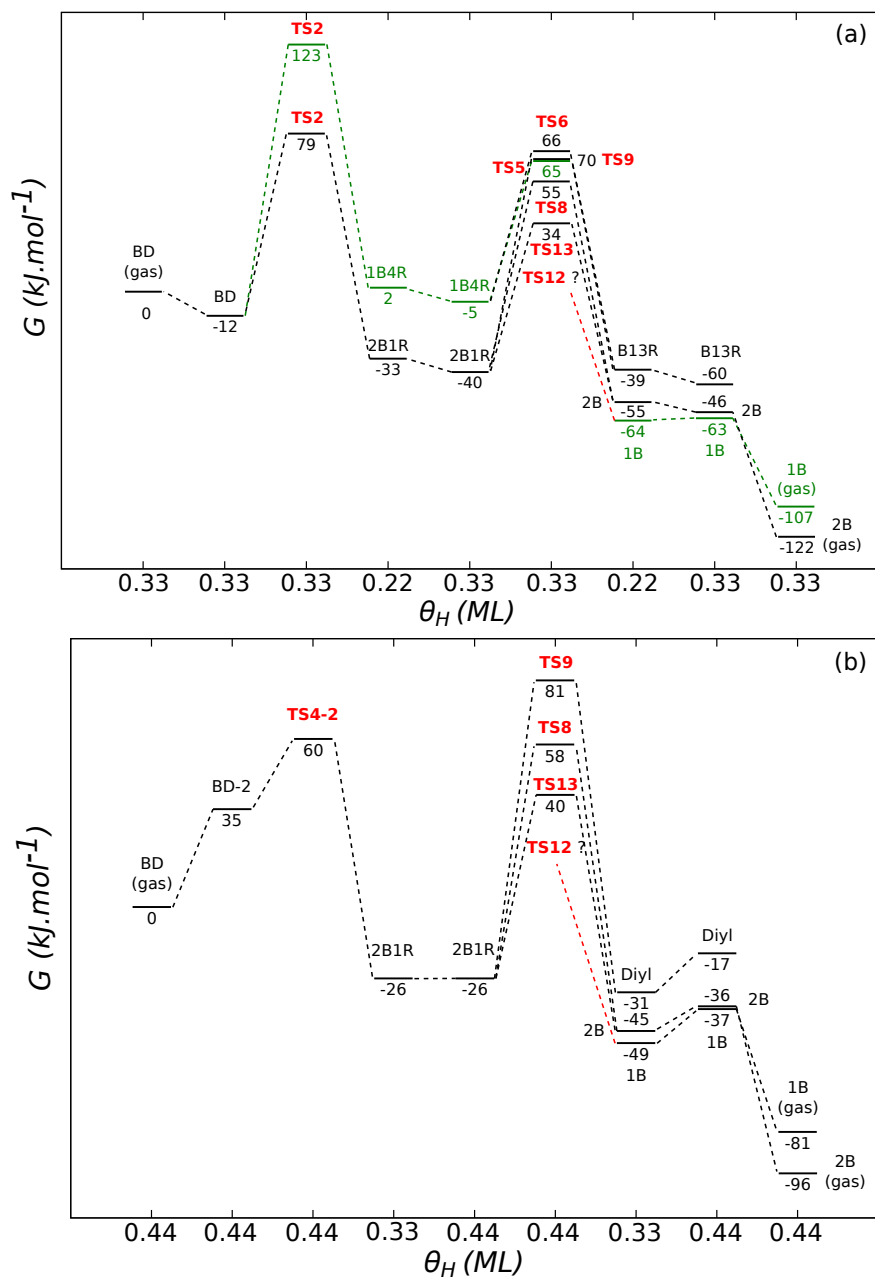


Figure 7.19: Butadiene hydrogenation pathway calculated with PBE for butadiene adsorbed in the $\text{cis-1,4di}\sigma\text{-}2,3\pi$ mode for $\theta_H = 0.33$ ML (a) and the $\text{di}\sigma$ mode for $\theta_H = 0.44$ ML (b) on Sn/Pt-Pt(111)

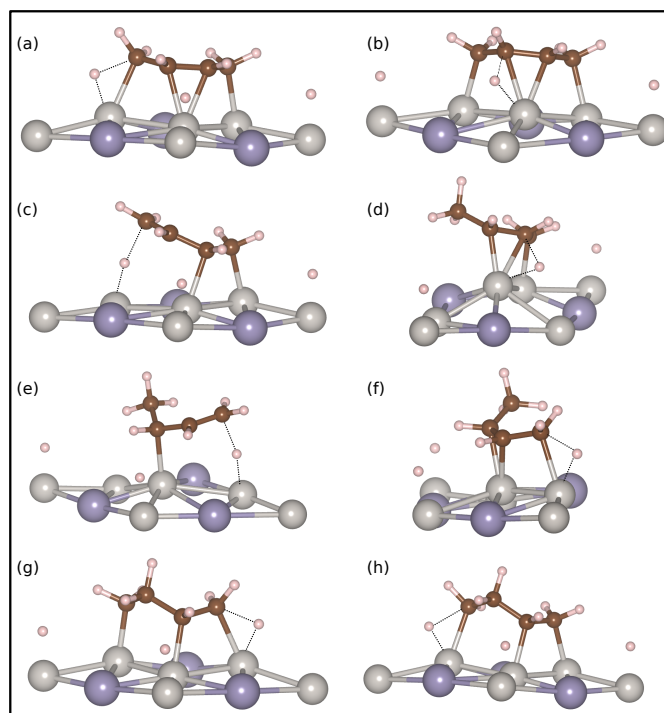


Figure 7.20: Geometrical structures of TS1 (a), TS2 (b), TS4-2 (c), TS9 (d), TS13 (e), TS8 (f), TS6 (g) and TS5 (h) corresponding to the reaction pathway of $\theta_H = 0.33$ ML on Sn/Pt-Pt(111), calculated with PBE

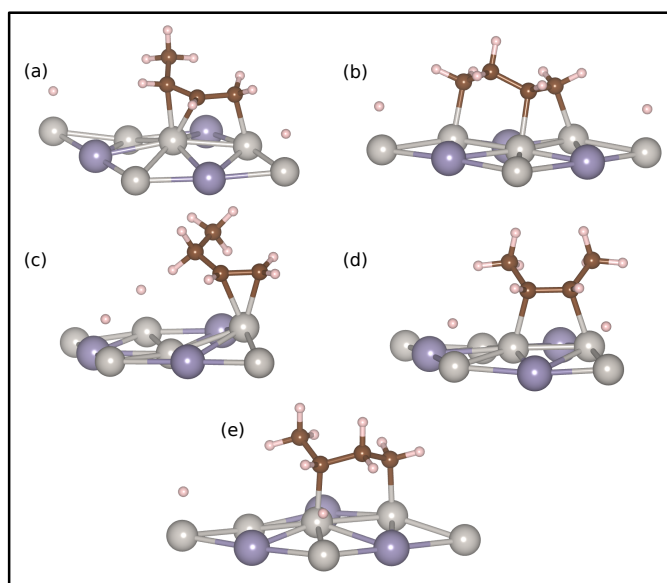


Figure 7.21: Geometrical structures of 2B1R (a), 1B4R (b), 1B (c), 2B (d) and B13R (e) corresponding to the reaction pathway of $\theta_H = 0.22$ ML on Sn/Pt-Pt(111), calculated with PBE

adsorption in the $di\sigma$ conformation is destabilizing the system which causes a crossing of the pathways. However, the barrier leading to TS4-2 is $35 \text{ kJ}\cdot\text{mol}^{-1}$ lower than the one leading to TS2 which makes the blue pathway the most favourable one.

The pathway obtained with optPBE is shown in Figure 7.23. As $\theta_H^* = 0.33 \text{ ML}$ for both the *tetra* and the $di\sigma$ mode, their hydrogenation route are presented in the same figure. TS1 and the pathway corresponding to that precursor are not reported here as this route is largely unfavoured. The adsorption of butadiene on both sites is stabilized by the change of functional, as observed at low coverage. This results in the destabilization of the desorption process. Thus, B13R and the adsorbed butenes are now close in energy. However, the desorption process is favoured with a very low barrier for 1B and an exothermic process for 2B. The adsorption of butadiene in the $di\sigma$ mode which was slightly endothermic with PBE becomes exothermic with $-10 \text{ kJ}\cdot\text{mol}^{-1}$. However, the effective barrier of TS4-2 is not affected by the use of optPBE and remains $30 \text{ kJ}\cdot\text{mol}^{-1}$. TS2 is also not affected by the change of functional. Thus, the hydrogenation route starting from the partially decoordinated mode is even more favoured using optPBE than using PBE.

7.3.3 Conclusion. Comparison with Pt(111)

On Sn/Pt, the low and intermediate coverage study shows that the reaction route opened by the $di\sigma$ mode is always preferred to the $cis-1,4di\sigma-2,3\pi$ mode using PBE and optPBE. We saw that this adsorption site is thermodynamically unfavoured relatively to the fully coordinated one. However it systematically allows a lower first hydrogenation barrier. The main difference with Pt(111) is that even at low coverage, this partially decoordinated mode opens a favoured reaction pathway. This is due to the presence of tin atoms that modify the electronic structure of the surface which destabilizes the total coordination as compared to the partial decoordination. On the platinum surface, only the presence of a certain amount of hydrogen can cause this relative stability balance that

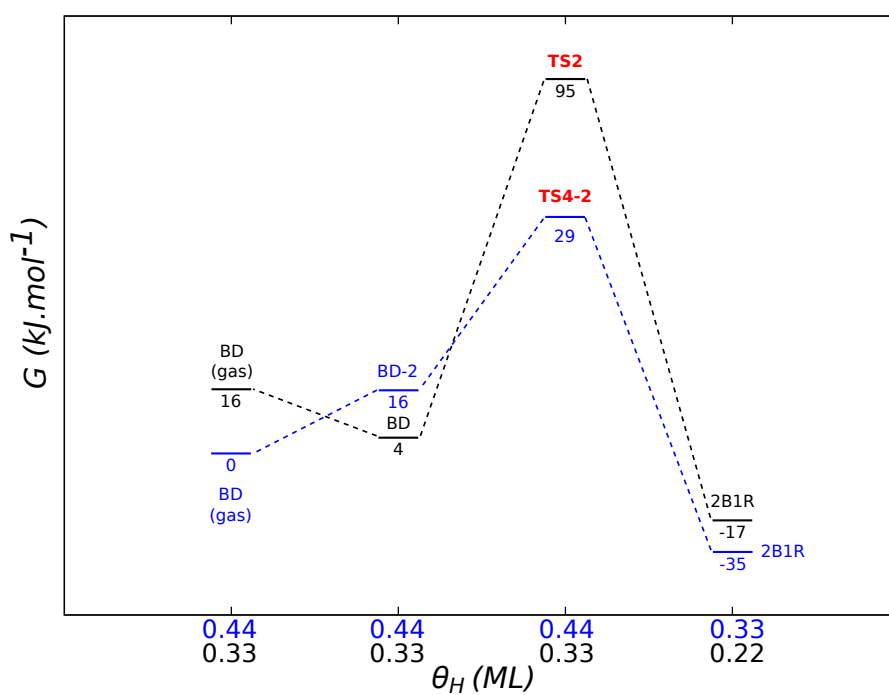


Figure 7.22: Superposition of the pathway obtained from the di σ mode at $\theta_H = 0.44$ ML (blue) and from the cis-1,4di σ -2,3 π mode at $\theta_H = 0.33$ ML (black) on Sn/Pt-Pt(111)

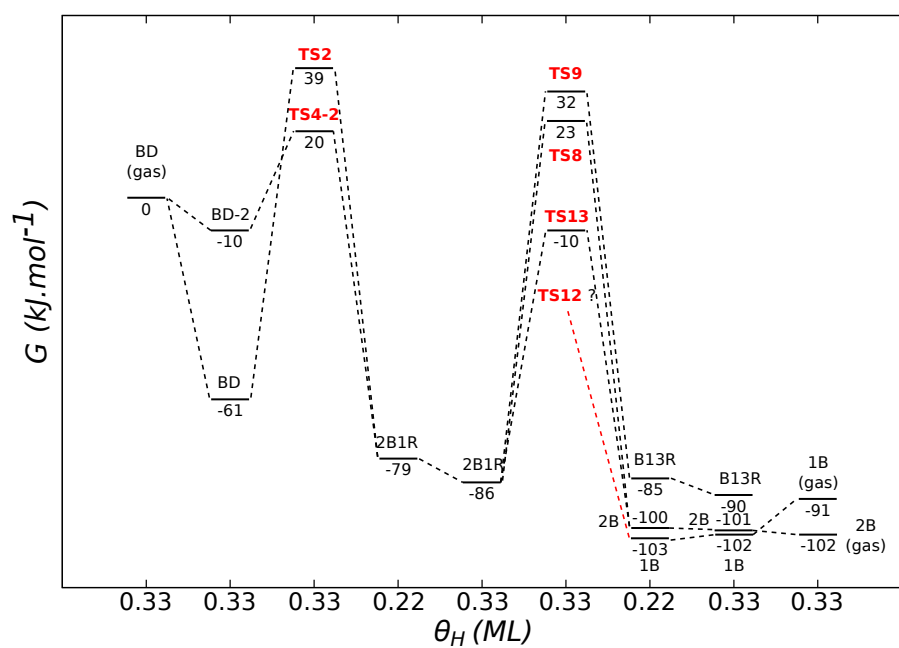


Figure 7.23: Butadiene hydrogenation pathway calculated with optPBE on Sn/Pt-Pt(111) for $\theta_H = 0.33$ ML and with butadiene adsorbed in the cis-1,4di σ -2,3 π (BD) and the di σ (BD-2) mode

favours the $di\sigma$ mode. Hence our interest on the $di\sigma$ adsorption site only at intermediate coverage for Pt(111). We also conclude that the selectivity of this reaction on Sn/Pt is not affected by the increase of hydrogen coverage, neither by the change of functional. The weaker adsorption of butadiene on this catalyst is the key of a higher selectivity, and is also the reason of lower effects on the system when changing the coverage or the functional.

Since the conclusion of the co-adsorption study promoted the fully Sn/Pt hydrogenated surface over a co-adsorbed system when using PBE (see Chapter 6), it is of great importance to investigate the reaction pathways starting from a physisorbed butadiene. This has been initiated and is well under way but cannot be presented in this document already. Considering the results obtained on Pt(111), we may find a preferred route opened by a physisorbed state over a chemisorbed one. Indeed, a strict comparison of the different pathways must be established as done for the systems studied on Pt. Only then, one will be able to conclude on the reaction mechanism occurring on Sn/Pt-Pt(111) at $T = 300$ K and $P_{H_2} = P_{But} = 1$ bar when the thermodynamic equilibrium is reached. Also, a complete thermodynamic study of the intermediates would bring new insights and rule on the accuracy of the slow diffusion hypothesis.

Chapter 8

Conclusion

Through the different studies presented in this work, we saw that it is very important to accurately describe the lateral interaction between hydrogen and the unsaturated molecule on the surface. Indeed, this is conditioning their relative stability which is itself dictating the reaction mechanism occurring on the surface.

We saw in Chapter 3 that functionals are now available to describe better the dispersion forces involved in many adsorption processes. We compared the adsorption energy and the electronic and geometric structures of a group of molecules calculated with the vdW functionals to the more traditional one, the PBE GGA functional. Most importantly, we confronted our results to experimental data obtained with microcalorimetry, in order to know the best functional to use for such systems. It appeared that optPBE-vdW gives results in best agreement with the experimental data set. Even though no experimental adsorption energy was measured for butadiene, the results obtained with optPBE-vdw on unsaturated hydrocarbons were very convincing and encouraged a parallel study of butadiene and hydrogen co-adsorption and reactivity with both functionals. In contrast PBE gives a marked underestimation of the adsorption energy (in absolute value).

The study of hydrogen adsorption on Pt(111) (Chapter 4) brought to the conclusion that the surface is completely covered with 1 ML at 300 K and 1 bar. On Sn/Pt-Pt(111), the coverage at these conditions is of only 0.67 ML because of Sn atoms that do not allow any adsorption. When changing the functional from PBE to optPBE, hydrogen is destabilized of about 0.1 eV which has consequences on the relative stability of hydrogen and butadiene. The use of optPBE does not impact the operating coverage in the case of Pt(111) which stays 1 ML but has an influence on the Sn/Pt-Pt(111) alloy and decreases the coverage from 0.67 to 0.44 ML since this functional yields a weaker adsorption for hydrogen. Moreover, in the case of Pt(111), it does impact strongly the preferred adsorption site of hydrogen which changes from fcc with PBE to top with optPBE. On the surface alloy, the preferential site stays the top site with both functionals. Finally, hydrogen is destabilized of about 0.1 eV when changing the functional from PBE to optPBE which has consequences on the relative stability of hydrogen and butadiene.

We then extended this thermodynamic model to the study of the co-adsorption of hydrogen and butadiene (Chapter 5 and 6) on both surface catalyst using both functional. For Pt(111), the use of PBE suggests that when the thermodynamic equilibrium is reached, the surface is covered with 1 ML of hydrogen and butadiene remains in the gas phase. On the contrary, using optPBE favours a chemisorption of butadiene in the trans-tetra σ mode, co-adsorbed with 0.56 ML of hydrogen. This is due to the change of relative stability of hydrogen and butadiene when changing the functional. The two different conclusions obtained with PBE and optPBE confirm that the choice of an appropriate method is crucial to allow accurate conclusions. Indeed, the surface entirely covered by hydrogen implies the physisorption of butadiene which directed our attention towards the Eley-Rideal mechanism. On the opposite, the chemisorption of buta-

diene and hydrogen announces the mechanism to be of Langmuir-Hinshelwood type. On Sn/Pt-Pt(111), the conclusions are similar to those obtained on Pt(111), but adapted to the surface structure regarding the operating coverage. Indeed, a complete hydrogen coverage (0.67 ML) and a metastable physisorption of butadiene is observed with PBE, while a co-adsorption of butadiene in the *cis*-1,4- $\text{di}\sigma$ -2,3 π conformation with 0.33 ML of hydrogen is obtained with optPBE.

We saw that at the thermodynamic equilibrium, PBE and optPBE gave different results, suggesting a fully hydrogenated surface in the case of PBE, and a chemisorption simultaneously of butadiene and hydrogen in the case of optPBE, this on both surface catalyst. This results implies two different reaction mechanisms that are Eley-Rideal on the surface fully covered by H atoms, and Langmuir-Hinshelwood for the co-adsorption.

The mechanistic study of butadiene hydrogenation, based on the results obtained in the co-adsorption study, was presented in Chapter 7. We saw that it is not trivial to investigate the possible pathways of this reaction as the first conclusions brought by the thermodynamics are not enough to conclude on the mechanism involved. Indeed, the most stable surface species is not always leading to the most favourable reaction path. It depends also on the hydrogenation barriers. We found out that the completely coordinated mode (*trans*-tetra σ) always leads to higher barriers than the partially de-coordinated one (*di* σ). On Pt(111), the latter is thermodynamically unfavoured at intermediate and high coverage. However, leading to lower barriers, the hydrogenation pathways starting from this conformation is favoured to the ones starting from the completely coordinated mode, using PBE and optPBE. The increase of hydrogen coverage is responsible for this new route on Pt(111) as it renders the *di* σ adsorption mode competitive with regards to the *trans*-tetra σ mode, when no competition was possible at low coverage. With this, we put forward the importance of the coverage dependency on Pt(111). On Sn/Pt-Pt(111), the partially de-coordinated mode was already stable at low

coverage because of the nature of the surface alloy. We observed that the increase of hydrogen atoms until an intermediate coverage did not affect the reactivity of butadiene. We also concluded that the use of the optPBE vdW functional did not impact on the selectivity of the reaction on this catalyst. We attributed this low effects to the fact that the adsorption of butadiene is quite weak on Sn/Pt compared to pure Pt.

The reactivity study on Pt(111) let us conclude that the pathway opened by the physisorbed state is the most favoured one using PBE, and thus, the Eley-Rideal mechanism is most likely to happen in this case. Using optPBE, the partially decoordinated mode ($di\sigma$) opens a route leading to a six-center unit TS that is more stable of about $50 \text{ kJ}\cdot\text{mol}^{-1}$ than the classical three-center unit TS resulting from a total coordination of the precursor ($trans\text{-}tetra\sigma$), and of about $70 \text{ kJ}\cdot\text{mol}^{-1}$ than the Eley-Rideal transition state. On Sn/Pt-Pt(111), the study is still under construction and cannot be presented yet.

The hypothesis we chose to approach the reactivity study of this reaction is to consider a constant coverage of hydrogen. Thus we do not allow the systems to reach the thermodynamic equilibrium between each hydrogenation step. This is a needed approximation at low coverage as one needs to refill the surface with one H atom to do the second hydrogenation. When we investigate the reactivity at higher coverage, we have two possibilities: either we consume the hydrogen atoms along the path, choosing the slow adsorption of H atoms as a hypothesis, or we study the thermodynamic of H adsorption around each intermediate along the path, thinking that a fast return to the equilibrium is the best hypothesis. At low coverage, we know that the dissociation of H_2 on the surface is a very fast process with no barrier. We still need to investigate this process at high coverage. Indeed, the surface being already quasi saturated, it is not trivial to know if the dissociation of H_2 will occur as easily as at low coverage. Thus the question of a fast return to the thermodynamic equilibrium remains unsolved for now but is relevant for the accuracy of this study and would improve our model.

The set of tools used until now to investigate butadiene hydrogenation has to be extended. Static DFT calculations provide important information on the energy profiles, but it would be important in a second step to use these profiles for the direct simulation of the catalytic reactivity. Other powerful methods such as microkinetics and kinetic Monte-Carlo would be very useful to complete the DFT tool, as they could provide missing informations at another scale. Both approaches would allow us to link the elementary step barriers with the global kinetic behavior of the system. Kinetic Monte Carlo would also allow us to describe the specific co-adsorption configurations between H atoms and butadiene. Even though the change of coverage remains a delicate issue in the treatment of such systems, these methods have already proven, through their performance, that they are essential in the development of heterogeneous catalysis. The methodology proposed in this work was developed to give insights at the microscale and is absolutely necessary to investigate properly the reactivity of catalyzed reactions. They should be now coupled with other methods making the link with the meso and macro scale. A multiscale study of butadiene hydrogenation involving simulated reactors is one possible way to improve the production of butene.

Appendices

Appendix A

Hydrogen adsorption sites on a (2×2) cell of Pt(111)

Each table contains all the possible adsorption configurations of hydrogen in fcc (f), hcp (h), top (t), tetrahedral (T) and octahedral (O) sites at the concerned coverage. The star (*) means that the z coordinate of the position of the atom was frozen in order to evaluate the energy of the site. Indeed, hydrogen is not stable in the octahedral site and always comes back to the fcc site during the optimization. The sign "-" means that the final site is the same as the initial site. The letter r means that we observed a high reconstruction of the surface.

Initial Site	E_{ads} (eV)	E_{ads}/at (eV)	Final Site
f	-0.53	-0.53	-
h	-0.49	-0.49	-
t	-0.49	-0.49	-
O*	0.39	0.39	-
T	0.22	0.22	-

Table A.1: $\theta_H = 0.25$ ML

Initial Site	E_{ads} (eV)	E_{ads}/at (eV)	Final Site
ff	-1.02	-0.51	-
tf2	-0.97	-0.49	-
fh2	-0.96	-0.48	-
hh	-0.93	-0.47	-
tt	-0.91	-0.45	-
tf1	-0.91	-0.45	-
th1	-0.92	-0.46	-
th2	-0.86	-0.43	-
fh1	-0.80	-0.40	-

Table A.2: $\theta_H = 0.5$ ML

Initial Site	E_{ads} (eV)	E_{ads}/at (eV)	Final Site
tff	-1.46	-0.49	fff
hff	-1.46	-0.49	fff
fff	-1.46	-0.49	fff
thf1	-1.33	-0.44	-
hhh	-1.33	-0.44	-
fhh	-1.33	-0.44	hhh
ttt	-1.28	-0.43	-
htt	-1.24	-0.41	-
ftt	-1.18	-0.39	-
thh	-1.17	-0.39	-
thf2	-1.11	-0.37	-

Table A.3: $\theta_H = 0.75$ ML

Initial Site	E_{ads} (eV)	E_{ads}/at (eV)	Final Site
hfff	-1.87	-0.47	ffff
ffhh	-1.87	-0.47	ffff
tfhh	-1.62	-0.41	tfff
thhh	-1.50	-0.37	-
httt	-1.48	-0.37	-
fftt	-1.48	-0.37	-
fttt	-1.40	-0.35	-
tfff	-1.38	-0.35	-
hftt	-1.38	-0.35	-
tffh	-1.38	-0.35	tfff
hhtt	-1.38	-0.35	-
fhhh	-1.00	-0.25	-

Table A.4: $\theta_H = 1$ ML

Initial Site	E_{ads} (eV)	E_{ads}/at (eV)	Final Site
thhff	-1.73	-0.35	tffff
tffff	-1.73	-0.35	-
htfff	-1.73	-0.35	tffff
hfttt	-1.72	-0.34	ftttt
ftttt	-1.72	-0.34	-
hfftt	-1.68	-0.34	hhhtt
tffff	-1.68	-0.34	-
htttt	-1.66	-0.34	-
fhhtt	-1.64	-0.33	fbttt
hhhtt	-1.58	-0.32	-
ftttt	-1.55	-0.31	-
hhfff	-1.54	-0.31	hhbbb
thhhh	-1.54	-0.31	-
fthhh	-1.54	-0.31	thhhh
tthhh	-1.53	-0.31	-
ffhhh	-1.46	-0.29	hhbbb
Offff	-1.46	-0.29	-
Tffff	-1.45	-0.29	-
hffff	-1.36	-0.27	-
fhhhh	-1.24	-0.25	-
Ohhhh	-1.13	-0.23	Thhhh
Thhhh	-1.13	-0.23	-

Table A.5: $\theta_H = 1.25$ ML

Initial Site	E_{ads} (eV)	E_{ads}/at (eV)	Final Site
ffttt	-1.69	-0.28	hhttt
fhhtt	-1.69	-0.28	ffttt
hhttt	-1.57	-0.26	-
htfff	-1.56	-0.26	hfttt
hfttt	-1.56	-0.26	-
ttfff	-1.50	-0.25	-
hfttt	-1.49	-0.25	ffttt
ffttt	-1.49	-0.25	-
ttthh	-1.48	-0.25	-
tffhh	-1.35	-0.23	ttbbh
tfhhh	-1.32	-0.22	ttbhh
tthhh	-1.32	-0.22	-
ftthh	-1.29	-0.22	ftthb
thfff	-1.29	-0.21	tbbff
OOfff	-1.10	-0.18	-
ffhhh	-1.04	-0.17	-
hhfff	-1.03	-0.17	hhffb
ffhhh	-1.03	-0.17	ffbhh
TThhh	-0.98	-0.16	-
oohhh	-0.96	-0.16	-
thfff	-0.84	-0.14	-
TTfff			
Ofttt	-1.35	-0.23	-
Ohttt	-1.32	-0.22	-
Otfff	-1.32	-0.22	-
Othhh	-1.15	-0.19	-
Tfttt	-1.33	-0.22	-
Thttt	-1.04	-0.17	-
Ttfff	-1.19	-0.20	-
Tthhh	-0.90	-0.15	-

Table A.6: $\theta_H = 1.5$ ML

Initial Site	E_{ads} (eV)	E_{ads}/at (eV)	Final Site
hfftttt	-1.32	-0.19	ffftttt
htttfff	-1.32	-0.19	ttttfff
ffftttt	-1.32	-0.19	-
hhtttff	-1.16	-0.17	tttfbbb
hhffttt	-1.16	-0.17	tttfbbb
hhhtttt	-1.13	-0.16	-
fhhtttt	-1.15	-0.16	bhhtttt
ftthhhh	-1.15	-0.16	ftthhbb
tttfff	-1.12	-0.16	-
hhhfff	-1.00	-0.14	-
TTTfff	-1.00	-0.14	-
ftthhhh	-0.96	-0.14	ftthhbb
ttthhhh	-0.93	-0.13	-
thhhfff	-0.87	-0.12	tthhbbb
OOOfff	-0.78	-0.11	-
ffthhhh	-0.72	-0.10	ttffhbb
OOOhhhh	-0.67	-0.10	-
TTThhhh	-0.67	-0.10	-
htttfff	-0.62	-0.09	httfbb
thhfff	-0.61	-0.09	tfffhhh
tffhhhh	-0.61	-0.09	tfffhhh
fffhhhh	-0.53	-0.08	-

Table A.7: $\theta_H = 1.75$ ML

Initial Site	E_{ads} (eV)	E_{ads}/at (eV)	Final Site
tfffhhhh	-1.13	-0.14	r
TTTTffff	-1.05	-0.13	-
thhhffff	-0.88	-0.11	r
TTTThhhh	-0.82	-0.10	-
OOOOffff	-0.57	-0.07	-
OOOOhhhh	-0.50	-0.06	-
tttffff	-0.46	-0.06	-
hhtffff	-0.46	-0.06	-
tfffhhhh	-0.39	-0.05	-
hhftttt	-0.27	-0.03	-
tttthhhh	-0.22	-0.03	-
tfffhhh	-0.14	-0.01	ttffhbb
fttthhhh	-0.11	-0.01	fttthbb
fftthhhh	-0.11	-0.01	ttthfbb
hhtttfff	-0.11	-0.01	ttfhbb
fhhtttt	0.06	0.00	-
hfftttt	-0.05	-0.00	-
htttfff	-0.00	-0.00	-
ffffhhhh	2.73	0.34	-

Table A.8: $\theta_H = 2$ ML

Appendix B

Screening of hydrogen adsorption sites on a (3×3) cell of Pt(111)

In the following tables are reported all the possible fcc sites for hydrogen to adsorb around one molecule of butadiene, using PBE and on Pt(111). Each table corresponds to a different adsorption mode of butadiene.

Initial site	ΔE_{ads} (eV,total)	ΔE_{ads} (eV,but.)	Final Site	Nbr of Pt(-C) at.
1	-1.80	-1.29	Hcp3	0
1 Fr.	-1.58		Fcc1	1
2	-1.81		Fcc8	1
2 Fr.	-1.18		Fcc2	2
3	-1.83	-1.32	Fcc3	1
4	-1.79	-1.27	Fcc4	1
5	-1.15	-0.64	Fcc5	2
6	-1.87		Fcc7	0
6 Fr.	-1.61		Fcc6	1
7	-1.87	-1.36	Fcc7	0
8	-1.81	-1.30	Fcc8	1
9	-1.84	-1.33	Fcc9	0

Table B.1: Adsorption energies (in eV) of hydrogen on the fcc sites ($\theta_H = 0.11$ ML) and butadiene in the cis-1,4di σ -2,3 π conformation on Pt(111) using PBE; "Fr." means that the H coordinates were frozen in the two directions of the surface (x and y) and optimized in the z direction; the sites that were not stable enough to have the H atom stay on it are marked in blue

Initial site	ΔE_{ads} (eV,total)	ΔE_{ads} (eV,but.)	Final Site	Nbr of Pt(-C) at.
1	-1.80	-1.29	Fcc1	1
2	-1.81		Fcc7	0
2 Fr.	-1.13		Fcc2	2
3	-1.74	-1.23	Fcc3	1
4	-1.83	-1.32	Fcc4	0
5	-1.83		Fcc4	0
5 Fr.	-1.13		Fcc5	2
6	-1.51	-0.10	Fcc6	2
7	-1.81	-1.30	Fcc7	0
8	-1.64	-1.13	Fcc8	0
9	-1.75		Fcc3	1
9 Fr.	-1.50		Fcc9	1

Table B.2: Adsorption energies (in eV) of hydrogen on the fcc sites ($\theta_H = 0.11$ ML) and butadiene in the cis-1, 2di σ -3, 4 π conformation on Pt(111) using PBE; "Fr." means that the H coordinates were frozen in the two directions of the surface (x and y) and optimized in the z direction; the sites that were not stable enough to have the H atom stay on it are marked in blue

Initial site	ΔE_{ads} (eV,total)	ΔE_{ads} (eV,but.)	Final Site	Nbr of Pt(-C) at.
1	-1.57	-1.05	Hcp3	0
1 Fr.	-1.39		Fcc1	1
2	-1.64		Fcc3	(0
2 Fr.	-1.30		Fcc2	1
3	-1.64	-1.13	Fcc3	0
4	-1.56	-1.05	Hcp6	0
4 Fr.	-1.42		Fcc4	1
5	-1.01	-0.50	Fcc5	2
6	-1.62	-1.11	Fcc6	0
7	-1.59	-1.08	Fcc7	0
8	-1.64		Fcc3	0
8 Fr.	-1.39		Fcc8	1
9	-1.62	-1.11	Fcc9	0

Table B.3: Adsorption energies (in eV) of hydrogen on the fcc sites ($\theta_H = 0.11$ ML) and butadiene in the trans- $di\pi$ conformation on Pt(111) using PBE; "Fr." means that the H coordinates were frozen in the two directions of the surface (x and y) and optimized in the z direction; the sites that were not stable enough to have the H atom stay on it are marked in blue

Initial site	ΔE_{ads} (eV,total)	ΔE_{ads} (eV,but.)	Final Site	Nbr of Pt(-C) at.
1	-1.47	-0.96	B1-1	1
1 Fr.	-1.39		Fcc1	1
2	-0.99	-0.48	Fcc2	2
3	-1.47	-0.96	B3-2	1
3 Fr.	-1.39		Fcc3	1
4	-1.54	-1.03	Fcc4	0
5	-1.49	-0.98	Hcp8	0
5 Fr.	-1.77		Fcc5	1
6	-1.49	-0.98	Hcp9	0
6 Fr.	-1.77		Fcc6	1
7	-1.54	-1.03	Fcc7	0
8	-1.55	-1.03	Fcc8	0
9	-1.57	-1.06	Fcc9	0

Table B.4: Adsorption energies (in eV) of hydrogen on the fcc sites ($\theta_H = 0.11$ ML) and butadiene in the cis-di π conformation on Pt(111) using PBE; "Fr." means that the H coordinates were frozen in the two directions of the surface (x and y) and optimized in the z direction; the sites that were not stable enough to have the H atom stay on it are marked in blue

Initial site	ΔE_{ads} (eV,total)	ΔE_{ads} (eV,but.)	Final Site	Nbr of Pt(-C) at.
1	-1.26	-0.75	Fcc1	0
2	-1.30		Fcc8	1
2 Fr.	-0.64		Fcc2	0
3	-1.26	-0.75	Fcc3	0
4	-1.31	-0.80	Fcc4	1
5	-1.15	-0.64	Fcc5	2
6	-1.15	-0.64	Fcc6	1
7	-1.31	-0.80	Fcc7	0
8	-1.30	-0.79	Fcc8	1
9	-1.30	-0.79	Fcc9	1

Table B.5: Adsorption energies (in eV) of hydrogen on the fcc sites ($\theta_H = 0.11$ ML) and butadiene in the $di\sigma$ conformation on Pt(111) using PBE; "Fr." means that the H coordinates were frozen in the two directions of the surface (x and y) and optimized in the z direction; the sites that were not stable enough to have the H atom stay on it are marked in blue

Appendix C

Molecular adsorption at Pt(111). How accurate are DFT functionals ?

Table C.1: Description of the benchmark set for molecular adsorption on Pt(111). The table lists the integral adsorption energy calculated from the experimental data, at the selected coverage. Mode: M: molecular, D: dissociative chemisorption, R: reaction as indicated ((g) is for gas, (a) for adsorbed species). INTF: integration between 0 and theta of a fit provided in ref. INTC: more or less accurate integration on the plot of E (coverage)

Molecule / reaction	Exp (eV) method	Mode	Coverage for E calc	Energy (eV)	tool	ref
C ₂ H ₄ (g) gives CCH ₃ (a) + H(a)	SCAC	R	1/9 ML	1.36	INTC	26(#)
Cyclohexene	SCAC	M	1/9 ML	1.273	INTF	32
c-C ₆ H ₁₀ (g) gives c-C ₆ H ₉ (a) + H(a)	SCAC	R	1/9 ML	1.433	INTF	32
C ₆ H ₆	SCAC	M	1/9 ML	1.72 (1.66)	INTF INTF	29,59
Naphthalene	SCAC	M	1/16 ML	2.763	INTF	75
CH ₄	TPD	M	1/9 ML	0.181	INTF	76
Ethane	TPD	M	1/9 ML	0.331	INTF	76
1/2(H ₂ gas)	Low energy recoil scatt	D	1/9 ML*	0.39 ± 0.02	INTC	77
1/2(H ₂ gas)	Nuclear micro-analysis	D	1/9 ML*	0.347 ± 0.04	INTC	78
CO ads	SCAC	M	1/9 ML 188	1.29 (1.31) 1.29	INTC (INTF) INTC	26(#), 29 28
1/2 (O ₂ gas)	SCAC	D	1/9 ML	1.10	INTC	79(#)
1/2 (O ₂ gas)	SCAC	D	1/9 ML	1.08	INTF	58

(*) adsorption energy is constant between 0 and 0.33 ML. (#) Published data incorrect due to wrong reflectivity of Pt(111). Scale factor of 0.7059 applied here.

Table C.2: Adsorption energies (in eV) for various systems and density functional approximations as well as the experimental reference value when available. All calculations were conducted with a slab of 6 layers in a (3×3) supercell except for adsorption of naphthalene where a (4×4) supercell was used.

Kpts	System	PBE	optPBE	optB86b	BEEF	PBE-dDsC	dDsC(a)	Exp
7x7x1	Ethylene	-1.21	-1.44	-1.73	-1.12	-1.51	-0.33	NA
7x7x1	Ethylidyne+H	-1.74	-1.75	-2.15	-1.43	-1.99	-0.28	-1.36
7x7x1	Butene cis	-0.93	-1.52	-1.85	-1.05	-1.51	-0.61	NA
7x7x1	Butene trans	-0.93	-1.53	-1.86	-1.06	-1.51	-0.61	NA
7x7x1	Cyclohexene (boat down)	-0.69	-1.31	-1.62	-0.90			
7x7x1	Cyclohexene (chair trans)	-0.74	-1.37	-1.69	-0.69			
7x7x1	Cyclohexene (chair cis)	-0.75	-1.45	-1.80	-0.95			
7x7x1	Cyclohexene (boat up)	-0.84	-1.51	-1.84	-1.03			
9x9x1	Cyclohexene (boat up)	-0.84	-1.51	-1.83	-1.04	-1.50	-0.66	-1.27
7x7x1	C ₆ H ₉ +H	-1.00	-1.63	-2.18	-0.97	-1.73	-0.74	-1.43
9x9x1	C ₆ H ₉ +H	-1.01	-1.63	-2.18	-0.98	-1.73	-0.74	-1.43
5x5x1	Butadiene (<i>cis</i> 1, 2 <i>di</i> σ 3, 4 π)	-1.57	-1.99	-2.49	-1.50			
5x5x1	Butadiene (<i>di</i> σ)	-1.00	-1.51	NA	-1.33			
5x5x1	Butadiene(<i>tetra</i> σ)	-1.82	-2.23	-2.78	-1.71			
7x7x1	Butadiene(<i>tetra</i> σ)	-1.89	-2.30	-2.86	-1.75	-2.43	-0.58	NA
9x9x1	Butadiene(<i>tetra</i> σ)	-1.89	-2.30	-2.86	-1.76	NA		
7x7x1	Benzene bri30	-1.12	-1.65	-2.34	-1.03	-1.76	-0.71	-1.72
9x9x1	Benzene bri30	-1.12	-1.65	-2.34	-1.04	-1.76	-0.69	-1.72
11x11x1	Benzene bri30	-1.13	-1.66	-2.35	-1.05	-1.76	-0.68	-1.72
11x11x1	Benzene hcp0	-0.86	-1.40	-2.05	-0.82			
7x7x1	Naphtalene(b)	-1.48	-2.32	-3.42	-1.41	-2.57	-1.18	-2.76
9x9x1	Naphtalene(b)	-1.46	-2.30	-3.39	-1.39	-2.51	-1.14	-2.76
7x7x1	Methane	-0.01	-0.23	-0.21	-0.12	-0.17	-0.10	-0.18
7x7x1	Ethane	-0.03	-0.36	-0.39	-0.22	-0.32	-0.28	-0.33
7x7x1	Hydrogen, fcc site	-0.52	-0.38	-0.50	-0.27	-0.55	-0.05	-0, 37
7x7x1	Hydrogen, top site	-0.48	-0.42	-0.50	-0.30	-0.52	-0.06	NA
7x7x1	CO (top)	-1.71	-1.68	-1.87	-1.49	-1.86	-0.16	-1.29
7x7x1	O (fcc)	-1.29	-1.43	-1.50	-1.15	-1.32	-0.07	-1.10

(a) Contribution of the dispersion correction dDsC to the adsorption energy. (b) (4×4) supercell.

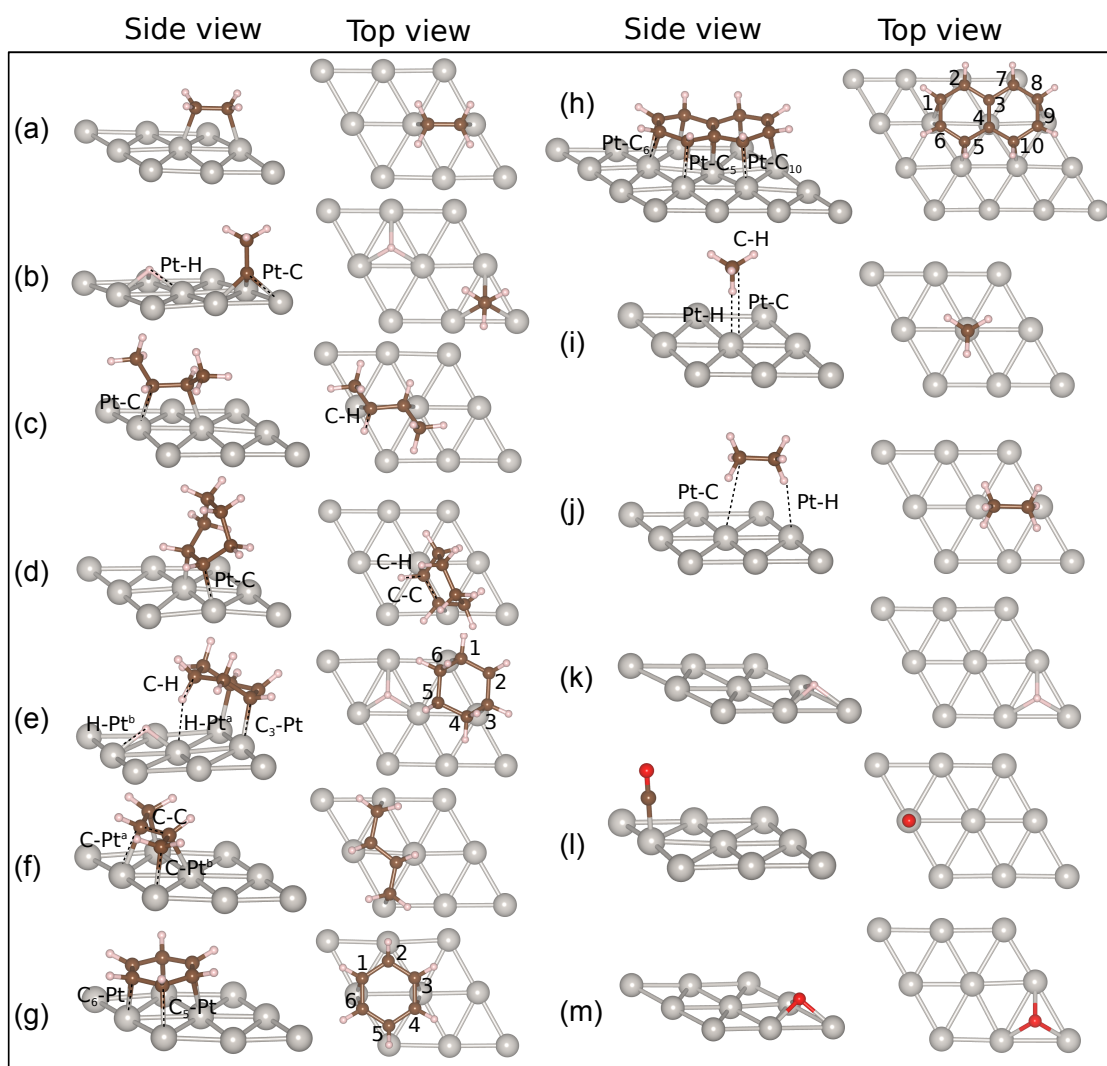


Figure C.1: Adsorption geometries with characteristic distances indicated. See Tables C.3 to C.17 for more details. a: ethylene C_2H_4 , b: ethylidyne CCH_3 and one H, c: trans 2-butene C_4H_8 , d: cyclohexene C_6H_{10} boat up, e: C_6H_9 and one H, f: butadiene C_4H_6 , g: benzene C_6H_6 , h: naphthalene $C_{10}H_8$, i: methane CH_4 , j: ethane C_2H_6 , k: H atom in fcc position, l: CO, m: O atom.

Table C.3: Characteristic distances (in Å) of ethylene

Distances	Pt-C	C-C	C-H
PBE	2.110	1.489	1.097
optPBE	2.127	1.491	1.097
optB86b	2.111	1.49	1.1
BEEF	2.121	1.487	1.091
PBE-dDsC	2.107	1.487	1.097

Table C.4: Characteristic distances (in Å) of ethylidyne+H

Distances	Pt-C	C-C	Pt-H
PBE	2.013	1.491	1.862
optPBE	2.022	1.496	1.876
optB86b	2.013	1.488	1.871
BEEF	2.012	1.496	1.865
PBE-dDsC	2.011	1.488	1.86

Table C.5: Characteristic distances (in Å) of trans butene

Distances	Pt-C	C-C	C-H
PBE	2.120	1.506	1.102
optPBE	2.133	1.509	1.101
optB86b	2.117	1.506	1.105
BEEF	2.127	1.506	1.095
PBE-dDsC	2.117	1.503	1.101

Table C.6: Characteristic distances (in Å) of cyclohexene

Distances	Pt-C	C-C	C-H
PBE	2.126	2.126	2.126
optPBE	2.138	2.138	2.138
optB86b	2.120	2.120	2.120
BEEF	2.131	2.131	2.131
PBE-dDsC	2.120	2.120	2.120

Table C.7: Characteristic distances (in Å) of C₆H₉+H (first part)

Distances	C ₁ -C ₂	C ₂ -C ₃	C ₃ -C ₄	C ₄ -C ₅	C ₅ -C ₆	C ₆ -C ₁
PBE	1.496	1.497	1.526	1.522	1.523	1.527
optPBE	1.500	1.500	1.532	1.528	1.529	1.534
optB86b	1.498	1.498	1.526	1.522	1.523	1.527
BEEF	1.496	1.496	1.529	1.525	1.526	1.531
PBE-dDsC	1.494	1.494	1.522	1.519	1.519	1.524

Table C.8: Characteristic distances (in Å) of C₆H₉+H (second part)

Distances	H-Pt ^a	H-Pt ^b	C ₂ -Pt	C ₃ -Pt	Pt-H
PBE	4.089	1.848	2.153	3.081	1.101
optPBE	4.084	1.854	2.176	3.09	1.102
optB86b	4.002	1.842	2.152	3.062	1.104
BEEF	4.135	1.846	2.164	3.09	1.096
PBE-dDsC	4.032	1.847	2.15	3.067	1.1

Table C.9: Characteristic distances (in Å) of butadiene

Distances	C-C	C-Pt-a	C-Pt-b
PBE	1.486	2.159	2.097
optPBE	1.489	2.181	2.112
optB86b	1.487	2.16	2.097
BEEF	1.485	2.174	2.106
PBE-dDsC	1.484	2.156	2.094

Table C.10: Characteristic distances (in Å) of benzene (first part)

Distances	C ₁ -C ₂	C ₂ -C ₃	C ₃ -C ₄	C ₄ -C ₅
PBE	1.474	1.474	1.435	1.473
optPBE	1.476	1.475	1.433	1.475
optB86b	1.474	1.474	1.435	1.474
BEEF	1.472	1.472	1.431	1.472
PBE-dDsC	1.472	1.471	1.433	1.471

Table C.11: Characteristic distances (in Å) of benzene (second part)

Distances	C ₅ -C ₆	C ₆ -C ₁	Pt-C ₅	Pt-C ₁	Pt-C ₆
PBE	1.473	1.435	2.158	2.197	2.189
optPBE	1.475	1.433	2.181	2.23	2.223
optB86b	1.474	1.435	2.16	2.203	2.194
BEEF	1.472	1.431	2.173	2.219	2.21
PBE-dDsC	1.471	1.434	2.156	2.193	2.186

Table C.12: Characteristic distances (in Å) of Naphthalene (first part)

Distances	C ₁ -C ₂	C ₂ -C ₃	C ₃ -C ₄	C ₄ -C ₅	C ₅ -C ₆
PBE	1.469	1.485	1.454	1.485	1.469
optPBE	1.471	1.486	1.452	1.487	1.47
optB86b	1.470	1.484	1.452	1.485	1.469
BEEF	1.467	1.483	1.452	1.483	1.466
PBE-dDsC	1.467	1.482	1.452	1.482	1.467

Table C.13: Characteristic distances (in Å) of Naphthalene (second part)

Distances	C ₆ -C ₁	C ₃ -C ₇	C ₇ -C ₈	C ₈ -C ₉	C ₉ -C ₁₀
PBE	1.428	1.485	1.469	1.428	1.469
optPBE	1.425	1.486	1.47	1.425	1.471
optB86b	1.427	1.485	1.47	1.427	1.469
BEEF	1.423	1.483	1.467	1.423	1.467
PBE-dDsC	1.427	1.482	1.467	1.427	1.467

Table C.14: Characteristic distances (in Å) of Naphthalene (third part)

Distances	C ₁₀ -C ₄	Pt-C ₁	Pt-C ₆	Pt-C ₅	Pt-C ₁₀
PBE	1.484	2.225	2.215	2.221	2.138
optPBE	1.487	2.272	2.256	2.261	2.158
optB86b	1.485	2.234	2.222	2.229	2.139
BEEF	1.483	2.256	2.246	2.242	2.153
PBE-dDsC	1.482	2.223	2.213	2.217	2.136

Table C.15: Characteristic distances (in Å) of methane

Distances	Pt-C	C-C	Pt-H
PBE	3.809	1.102	2.713
optPBE	3.702	1.103	2.606
optB86b	3.416	1.113	2.307
BEEF	3.806	1.093	2.719
PBE-dDsC	3.867	1.096	2.766

Table C.16: Characteristic distances (in Å) of ethane

Distances	Pt-C	C-C	Pt-H
PBE	3.86	1.525	2.68
optPBE	3.628	1.53	2.496
optB86b	3.465	1.522	2.232
BEEF	3.865	1.528	2.721
PBE-dDsC	3.874	1.522	2.484

Table C.17: Characteristic distances (in Å) of H, O and CO

System	H	O	CO	
Distances	Pt-H	Pt-O	Pt-C	C-O
PBE	1.868	2.040	1.841	1.157
optPBE	1.878	2.050	1.853	1.157
optB86b	1.872	2.038	1.845	1.156
BEEF	1.869	2.051	1.85	1.156
PBE-dDsC	1.861	2.040	1.84	1.157

Bibliography

- [1] Morin, C.; Simon, D.; Sautet, P. *J. Phys. Chem. B* **2003**, *107*, 2995–3002.
- [2] Morin, C.; Simon, D.; Sautet, P. *Surface Science* **2006**, *600*, 1339–1350.
- [3] Michalak, W. D.; Krier, J. M.; Komvopoulos, K.; Somorjai, G. A. *J. Phys. Chem. C* **2013**, *117*, 1809–1817, WOS:000314492400034.
- [4] Valcárcel, A.; Clotet, A.; Ricart, J. M.; Delbecq, F.; Sautet, P. *J. Phys. Chem. B* **2005**, *109*, 14175–14182.
- [5] Li, J.; Fleurat-Lessard, P.; Zaera, F.; Delbecq, F. *Journal of Catalysis* **2014**, *311*, 190–198.
- [6] Kresse, G.; Hafner, J. *Phys. Rev. B* **1993**, *47*, 558–561.
- [7] Kresse, G.; Furthmüller, J. *Computational Materials Science* **1996**, *6*, 15–50.
- [8] Zhao, H.; Koel, B. E. *Surface Science* **2004**, *572*, 261–268.
- [9] Zhao, H.; Koel, B. E. *Journal of Catalysis* **2005**, *234*, 24–32.
- [10] Valcárcel, A.; Clotet, A.; Ricart, J. M.; Delbecq, F.; Sautet, P. *Surface Science* **2004**, *549*, 121–133.
- [11] Kohn, W.; Sham, L. J., **1965**, *140*, A1133–A1138.

- [12] Perdew, J. P.; Burke, K.; Ernzerhof, M. *Phys. Rev. Lett.* **1996**, *77*, 3865–3868.
- [13] Klimeš, J.; Bowler, D. R.; Michaelides, A. *J. Phys.: Condens. Matter* **2010**, *22*, 022201.
- [14] Somorjai, G. A. *Progress in Surface Science* **1995**, *50*, 3–29.
- [15] King, D. A. *Surface Science* **1994**, *299–300*, 678–689.
- [16] Lytken, O.; Lew, W.; Campbell, C. T. *Chemical Society Reviews* **2008**, *37*, 2172.
- [17] Hoffmann, R. *Rev. Mod. Phys.* **1988**, *60*, 601–628.
- [18] Nilsson, A.; Pettersson, L. G. M. *Surface Science Reports* **2004**, *55*, 49–167.
- [19] Whitten, J. L.; Yang, H. *Surface Science Reports* **1996**, *24*, 55–124.
- [20] J. P. Perdew,; K. Schmidt, *Density Functional Theory and Its Applications to Materials*, american institute of physics ed.; V. E. Van Doren, K. Van Alsenoy, and P. Geerlings: Melville, NY, 2001.
- [21] W. Koch,; M.C. Holthausen, *A Chemist's Guide to Density Functional Theory, 2nd Edition*; Wiley-VCH: Weinheim, 2001.
- [22] Becke, A. D. *The Journal of Chemical Physics* **1993**, *98*, 5648–5652.
- [23] Paier, J.; Marsman, M.; Kresse, G. *The Journal of Chemical Physics* **2007**, *127*, 024103.
- [24] Schimka, L.; Harl, J.; Stroppa, A.; Grüneis, A.; Marsman, M.; Mittendorfer, F.; Kresse, G. *Nat Mater* **2010**, *9*, 741–744.
- [25] Klimeš, J.; Michaelides, A. *The Journal of Chemical Physics* **2012**, *137*, 120901.
- [26] Brown, W. A.; Kose, R.; King, D. A. *Chem. Rev.* **1998**, *98*, 797–832.

- [27] Lew, W.; Lytken, O.; Farmer, J. A.; Crowe, M. C.; Campbell, C. T. *Review of Scientific Instruments* **2010**, *81*, 024102.
- [28] Fischer-Wolfarth, J.-H.; Hartmann, J.; Farmer, J. A.; Flores-Camacho, J. M.; Campbell, C. T.; Schauerer, S.; Freund, H.-J. *Review of Scientific Instruments* **2011**, *82*, 024102.
- [29] Schießer, A.; Hörtz, P.; Schäfer, R. *Surface Science* **2010**, *604*, 2098–2105.
- [30] Yeo, Y. Y.; Stuck, A.; Wartnaby, C. E.; King, D. A. *Chemical Physics Letters* **1996**, *259*, 28–36.
- [31] Gross, H.; Campbell, C. T.; King, D. A. *Surface Science* **2004**, *572*, 179–190.
- [32] Lytken, O.; Lew, W.; Harris, J. J. W.; Vestergaard, E. K.; Gottfried, J. M.; Campbell, C. T. *J. Am. Chem. Soc.* **2008**, *130*, 10247–10257.
- [33] Dion, M.; Rydberg, H.; Schröder, E.; Langreth, D. C.; Lundqvist, B. I. *Phys. Rev. Lett.* **2004**, *92*, 246401.
- [34] Wellendorff, J.; Lundgaard, K. T.; Møgelhøj, A.; Petzold, V.; Landis, D. D.; Nørskov, J. K.; Bligaard, T.; Jacobsen, K. W. *Phys. Rev. B* **2012**, *85*, 235149.
- [35] Lee, K.; Morikawa, Y.; Langreth, D. C. *Phys. Rev. B* **2010**, *82*, 155461.
- [36] Steinmann, S. N.; Corminboeuf, C. *The Journal of Chemical Physics* **2011**, *134*, 044117.
- [37] Steinmann, S. N.; Corminboeuf, C. *J. Chem. Theory Comput.* **2011**, *7*, 3567–3577.
- [38] Grimme, S.; Antony, J.; Ehrlich, S.; Krieg, H. *The Journal of Chemical Physics* **2010**, *132*, 154104.
- [39] Grimme, S.; Ehrlich, S.; Goerigk, L. *J. Comput. Chem.* **2011**, *32*, 1456–1465.

- [40] Tkatchenko, A.; Scheffler, M. *Phys. Rev. Lett.* **2009**, *102*, 073005.
- [41] Tkatchenko, A.; DiStasio, R. A.; Car, R.; Scheffler, M. *Phys. Rev. Lett.* **2012**, *108*, 236402.
- [42] Bučko, T.; Lebègue, S.; Hafner, J.; Ángyán, J. G. *Phys. Rev. B* **2013**, *87*, 064110.
- [43] Brémond, É.; Golubev, N.; Steinmann, S. N.; Corminboeuf, C. *The Journal of Chemical Physics* **2014**, *140*, 18A516.
- [44] Delbecq, F.; Zaera, F. *J. Am. Chem. Soc.* **2008**, *130*, 14924–14925.
- [45] Delbecq, F.; Vigné-Maeder, F.; Becker, C.; Breitbach, J.; Wandelt, K. *J. Phys. Chem. C* **2008**, *112*, 555–566.
- [46] Avery, N. R.; Sheppard, N. *Proceedings of the Royal Society of London A: Mathematical, Physical and Engineering Sciences* **1986**, *405*, 1–25.
- [47] Avery, N. R.; Sheppard, N. *Proceedings of the Royal Society of London A: Mathematical, Physical and Engineering Sciences* **1986**, *405*, 27–39.
- [48] Bertolini, J. C.; Cassuto, A.; Jugnet, Y.; Massardier, J.; Tardy, B.; Tourillon, G. *Surface Science* **1996**, *349*, 88–96.
- [49] Sautet, P.; Paul, J.-F. *Catal Lett* **1991**, *9*, 245–260.
- [50] Mittendorfer, F.; Thomazeau, C.; Raybaud, P.; Toulhoat, H. *J. Phys. Chem. B* **2003**, *107*, 12287–12295.
- [51] Saeys, M.; Reyniers, M.-F.; Marin, G. B.; Neurock, M. *J. Phys. Chem. B* **2002**, *106*, 7489–7498.
- [52] Morin, C.; Simon, D.; Sautet, P. *J. Phys. Chem. B* **2004**, *108*, 5653–5665.

- [53] Liu, W.; Carrasco, J.; Santra, B.; Michaelides, A.; Scheffler, M.; Tkatchenko, A. *Phys. Rev. B* **2012**, *86*, 245405.
- [54] Liu, W.; Ruiz, V. G.; Zhang, G.-X.; Santra, B.; Ren, X.; Scheffler, M.; Tkatchenko, A. *New J. Phys.* **2013**, *15*, 053046.
- [55] Yildirim, H.; Greber, T.; Kara, A. *J. Phys. Chem. C* **2013**, *117*, 20572–20583.
- [56] Wander, A.; Held, G.; Hwang, R.; Blackman, G.; Xu, M.; Deandres, P.; Vanhove, M.; Somorjai, G. *Surf. Sci.* **1991**, *249*, 21–34, WOS:A1991FV26700016.
- [57] Morin, C.; Simon, D.; Sautet, P. *J. Phys. Chem. B* **2004**, *108*, 12084–12091.
- [58] Karp, E. M.; Campbell, C. T.; Studt, F.; Abild-Pedersen, F.; Nørskov, J. K. *J. Phys. Chem. C* **2012**, *116*, 25772–25776.
- [59] Ihm, H.; Ajo, H. M.; Gottfried, J. M.; Bera, P.; Campbell, C. T. *J. Phys. Chem. B* **2004**, *108*, 14627–14633.
- [60] Augustine, R. L. *Heterogeneous Catalysis for the Synthetic Chemist*; CRC Press, 1995.
- [61] Bartók, M. *Stereochemistry of Heterogeneous Metal Catalysis*; John Wiley & Sons Canada, Limited, 1985.
- [62] Bauer, K.; Garbe, D.; Surburg, H. *Common Fragrance and Flavor Materials: Preparation, Properties and Uses*; John Wiley & Sons, 2008.
- [63] Marinelli, T. B. L. W.; Nabuurs, S.; Ponec, V. *Journal of Catalysis* **1995**, *151*, 431–438.
- [64] Olsen, R. A.; Kroes, G. J.; Baerends, E. J. *The Journal of Chemical Physics* **1999**, *111*, 11155–11163.

- [65] Watson, G. W.; Wells, R. P. K.; Willock, D. J.; Hutchings, G. J. *J. Phys. Chem. B* **2001**, *105*, 4889–4894.
- [66] Bădescu, Ș. C.; Salo, P.; Ala-Nissila, T.; Ying, S. C.; Jacobi, K.; Wang, Y.; Bedürftig, K.; Ertl, G. *Phys. Rev. Lett.* **2002**, *88*, 136101.
- [67] Eberhardt, W.; Greuter, F.; Plummer, E. W. *Phys. Rev. Lett.* **1981**, *46*, 1085–1088.
- [68] Umezawa, K.; Ito, T.; Asada, M.; Nakanishi, S.; Ding, P.; Lanford, W. A.; Hjörvarsson, B. *Surface Science* **1997**, *387*, 320–327.
- [69] Légaré, P. *Surface Science* **2004**, *559*, 169–178.
- [70] Chizallet, C.; Bonnard, G.; Krebs, E.; Bisson, L.; Thomazeau, C.; Raybaud, P. *J. Phys. Chem. C* **2011**, *115*, 12135–12149.
- [71] Castillo, S.; Poulain, E.; Bertin, V.; Cruz, A. *Int. J. Quantum Chem.* **1995**, *56*, 207–215.
- [72] Atrei, A.; Bardi, U.; Wu, J. X.; Zanazzi, E.; Rovida, G. *Surface Science* **1993**, *290*, 286–294.
- [73] Thomazeau, C.; Cseri, T.; Bisson, L.; Aguilhon, J.; Minh, D. P.; Boissiere, C.; Durupthy, O.; Sanchez, C. *Top. Catal.* **2012**, *55*, 690–699, WOS:000307778600002.
- [74] Vigné, F.; Haubrich, J.; Loffreda, D.; Sautet, P.; Delbecq, F. *Journal of Catalysis* **2010**, *275*, 129–139.
- [75] Gottfried, J. M.; Vestergaard, E. K.; Bera, P.; Campbell, C. T. *J. Phys. Chem. B* **2006**, *110*, 17539–17545.
- [76] Tait, S. L.; Dohnálek, Z.; Campbell, C. T.; Kay, B. D. *The Journal of Chemical Physics* **2006**, *125*, 234308.

- [77] Koeleman, B. J. J.; de Zwart, S. T.; Boers, A. L.; Poelsema, B.; Verhey, L. K. *Nuclear Instruments and Methods in Physics Research* **1983**, *218*, 225–229.
- [78] Norton, P. R.; Davies, J. A.; Jackman, T. E. *Surface Science* **1982**, *121*, 103–110.
- [79] Fiorin, V.; Borthwick, D.; King, D. A. *Surface Science* **2009**, *603*, 1360–1364.